Numerical study of vertical axis wind turbine performance in turbulent flows and behind turbine wakes

Belkacem Belabes

A Thesis

In

The Department

Of

Mechanical, Industrial, and Aerospace Engineering

Presented in Partial Fulfillment of the Requirements

for the Degree of

Doctor of Philosophy (Mechanical Engineering) at

Concordia University

Montreal, Quebec, Canada

July 2023

CONCORDIA UNIVERSITY

School of Graduate Studies

This is to certify that the thesis prepared,

By: **Belkacem Belabes**

Entitled: **Numerical study of vertical axis wind turbine performance in turbulent flows and behind turbine wakes**

And submitted in partial fulfillment of the requirements of the degree of

Doctor of Philosophy (Mechanical Engineering)

Complies with the regulations of this University and meets the accepted standards with respect to originality and quality.

Signed by the Final Examining Committee:

Dr. Todd Eavis	Chair
Dr. Mathieu Olivier	External Examiner
Dr. Lyes Kadem	Examiner
Dr. Sheng Samuel Li	Examiner
Dr. Mojtaba Kheiri	Examiner
Dr. Marius Paraschivoiu	Thesis Supervisor

Approved by

Martin D. Pugh, Chair
Department of Mechanical, Industrial and Aerospace Engineering

September 15th, 2023
Date of Defense

Mourad Debbabi, Dean
Gina Cody School of Engineering and Computer Science

Abstract

Numerical study of vertical axis wind turbine performance in turbulent flows and behind turbine wakes

Belkacem Belabes, Ph.D.

Concordia University, 2023.

Wind energy is a clean, renewable, and cost-effective alternative to conventional power sources. It does not require fuel, does not emit pollution, and can be installed near the places where electricity is needed, reducing transmission losses. Vertical Axis Wind Turbines (VAWTs) are a type of wind energy technology that have some advantages over Horizontal Axis Wind Turbines (HAWTs), such as being able to able to harvest wind from all directions, generate less noise, and offering a simpler structure. However, VAWTs also have lower efficiency than HAWTs, and their performance is affected by the wake, which is a lower-velocity turbulent flow behind the rotating blades.

The wake can interfere with the operation of other wind turbines downstream, but it can also enhance the performance of smaller VAWTs. The aim of this research is to use Computational Fluid Dynamics (CFD) to study the effect of wake on different sizes of VAWTs, and to understand how the turbulence generated by the wake influences the power output of these turbines. This thesis presents a CFD methodology and identifies the strengths and weaknesses of CFD for the simulation of the interaction of the wake with downstream VAWTs. The contributions are threefold. First, the understanding of how turbulence intensity affects the VAWT's performance. Second, calculating the performance of a wind turbine that is in the wake of another turbine and the study of some particular VAWTs placement configurations. Third, quantifying the limitations of CFD and identifying when it is appropriate to use two-dimensional models for flow simulations of multiple VAWTs. This research has documented an increased performance of about 20% for small turbines in high turbulence intensity flows. Furthermore, a 20% increase in power output from an optimization array of VAWTs was identified. Finally, this work suggests that two-dimensional CFD simulations are adequate for simulation pairs of upstream and downstream turbines if the turbines are low-solidity and low aspect ratio turbine types.

Acknowledgments

I want to express my sincere gratitude to my supervisor, Prof. Marius Paraschivoiu, for his continuous support of my Ph.D. study. Without his motivation, knowledge, insightful comments, encouragement, and challenging questions that triggered several innovative solutions while researching and writing the thesis, this accomplishment would not have occurred.

I am also grateful to my fellow lab-mates for the stimulating discussions and the laughter moments, which decreased the pressure of hard work. I want to thank my friends for expecting nothing less than triumph during my Ph.D. program.

We gratefully acknowledge funding support from Concordia University.

Dedication

To my wonderful family, for their measureless support and unconditional love.
Dedicated to my loving parents.

Contribution of the authors

This thesis is prepared in manuscript-based format. Chapters 1 and 5 are the introduction and conclusion of the thesis, respectively. The rest of the chapters are reprinted from published papers or submitted to scientific journals. The first author of all manuscripts is Mr. Belabes, the author of this thesis and the manuscripts. He has implemented and developed numerical simulations and post-processed the results. He was also responsible for designing, conducting, and interpreting the obtained results. The paper titles, journal names, volume numbers, page numbers, and the contribution of the co-authors will be given in detail as follows.

Chapter 2, entitled "Numerical study of the effect of turbulence intensity on VAWT performance" is published in the Energy Journal, Volume 233, pages 121139, 2021 (https://doi.org/10.1016/j.energy.2021.121139). This work has been co-authored by Prof. Marius Paraschivoiu. Prof. Marius Paraschivoiu is the supervisor of the project.

Chapter 3, entitled "CFD modeling of vertical-axis wind turbine wake interaction" is published in the Journal of Transactions of the Canadian Society for Mechanical Engineering, 00: 1–10 (2023) (https://dx.doi.org/10.1139/tcsme-2022-0149). This work has been co-authored by Prof. Marius Paraschivoiu. Prof. Marius Paraschivoiu is the supervisor of the project.

Chapter 4, entitled "CFD modeling of vertical axis wind turbine wake interaction with a full rotor in the near and far wake" is a submitted paper in the Journal of Energy Resources Technology. This work has been co-authored by Prof. Marius Paraschivoiu. Prof. Marius Paraschivoiu is the supervisor of the project.

Table of Contents

Table of figures ..... **IX**

1 CHAPTER 1. Introduction **1**

1.1 Vertical Axis Wind Turbine 3

1.2 Wind turbine farms 4

1.3 Wake around VAWTs and wind farms 5

1.4 Turbulence intensity definition 6

1.5 Turbulence intensity studies 8

1.5.1 Wind tunnel study 9

1.5.2 Wind data acquisition and treatment 11

1.5.3 CFD treatment 13

1.6 Wind Turbine Simulation Models 14

1.7 Research Objectives 17

1.8 Outline of thesis 18

2 CHAPTER 2. ARTICLE 1: Numerical study of the effect of turbulence intensity on VAWT performance **20**

2.1 Introduction 20

2.2 Wind Turbine Simulation Models 23

2.2.1 Turbine 1: Large Wind Turbine 28

2.2.2 Turbine 2: Small Wind Turbine 29

2.3 Numerical Methodology 30

2.3.1 Mesh topology 33

2.3.2 Wall treatment 35

2.3.3 Mesh independence study 38

2.3.4 Time step independence study 39

2.3.5 Influence of temporal scheme parameters 41

2.3.6 Solver settings 42

2.4 Model validation and analysis 44

2.4.1 Model validation 44

2.4.2 Effect of turbulence intensity 44

2.5 Conclusions 60

3 CHAPTER 3. ARTICLE 2: CFD modeling of Vertical Axis Wind Turbine Wake Interaction 61
3.1 Introduction 61
3.2 Methodology 64
3.2.1 Turbine geometrical and operational characteristics 64
3.2.2 Model set-up 65
3.2.3 Computational domain 66
3.2.4 Mesh 67
3.3 Results and discussion 69
3.3.1 Validation 69
3.3.2 Effect of different configurations 71
3.4 Conclusion 81
4 CHAPTER 4. ARTICLE 3: CFD analysis of vertical axis wind turbine wake-rotor interaction: a comparison between 2 and 3-dimensional modeling 82
4.1 Introduction 82
4.2 Geometric model 87
4.3 Numerical method 89
4.3.1 Turbulence modeling 89
4.3.2 Computational domain 91
4.3.3 Computational grids and time step settings 92
4.3.1 Analysis of the computational domain size 93
4.3.1 2DValidation: comparison with field data 94
4.3.2 Verification: mesh refinement of the wake 98
4.4 Simulation results and analysis 101
4.4.1 Comparison between 2-dimensional and 3-dimensional simulations of the wake . 101
4.4.2 Velocity correction of the 2-Dimensional simulation 104
4.5 Conclusions 108
5 CHAPTER 5: Conclusion and future work 110
5.1 Conclusion 110
5.2 Future works 112
References 113

Table of figures

Figure 1-1: Types and shapes of wind turbines. (Reproduced from ref.[12]). 4

Figure 1-2: The turbulence created by the wind turbines in a wind parc. (from ref. [19]). 6

Figure 1-3: Set-up at the VUB wind tunnel, with turbine and hot-wire to control free flow. (From Molina et al. [24]). 9

Figure 1-4: Turbulence intensity measurement wind tunnel using Turbulence grids. (From Ref.[29]). 10

Figure 1-5: The Power as a function of mean wind cube with mean values and standard deviation for each bin (left), curves divided by TI with mean values for each bin (center). To the right, the TI-divided curves are presented as deviation from mean power f for each bin. Blue: Low TI (< 10%), Red: Medium TI (10% < TI < 15%), Green: High TI (> 15%). (Results from ref. [30]. .. 12

Figure 1-6: Turbulence intensity influence on (Cp) from 10 min mean values (left) and 1 min mean values (right). (Results from ref. [30]. 12

Figure 2-1: A two-bladed Darrieus wind turbine installation of 500kw (From: [63]). 29

Figure 2-2 : Set-up at the VUB wind tunnel, with turbine and hot-wire to control free flow speed [24]. 30

Figure 2-3 : The main dimensions of the computational domains: are (a) 2D and (b) 3D representation. 32

Figure 2-4: The finest mesh for the validation case: (a) Total domain 2D mesh, (b) Rotor sub-grid mesh for the bladed VAWT, (c) Airfoil mesh with 60-step boundary layer extrusion. d) 3D view. 35

Figure 2-5: Y^+ distribution on blade 1 profile for the Large Wind Turbine on the finest mesh. .. 36

Figure 2-6 : Turbulent viscosity ratio near the airfoil at different azimuthal positions, $\lambda = 4.5$ for the large wind turbine. 37

Figure 2-7: Cycle-averaged moment coefficient (Cm) for refining the mesh size. 38

Figure 2-8: Validation of the results against experimental results for the large H-Darrieus VAWT (D=35m). 40

Figure 2-9: Cycle-averaged coefficient of moment (Cm) against various time steps for the large wind turbine. 41

Figure 2-10: Instantaneous moment coefficient for the full 15 turbine revolution for different number of iterations by time step. 43

Figure 2-11: 3D Validation of present computational model for the small H-Darrieus VAWT (D=0.5m). Compared to experimental data [24]. 45

Figure 2-12: Validation of present computational model for the big H-Darrieus VAWT (D=35m). Compared to experimental data [63] and simulation of [62]. 46

Figure 2-13: Power coefficient curves compared against the corrected curve obtained at the CRIACIV wind tunnel, at a Re = 267K, Re = 300K, Re = 333K, and Re = 367K. 48

Figure 2-14: Instantaneous moment coefficient versus azimuth angle for 2 turbine revolutions for one blade and two blades. 50

Figure 2-15: Power coefficient obtained by present simulations against different intensity turbulence levels. 51

Figure 2-16: Power coefficient curves for different turbulent intensities compared against experiment data. 52

Figure 2-17: Instantaneous velocity (a) and pressure (b) contours around the blades for NACA0018-0.5m and NACA0018-35m with turbulence intensity of Iu=14.8 % at θ = 150°. 54

Figure 2-18: Instantaneous vorticity magnitude contours around the blade for NACA0018-0.5m and NACA0018-35m with turbulence intensity of Iu=14.8 % at θ = 150°. (a) Top view of 2 blades, (b) Zoom on one blade. 57

Figure 2-19: Instantaneous vorticity magnitude contours around the blade turbulence intensity of Iu=14.8 % at θ = 168°. (a) NACA0018-0.5m, (b) NACA0018-35m. 58

Figure 2-20: Instantaneous vorticity magnitude contours around the small turbine blade at θ = 168°. (a) Iu=0.07 %, (b) Iu=14.8 %. 59

Figure 3-1: Important characteristics of the large vertical axis wind turbine selected. 65

Figure 3-2: Schematic of computational domain with x and y distance indicated. 66

Figure 3-3: 2-dimensional computational grid for a sample double rotor arrangement. 67

Figure 3-4: Y^+ distribution on all blade profiles for Wind Turbines on the finest mesh. 68

Figure 3-5: Mesh extension according to the evolution of distance. 69

Figure 3-6: Validation of the present computational model [76]. 70

Figure 3-7: The power coefficient against the different positions of turbines 2. **Turbine 2 at Y= -R (Starboard side).** 73

Figure 3-8: Vorticity distribution downstream of the VAWTs for different distances TI=14.8% **(Starboard side).** 74

Figure 3-9: The power coefficient against the different positions of turbines 2. **Turbine 2 at Y=R (Port side).** 75

Figure 3-10: Vorticity distribution downstream of the VAWTs for different distances at TI=14.8% (**Port side**). 76

Figure 3-11: Vorticity contours for an array of 3 turbines (TI=14.8%). 77

Figure 3-12: Velocity Contours for an array of 5 turbines. All Turbines have counter–clockwise directions. 78

Figure 3-13: Moment convergence for wind turbines 1, 2, and 4. 80

Figure 3-14: Vorticity contours for an array of 5 turbines. All Turbines have counter–clockwise directions. 80

Figure 4-1: VAWT 850 installation [63]. 88

Figure 4-2: The Wind turbine installed in Wind tunnel [111]. 88

Figure 4-3: Three VAWTs at experimental wind farm [112]. 88

Figure 4-4: Overall view schematic of the computational domain: **a)** Configuration, (D=1.2m, Ls=10D); **b)** Configuration (D=35m, Ls=2.5D). 92

Figure 4-5: Computational domain of two wind turbines for two configurations. Configuration of (D=35m, Ls=2.5D), and Configuration (D=35m, Ls=10D). 92

Figure 4-6: Computational grid. **a**: 2D Mesh, **b**: 3D Mesh, **c**: Leading-edge boundary layer, **d**: Trailing-edge refinement, **e**: Trailing-edge boundary layer. 93

Figure 4-7: Velocity contours for simulations with a **Small Domain.** 95

Figure 4-8: Velocity contours for simulations with a **Large Domain.** 95

Figure 4-9: Photograph of the VAWT array [14]. 95

Figure 4-10: Sketch of the VAWT array [14]. 95

Figure 4-11: Schematic of the computational domain of 9 double rotor arrangement. 96

Figure 4-12: Computational grid for 9 double rotor arrangement. 96

Figure 4-13: Average mean horizontal flow velocity at rotor mid-height normalized by the inflow velocity. 96

Figure 4-14: Vorticity Contour of the entire wind farm and location of the points where average velocity is collected. 97

Figure 4-15: Velocity Contour of the entire wind farm. 97

Figure 4-16: The Moment coefficient (Cm) convergence for three different meshes. 99

Figure 4-17: Velocity magnitude on line at L=8D. 99

Figure 4-18: The instantaneous Velocity contours for the coarse, medium, and fine mesh after convergence. 100

Figure 4-19: Velocity magnitude at horizontal plan of L=8D. 102

Figure 4-20: Velocity contours at the vertical plane at the middle of the balades for the **3-dimensional** simulations. 103

Figure 4-21: Velocity contours for the **2-dimensional** simulations. 103

Figure 4-22: Velocity magnitude at the horizontal plane of L=8D **Corrected vs. Not-Corrected cases.** 107

Figure 4-23: Velocity contours for the case of the **Corrected** simulation. 108

Figure 4-24: Velocity contours for the case of the **not Corrected** simulation. 108

List of tables

Table 2-1: Main geometrical features of the large wind turbine [62]. 28

Table 2-2: Main geometrical features of the small wind turbine [24]. 29

Table 2-3: Sets of generated mesh for mesh sensitivity study. 39

Table 2-4: Coefficient of moment as a function of Time step for the large wind turbine. 40

Table 2-5: The main parameters used in 2D and 3D simulations. 41

Table 2-6: Influence of different parameter on Time step. 42

Table 3-1: A summary of the research on Darrieus VAWT farms. 63

Table 3-2: Geometrical and operation characteristics of the turbines [63]. 65

Table 3-3: Cycle-averaged moment coefficient (Cm) for refining the mesh size. 68

Table 3-4: Mesh detail for each distance case. 69

Table 3-5: Comparison between 2D and 3D simulations. 71

Table 3-6: The power coefficient (Cp) against the different positions of turbines. (3 Turbines). 77

Table 3-7: The power coefficient against the different positions of turbines. (5 Turbines) 79

Table 4-1: Geometrical and operation characteristics of the selected VAWT. 88

Table 4-2: Turbulence model and Solver settings. 90

Table 4-3 : Comparison between small and large domain for different wind turbines sizes..... 94

Table 4-4: The power coefficient obtained by the three different meshes. 98

Table 4-5: The power coefficient (Cp) for Wind turbine diameter **D=35m**. 103

Table 4-6: The power coefficient (Cp) for Wind turbines diameter **D=1.2m** and **D=0.5m**. 104

Table 4-7: Comparison between the calculated and the corrected power coefficients with different distances for the large wind turbine. 106

Table 4-8: Comparison between the calculated and the corrected power coefficients with different distances for the small wind turbine. 107

1 CHAPTER 1. Introduction

Wind energy is a clean, renewable, and widely available source of power that can help reduce greenhouse gas emissions and dependence on fossil fuels. Many countries are investing heavily in wind energy to meet their growing energy needs. Canada is one of the world leaders in wind power production, with an installed capacity of 12,400 MW in 2017 according to Afsharian et al. [1]. At the end of December 2021, the wind power generating capacity increased to 14,300 MW which is about 5.5% of the total Canadian electricity demand. The Canadian Wind Energy Association (CanWEA) has recently released a new vision for wind energy in Canada by 2025. The publication highlights the positive outcomes of wind energy, including job creation and environmental impact reduction. It also emphasizes that Canada's electricity system has the capacity to incorporate a significant amount of wind energy, with the goal of obtaining 20% of Canada's electricity from wind power by 2025. Achieving this target would necessitate the installation of 22,000 wind turbines across 450 locations as mentioned by Brahimi et al. [2] and in CanWEA [3]. Wind energy is also one of the most environmentally friendly forms of electricity generation.

The most common type of wind turbine used for generating electricity is the Horizontal Axis Wind Turbine (HAWT), nevertheless, Vertical Axis Wind Turbines (VAWTs) have several benefits that make them superior to HAWT in many aspects. VAWTs can capture wind from any direction, reduce noise and visual pollution, and lower maintenance and installation costs. For these reasons, there has been a recent shift in wind turbine research toward vertical-axis wind turbines. The development and limitations of large vertical axis wind turbines (VAWTs) are impacted by the scale effect, with the Reynolds number being a significant factor in distinguishing between small and large-scale turbines. In this sense, a dimensionless analysis was initially conducted, revealing that scaling the entire wind turbine primarily changes the Reynolds number while keeping another key factor constant. Building upon this understanding, a univariate analysis was performed by Gaohua et al. [4] to explore the impact of Reynolds number variation, resulting from scaling effects, on the aerodynamic performance of VAWTs. This study employed a simplified single-bladed VAWT model, subjected to a series of high-resolution numerical simulations. By scaling the model size directly, the operating Reynolds number of the wind turbine was varied within the range of 1×10^4 to 5×10^6, maintaining specific solidity and reduced

frequency. The analysis demonstrated that, across the investigated Reynolds number range, an increase in the wind turbine model size led to reduced flow separation near the blade, a weaker dynamic stall vortex, and a general tendency of increasing power coefficient for wind energy extraction. These findings suggest that larger-scale wind turbines generally offer improved aerodynamic performance. Specifically, within a Reynolds number range of 5×10^4 to 5×10^5, the power coefficient exhibited a significant increase with the size of the wind turbine. However, in the range of 5×10^5 to 5×10^6, the power coefficient continued to rise, albeit with a decreasing rate of increment.

Regarding the manufacturing of VAWT blades, Suresh et al. [5] focus on the design and analysis of two airfoil profiles, namely NACA 0012 and NACA 0018. The structural stability, specifically the deformation of Aluminum blades, under varying wind speeds during the energy conversion process is investigated. The developed airfoil models exhibit remarkable structural stability, even under high-pressure conditions, with minimal deformation, stress, and strain. The velocity and pressure distributions at different wind speeds (3 m/s, 5 m/s, and 10 m/s) are analyzed. The results indicate that the turbine blades maintain uniform rotation even in turbulent flow conditions. The analysis of the developed models demonstrates a good agreement in predicting torque and power outputs. Therefore, the findings suggest that these models can be practically implemented and joined using Friction Stir Processing. This research paves the way for the effective utilization of VAWTs with the studied airfoil profiles, contributing to the advancement of wind energy conversion technologies.

Gerrie et al. [6] focus on analyzing the performance of a small-scale hybrid vertical-axis wind turbine capable of transitioning between different turbine types by adjusting the blade orientation. The analysis utilizes 3D computational fluid dynamics (CFD), complemented by wind tunnel experiments to validate the findings. Various design parameters, including blade length, diameter, and number of blades, were varied during the analysis to explore potential areas for improvement in the turbine's design. The results demonstrate that the current design of the turbine achieves optimal efficiency of 12.5%.

Considering urban environments, the wind has several characteristics that make its harvest more complicated; knowing that the conglomerate of buildings that shape the cities increases the terrain roughness length, shifting the atmospheric boundary layer upwards. This wind presents very high levels of turbulence as found by Janajreh et al. [7] and in some locations, the wind

turbines would receive incident wind with considerable skew angles as confirmed by Balduzzi et al. [8]. According to these complications, the true suitability of wind turbines for use in the urban environment is not yet proven. Bianchi et al. [9] and Bianchini et al. [10] declare that most of the past wind installations failed to reach the expected energy yield, resulting in underperforming turbines and bad press for the technology. A careful analysis of wind turbine conditions is therefore mandatory for this technology to reach its maturity and economic viability in an acceptable time horizon.

1.1 Vertical Axis Wind Turbine

Wind turbines can be classified according to their axis of rotation. Thus, there are two types of wind turbines: horizontal axis wind turbines (HAWT or Horizontal Axis Wind Turbines) and Vertical axis wind turbines (VAWT Vertical Axis Wind Turbines) as shown in Figure 2. A VAWT wind turbine is a wind turbine whose main rotor is perpendicular to the direction of the wind speed; the generator is placed close to the ground, which makes maintenance and repairs easy compared to HAWT wind turbines.

Most wind turbines currently installed on is horizontal axis. However, there are some important advantages of vertical axis turbines that they are applied in urban areas. In addition to ease of maintenance, VAWT wind turbines offer several advantages, the most important of which is that they can be placed next to each other. Therefore, less space is occupied compared to HAWT wind turbines. Besides, less noise is produced, and the starting wind speed is much lower than that of HAWT wind turbines.

Generally, HAWT wind turbines perform better when the wind varies little, but their performance becomes less when the wind direction fluctuates; in contrast, VAWT wind turbines work for any direction, non-uniformity, or even rapid fluctuations in the wind, as concluded by Eriksson et al. [11]. A vertical axis wind turbine (VAWT) has blades mounted on the top of the main shaft structure, rather than in the front like an aircraft rotor. Despite the VAWTs being less often used than their horizontal counterparts, VAWTs are more practical in urban areas. There are two common designs including a turbine that resembles two halves of the drum, each mounted to the rotating element (Savonius rotor), and a smaller model that looks somewhat like an eggbeater (Darrieus model) as shown in Figure 1-1. The vertical axis wind turbines let the wind in through a

hub to turn a generator; the turbine spins via rotational momentum when air passes through the blades.

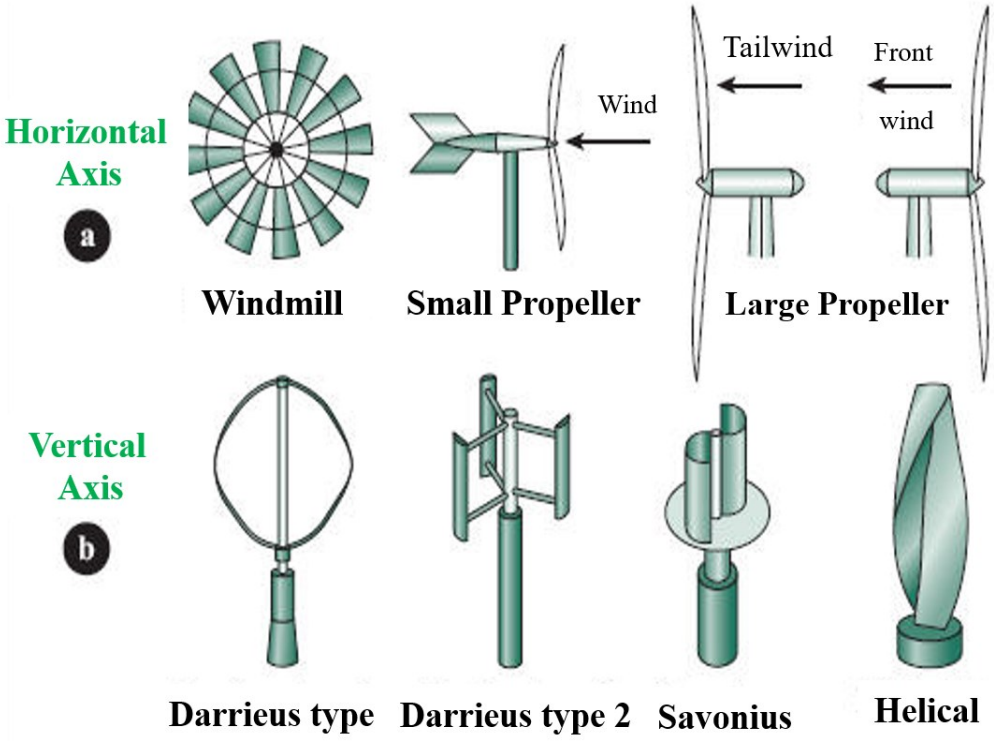

Figure 1-1: Types and shapes of wind turbines. (Reproduced from ref. [12]).

New concepts that combine both Savonius and Darrieus turbines have also been proposed. Gerrie et al. [6] proposed a small-scale hybrid vertical-axis wind turbine capable of transitioning between a Savonius and a Darrieus turbine by adjusting the blade orientation. An analysis based on 3D computational fluid dynamics (CFD) and complemented by wind tunnel experiments, nevertheless showed a very low performance.

1.2 Wind turbine farms

One of the drawbacks of HAWTs is that they need significant land space to avoid interference from the wakes of neighboring and upstream turbines. This reduces the power density of HAWT farms, which is the amount of power that can be harvested from a given area. A common solution is to build taller HAWTs that can capture stronger winds at higher altitudes, but this also increases the costs and impacts of wind energy on the environment, aesthetics, noise, and radar. Therefore, researchers are exploring the use of VAWTs, in particular dual turbines that rotate in

opposite directions to each other, which can increase the power density of wind farms by allowing more turbines to be packed in a smaller area.

A number of studies on VAWTs have shown the importance of spacing between the turbines (as well as the array configuration) to minimize wake loss. Recent studies on a closely spaced array of VAWTs by Dabiri and his team [13]–[16] have shown the possibility of achieving a much higher power density (i.e., power per unit farm area) compared to existing wind farms employing HAWTs. During their field measurements in Southern California in 2010 and 2011, Dabiri and his team [13]–[16]tested various configurations of pairs of counterrotating VAWTs closely spaced from each other, inspired by the hydrodynamic mechanism of "fish schooling" minimizing the wake loss. The performance of pairs of counter-rotating VAWTs has also been investigated numerically by Feng et al. [17] using a free vortex method with empirical wake models. More recently, Araya et al. [18] have proposed a low-order model of two-dimensional flow past pairs of VAWTs using the concept of a leaky Rankine body, showing the existence of two competing fluid dynamic mechanisms (namely the local acceleration of the flow and local deceleration of the flow) that contribute to the overall array performance.

1.3 Wake around VAWTs and wind farms

The wake effect plays a crucial role in the performance and efficiency of vertical axis wind turbines (VAWTs) and wind farms. As the wind interacts with the rotating blades, it creates a wake region behind the turbine. This wake consists of turbulent airflow characterized by reduced wind speeds and increased turbulence intensity. The wake effect becomes even more significant in wind farms, where multiple turbines are closely spaced. Understanding and managing the wake effect is essential for optimizing wind turbine placement and overall wind farm efficiency. The wake not only affects the performance of downstream turbines but also influences the fatigue loads experienced by the turbine structures. It is necessary to design wind farms with sufficient spacing between turbines to minimize wake interactions and maximize energy capture.

Researchers employ various methods, including computational modeling and field measurements, to study the wake behavior around VAWTs and wind farms. Advanced computational fluid dynamics (CFD) simulations help analyze the wake dynamics and provide insights into the flow patterns, turbulence characteristics, and wake recovery. Additionally, field

measurements using LiDAR (Light Detection and Ranging) and other instruments enable researchers to validate the CFD models and observe the wake behavior in real-world conditions.

Efforts are ongoing to develop wake control strategies to mitigate the negative effects of the wake, such as wake redirection or turbine wake steering. By redirecting or steering the wake away from downstream turbines, it is possible to reduce wake losses and enhance the overall energy production of the wind farm. Understanding the complex wake dynamics around VAWTs and wind farms is vital for improving their performance, increasing energy capture, and optimizing the layout and operation of wind energy systems in order to make wind power a more efficient and sustainable source of renewable energy. Figure 1-2 shows the wake generated during the rotation of the turbines of the wind farm and its direction.

Figure 1-2: The turbulence created by the wind turbines in a wind parc. (from ref. [19]).

1.4 Turbulence intensity definition

Turbulence is an important process in most fluid flows and contributes significantly to the transport of momentum, heat, and mass. Turbulence also plays a role in the generation of fluid friction losses and fluid-induced noise. In order to understand the behavior of fluid flows and in order to design and evaluate wind turbines, the airfoil of the aircraft, the Turbo reactor... To study the influence of turbulence on the performance of the wind turbines, it is necessary to measure the

turbulence intensity (TI), which it can be obtained using a cup anemometer normally used for measuring wind speed. Turbulence intensity is a measure of the wind turbulence and thus also the tendency of the wind to alter speed. The turbulence intensity (TI) is defined by the ratio of the vector norm of the fluctuating part (u') and the average of the mean velocity (U), as defined in equations (1-1), (1-2), and (1-3), respectively:

$$TI = \frac{u'}{U} \tag{1-1}$$

$$u' = \sqrt{\frac{1}{3}({u'_x}^2 + {u'_y}^2 + {u'_z}^2)} \tag{1-2}$$

$$U = \sqrt{(\bar{u}_x^2 + \bar{u}_{y+}^2 \bar{u}_z^2)} \tag{1-3}$$

where $\bar{u}_x$; $\bar{u}_y$ and $\bar{u}_z$ are the wind speed along the x-axis; y-axis; $\bar{u}_z$ and z-axis.

In view of the importance of analyzing turbulence, several studies have been carried out in this area. These studies are performed using suitable instruments such as hot wire anemometers (often called CTA or constant temperature anemometers with reference to the operating principle) or laser-Doppler anemometers (LDA) and more recently with velocimetry by imaging of particles (PIV). Generally, the data analysis obtained by these measurements is done using computer modeling (Programming like MATLAB, FORTRAN ... etc.). For this kind of measurement in order to have more accurate results, the time period used should be longer than the turbulent fluctuations, but shorter than the periods associated with long-term wind speed variations such as daytime effects, as revealed by Manwell et al. [20].

Usually, the specialists use a cup anemometer to measure the intensity of the turbulence. Therefore, using this device the total horizontal wind speed is measured. In order to calculate the mean kinetic energy (TKE) per unit of the mass associated with vortices in turbulent flow, a more precise quantity is needed to estimate the energy content of velocity fluctuations in a volume of air. The mean kinetic energy derives from the separate standard deviations of the x, y, and z directions, assuming isotropic turbulence as well as using a definition where TI derives from the mean velocity fluctuation of the three directions (as commonly used in CFD), it may be related to TI depending on Versteeg et al. [21]:

$$TKE = \frac{1}{2}\left(v'^2_{v_x} + v'^2_{v_y} + v'^2_{v_z}\right) = \frac{3}{2}(TI\bar{v})^2 \quad (1\text{-}4)$$

Measuring turbulence intensity with a cup anemometer may be problematic, as noted by Yahaya et al. [22]. For example, mainly the horizontal turbulence is accounted for as the vertical turbulence will have a small influence on the horizontal wind speed. Wharton et al. [23] confirm that is also generally the case that high TI is accompanied by convective atmospheric conditions and low wind shear. Wind shear affects power production since the mean wind speed varies within the rotor area, affecting the relation between the measured hub height wind speed and the effective mean wind speed for the rotor area. Using more advanced equipment such as a sonic detection and ranging (SODAR) or light detection and ranging (LIDAR) apparatus, the wind speed can be tracked over the entire height of the rotor and all components of the turbulence can be measured, thus eliminating uncertainties from vertical turbulence and atmospheric conditions. However, cup anemometers are commonly used for measuring TI and while the TI values may be underestimated, the cup anemometer measurements do seem to correctly track changes in turbulence level as found by Yahaya et al. [22], and Wharton et al. [23].

1.5 Turbulence intensity studies

The implementation of small vertical-axis wind turbines in urban environments is being studied by the scientific community to complement large wind farms in wind energy generation. The technology is, however, far from maturity due to the complexity of urban flows and the lack of knowledge in the field, as stated by Molina et al. [24] because the impact of turbulence intensity on the performance of the VAWTs is not fully understood. In the literature, various methods have been used to predict the performance of VAWTs, such as which experimentally using wind tunnels or data logger measurement and numerically using the Computational Fluid Dynamics (CFD) analysis method.

The high turbulence of the flow needs to be considered as it is a main feature of the flow in this environment. This turbulence is not only composed of high turbulence intensity but also of large velocity fluctuations with large vertical components due to the existence of buildings. Challenges related to rapidly changing wind direction in urban areas have been investigated by Battisti et al. [25] and, Anup et al. [26] and show that these large variations in the wind affect negatively the performance of all types of wind turbines.

Recent work on vertical-axis wind turbines (VAWT) indicates that the performance of this type of turbine increases with higher turbulent intensity for a homogeneous isotropic turbulent flow and maybe a better alternative to conventional horizontal-axis wind turbines (HAWT) in urban applications as found by Drew et al. [27] and, Balduzzi et al. [28].

1.5.1 Wind tunnel study

There are not many reports related to the effect of the turbulence intensity of the external flow on the wake behind a wind turbine generated in the wind tunnel. The concept is to obtain basic data to estimate wind turbine interference in wind farms like the wake generated and its influence on each other. The measurements of the velocity field, also the pressure in the wake are to be performed for different turbulence intensities in the main flow in a wind tunnel. The wind tunnel has a long open test section where the wind turbine is placed in the center as shown in Figure 1-3.

Figure 1-3: Set-up at the VUB wind tunnel, with turbine and hot-wire to control free flow. (From Molina et al. [24]).

The coordinate system is defined for the measurements, in which the x-axis, the y-axis, and the z-axis are set in the streamwise, lateral, and vertical directions, respectively. The origin is taken at the center of the wind turbine rotor. The wind profile in the wake is measured by using an I-type hot wire probe attached to a positioning device as shown in Figure 1-3.

In order to change the turbulence intensity, two turbulence grids that have different blockage ratios are applied. Figure 1-4 shows the setting positions and photographs of these grids. As shown in Figure 1-4(a), the coarse grid was set at the honeycomb section of the wind tunnel. Turbulent flows without the grid, with the coarse one, and with the coarse and fine ones were

described as “Low turbulence”, “Medium turbulence” and “High turbulence” respectively, in increasing order of averaged turbulence intensity as revealed by Maeda et al. [29].

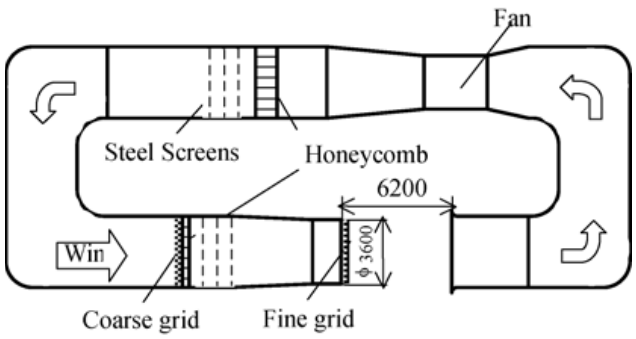

(a) Attachment positions of grids (Top view).

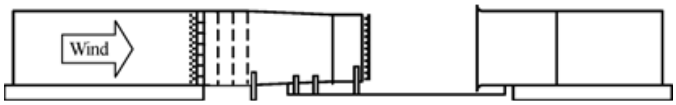

(b) Attachment positions of grids (Side view).

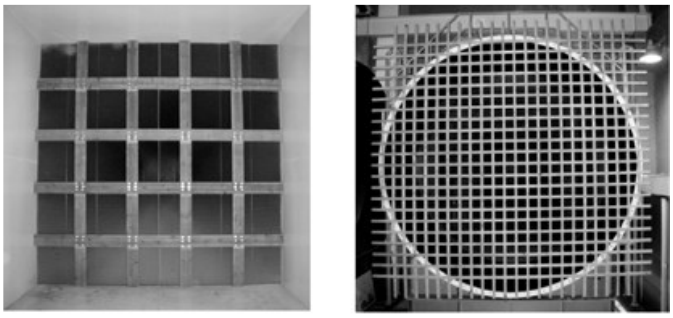

(c) Photographes of grids.

Figure 1-4: Turbulence intensity measurement wind tunnel using Turbulence grids. (From Ref. [29]).

In this paper, using the wind tunnel, the averaged wind profile and turbulence intensity profile in the wake is studied, when the turbulence intensity of the external wind was changed. This case study is like the influence of the wake in the horizontal wind turbine arrangement in a wind farm. A wind tunnel experiment is performed with a 500 mm-diameter wind turbine and the wind velocity in the wake. The objective is to take maximum advantage of the wind and to install many wind turbines. The wake is measured by an I-type hot wire probe. As a result, it is clarified

that high turbulence intensities enable to the entrainment of the main flow and the wake and to recover quickly the velocity in the wake as concluded by Maeda et al. [29].

1.5.2 Wind data acquisition and treatment

In this method; to quantify the Power performance of a wind turbine, the energy-production measurements of wind turbines are adopted. This implies using the recorded mean wind speed over a period of 10 min on the site when analyzing the relation between wind speed and performance. The hourly or daily average data for wind speed and direction, for one year or several years, to be measured.

To investigate the relationship between turbulence and performance of the wind turbines, several approaches are adopted. One of the important approaches is to compare the power coefficient Cp of the wind turbine to the turbulence intensity TI of the wind while eliminating the effect of the cubic factor. This way, the relations can be attributed to the actual behavior of the wind turbine, rather than the power of the wind that changes with the wind cube. The average wind energy flux, which is proportional to ($\overline{v^3}$) and represents the total amount of kinetic wind that passes a unit cross-section area per unit of time, is used to obtain an equivalent wind speed that considers both wind speed and wind shear as suggested by Möllerström [30], The wind energy flux for a given time period is the same as the mean wind cube as confirmed by Wagner, et al. [31] it is calculated from the mean wind and turbulence intensity of that period as shown in Figure 1-5. For example, the data is logged at a high enough frequency, so the mean wind cube can with the same result be retrieved from averaging the wind cube values. Therefore, the mean wind cube is used instead of the mean wind speed when calculating the aerodynamic power coefficient $\widetilde{C_p}$, the mean wind cube $\overline{v^3}$ and $\widetilde{C_p}$ is obtained as:

$$\overline{v^3} = \frac{1}{N}\sum_{i=1}^{N} v_i^3 \tag{1-5}$$

$$\widetilde{C_p} = \frac{\overline{P_{aero}}}{0.5\rho A\overline{v^3}} \tag{1-6}$$

When using a power wind speed relation, i.e. a power curve, to study how TI affects the turbine's energy extraction, it is also preferable to use $\overline{v^3}$ rather than $\bar{v}$. This is again because the

mean wind cube is directly proportional to the power of the wind, thus enabling the displaying of differences between different TIs without the cubic effect interfering.

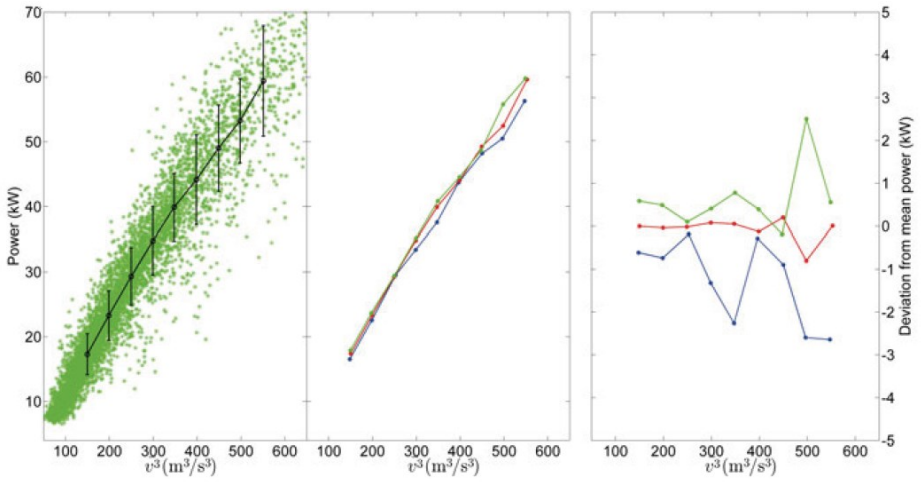

Figure 1-5: The Power as a function of mean wind cube with mean values and standard deviation for each bin (left), curves divided by TI with mean values for each bin (center). To the right, the TI-divided curves are presented as deviation from mean power f for each bin. Blue: Low TI (< 10%), Red: Medium TI (10% < TI < 15%), Green: High TI (> 15%). (Results from ref. [30].

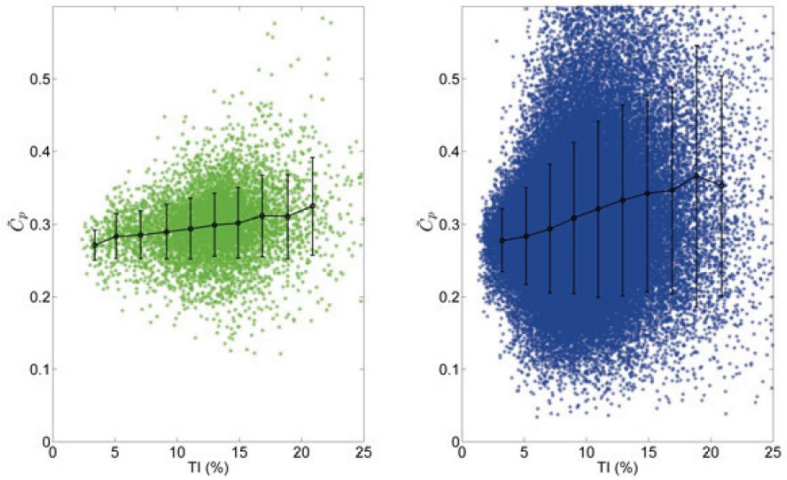

Figure 1-6: Turbulence intensity influence on (Cp) from 10 min mean values (left) and 1 min mean values (right). (Results from ref. [30].

Figure 1-5 and Figure 1-6 present the results that can be extracted by the method of wind Data acquisition and treatment. The presence of turbulent flow in cities with complex urban structures poses challenges to the effective utilization of distributed wind energy. Liu et al. [32] focus on analyzing turbulence intensity (TI), a crucial factor in wind turbine design and wind power evaluation. High-frequency observations were conducted on a 325-meter tower situated in

downtown Beijing, China. The results demonstrate significant differences in TI characteristics compared to higher heights. Diurnal variations, statistical distributions, and the relationship between TI and near-ground wind speeds exhibit distinct patterns. Furthermore, it is observed that the currently recommended parameters for the Normalized Turbulence Model (NTM) according to the International Electrotechnical Commission (IEC) standard do not fit the data well. As a result, new NTM parameters are determined through a least-square fitting approach. Additionally, a three-parameter model is identified as a good fit for the data and performs slightly better than the NTM with the least-square fitting parameters. These findings highlight the need for re-evaluating the NTM parameters specified in the IEC standard for urban areas.

1.5.3 CFD treatment

To analyze the performance of the VAWTs, we need to predict their performance characteristics and understand the flow field around them. One of the reliable and accurate methods for this is Computational Fluid Dynamics (CFD) analysis as Jin et al. [33] mentioned. CFD calculations can reveal the details of the flow that can help us comprehend the VAWTs better. However, two-dimensional CFD analyses have limitations in accuracy, as they neglect the three-dimensional effects such as tip vortices and struts. Many researchers like, Lanzafame et al. [34], Mohamed et al. [35], Danao et al. [36], Xiao, et al. [37], and Armstrong et al. [38] have used CFD modeling to study VAWTs]. For example, Lanzafame et al. [34] modeled and simulated an H-type Darrieus VAWT using ANSYS Fluent solver and found good agreement with experimental data. They also showed that the transition SST turbulence model can capture the flow behavior of wind around small-scale turbines.

Several studies of the turbulence intensity effect on the VAWT are performed, such as Lam et al. [39] studied the wakes velocity field and turbulence field from 1 to 10 turbine diameters (1D to 10D) downstream, using a low-solidity two-straight-bladed of the vertical axis wind turbine. In this study, both the transition shear stress transport (SST) and the detached eddy simulation (DES) models were used to close the unsteady Reynolds-averaged Navier-Stokes (URANS) equations. It defines the regions of the near and far wakes based on the occurrence of the maximum velocity deficit, where the velocity in the near wake suffered a drastic deficit of about 85%, however, in the far wake major velocity recovery occurred with the average stream-wise velocity reaching approximately 75% at 10D.

More details on how to study the influence of the turbulence intensity on the vertical axis wind turbine wind in the next section.

1.6 Wind Turbine Simulation Models

The common parameters in the field of wind turbines are reviewed. The power available from the wind for a cross-section area (A_s) is given by:

$$P_{wind} = 0.5\,\rho\,A_s U^3 \tag{1-7}$$

where ρ is the density of the air and U is the wind speed.

For an H-type vertical axis wind turbine, the swept area (A_s) is a rectangle, calculated as the turbine diameter multiplied by the blade length. The power coefficient is a measure of the wind turbine's ability to convert wind energy to mechanical energy which is defined as:

$$Cp = \frac{P_{wind\ turbine}}{P_{wind}} \tag{1-8}$$

where $P_{wind\ turbine}$ is the aerodynamic power output.

The power coefficient depends on the tip speed ratio TSR or λ, which is the ratio between the velocity of the blade and the wind speed, thus calculated as:

$$\lambda = \frac{\omega R}{U} \tag{1-9}$$

where ω is the angular velocity of the turbine and R is the turbine radius.

The Navier-Stokes equations in the case of the system rotate at the fixed angular velocity written as follows:

$$\rho\frac{D\vec{v}}{Dt} = -\nabla p + \mu\nabla^2\vec{v} - \rho[2\omega \times W + \omega \times \omega \times r] \tag{1-10}$$

where $\vec{v}$ is the velocity vector, $W = \sqrt{V_c^2 + V_n^2}$, which: *Vc, Vn* are the Chord and vertical component of the velocity respectively.

The term $2\omega \times W$ is the Coriolis acceleration, and the term $\omega \times \omega \times r$ is centrifugal acceleration. As can be seen, the associated terms with Coriolis acceleration and centrifugal acceleration due to the rotation of the system are added to Navier-Stokes equations.

In the vertical axis wind turbine fields, the wind passing through the wind turbine is considered an inertial system. In this case, the continuity equation and momentum conservation are included, and defined below:

$$\nabla . \vec{v} = 0 \tag{1-11}$$

$$\rho \left(\frac{D\vec{v}}{Dt} \right) = -\nabla p + \nabla . \tau \tag{1-12}$$

And the SST k–ω turbulence model was developed by Menter [40] as follows:
Transport equations of k:

$$\frac{\partial}{\partial t}(\rho k) + \frac{\partial}{\partial x_i}(\rho k u_i) = \frac{\partial}{\partial x_i}\left(\Gamma_k \frac{\partial k}{\partial x_j} \right) + G_k - Y_k + S_k + G_b \tag{1-13}$$

and transport equations of ω:

$$\frac{\partial}{\partial t}(\rho \omega) + \frac{\partial}{\partial x_i}(\rho \omega u_i) = \frac{\partial}{\partial x_i}\left(\Gamma_\omega \frac{\partial \omega}{\partial x_j} \right) + G_\omega - Y_\omega + S_\omega + G_{\omega b} \tag{1-14}$$

where ρ is the fluid density, p is the mean pressure, $\Gamma_U, \Gamma_k, and\ \Gamma_\omega$ are the effective diffusivities of the mean fluid speed U (V or W), turbulence kinetic energy k, and specific dissipation rate ω, respectively, which are expressed as:

$$\Gamma_U = \mu + \mu_t \tag{1-15}$$

$$\Gamma_k = \mu + \frac{\mu_t}{\sigma_k} \tag{1-16}$$

$$\Gamma_\omega = \mu + \frac{\mu_t}{\sigma_\omega} \tag{1-17}$$

and μ_t is the turbulent viscosity, which is defined as follows:

$$\mu_t = \frac{\rho k}{\omega} \frac{1}{max\left[\frac{1}{\alpha^*}, \frac{SF_2}{\alpha_1 \omega} \right]} \tag{1-18}$$

In these equations:

G_k represents the generation of turbulence kinetic energy due to mean velocity gradients.

G_ω represents the generation of ω.

$Y_k \; and \; Y_\omega$ represent the effective diffusivity of k and ω due to turbulence.

All the above terms are calculated as described below.

$S_k \; and \; S_\omega$ are user-defined source terms.

$G_b \; and \; G_{\omega b}$ account for buoyancy terms as described in Effects of Buoyancy on Turbulence in the k-ω models.

While the original model formulation has largely stayed unchanged from the formulation given by Menter [40], there have been several areas of improvement carried out within the small modifications of the SST Model, the complete formulation of the SST model is given, with the limited number of modifications given by Menter [41]:

$$\frac{\partial(\rho k)}{\partial t} + \frac{\partial(\rho U_i k)}{\partial x_i} = \tilde{P}_k - \beta^* \rho k \omega + \frac{\partial}{\partial x_i}\left[(\mu + \sigma_k \mu_t)\frac{\partial k}{\partial x_i}\right] \tag{1-19}$$

$$\frac{\partial(\rho \omega)}{\partial t} + \frac{\partial(\rho U_i \omega)}{\partial x_i} = \alpha \rho S^2 - \beta \rho \omega^2 + \frac{\partial}{\partial x_i}\left[(\mu + \sigma_\omega \mu_t)\frac{\partial \omega}{\partial x_i}\right] + 2(1 - F_1)\rho \sigma_{w2}\frac{1}{\omega}\frac{\partial k}{\partial x_i}\frac{\partial \omega}{\partial x_i} \tag{1-20}$$

where the blending function F1 is defined by:

$$F_1 = tanh\left\{\left\{min\left[max\left(\frac{\sqrt{K}}{\beta^* \omega y}, \frac{500v}{y^2 \omega}\right), \frac{4\rho \sigma_{\omega 2} k}{CD_{k\omega} y^2}\right]\right\}^4\right\} \tag{1-21}$$

with $CD_{k\omega} = max\left(2\rho\sigma_{\omega 2}\frac{1}{\omega}\frac{\partial k}{\partial x_i}\frac{\partial \omega}{\partial x_i}, 10^{-10}\right)$ and y is the distance to the nearest wall.

F1 is equal to zero away from the surface (k-ε model) and switches over to one inside the boundary layer (k-ω model).

The turbulent eddy viscosity is defined as follows:

$$v_t = \frac{a_1 k}{max(a_1 \omega, SF_2)} \tag{1-22}$$

where S is the invariant measure of the strain rate and F_2 is a second blending function defined by:

$$F_2 = tanh\left[\left[max\left(\frac{2\sqrt{k}}{\beta^* \omega y}, \frac{500v}{y^2 \omega}\right)\right]^2\right] \quad (1\text{-}23)$$

A production limiter is used in the SST model to prevent the build-up of turbulence in stagnation regions:

$$P_k = \mu_t \frac{\partial U_i}{\partial x_j}\left(\frac{\partial U_i}{\partial x_j} + \frac{\partial U_j}{\partial x_i}\right) \rightarrow \tilde{P}_k = \min(P_k, 10.\beta^* \rho k \omega) \quad (1\text{-}24)$$

All constants are computed by a blend from the corresponding constants of the k-ε and the k-ω model via:

$\alpha = \alpha 1F + \alpha 2\ (1 - F)$

The constants for this model are: $\beta^* = 0.09$, $\alpha_1 = \frac{5}{9}$, $\beta_1 = \frac{3}{4}$, $\sigma_{k1} = 0.85$, $\sigma_{k\omega 1} = 0.5$, $\alpha_2 = 0.44$ $\beta_2 = 0.0828$, $\sigma_{k2} = 1$, $\sigma_{k\omega 2} = 0.856$.

The only modifications from the original formulation are the use of the strain rate S, instead of the vorticity in equation (1-21) and the use of the factor 10 in the production limiter, instead of equation (1-20) as proposed by Menter [42].

In this work, a Reynold number based on the turbine diameter is used:

$$Re = \frac{\rho U D}{\mu} \quad (1\text{-}25)$$

where ρ is the air density and μ the air dynamic viscosity.

1.7 Research Objectives

This work conducts a comprehensive computational analysis of VAWT performance in the presence of turbine wakes and more generally in a turbulent flow. The goal is to identify and quantify the parameters that affect the performance of vertical axis wind turbines operating in non-uniform flows such as in the wake of another turbine or in urban environments where the turbulence intensity is high.

To do so, a combination of numerical investigations is needed. The following has been performed to achieve this objective:

1. Implement and validate efficient CFD methodology to simulate the flow around different sizes of VAWTs and resulting wake;
2. Investigating and understanding the interaction of VAWT with turbulent flow;
3. Investigating and understanding the interaction between VAWTs in close proximity to each other to harvest the maximum energy from the wind;
4. Test and implement a new methodology capturing the interaction of the wake with a VAWT.

This work aims to enhance the understanding of the turbulence intensity effect on the performance of a VAWT and the wake effect on the performance of a VAWT. The impact of this work is to offer knowledge and a CFD methodology that can be used toward the optimal placement of vertical axis wind turbines to maximize the power coefficient output of a wind farm.

1.8 Outline of thesis

This thesis is organized in a paper-based format which presents a Numerical study of VAWT performance behind turbine wakes. The intrinsic behavior of a wake is investigated through numerical studies that are validated with other experimental data. In addition, several numerical models are developed to simulate different types of wind turbines, with different sizes with the aim of improving their performance.

Chapter 1 provides an overview of the Vertical Axis Wind Turbine, a type of wind energy device that rotates around a vertical axis. The concepts of wake and turbulence intensity, which are important for understanding the interaction between upstream and downstream wind turbines, are introduced and explained. The chapter also reviews the existing literature on the wake effects and interactions among multiple vertical wind turbines in an array configuration. Finally, the chapter describes the research methodology and approach used to investigate the wake characteristics and optimization of vertical wind turbine arrays.

Chapter 2 demonstrates how CFD can accurately simulate the effect of flow turbulence intensity on the performance of vertical-axis wind turbines (VAWT). The CFD analysis covers two and three-dimensional cases for different straight-bladed Darrieus-type rotors. The rotors have NACA0018 blades and diameters of 0.5 m and 35 m, representing a small and a large H-Darrieus VAWT respectively. The computational results from a commercial CFD code (Star CCM+) are

validated against experimental measurements. The simulations are based on full URANS calculations with different settings. The settings studied include time step, number of iterations per time step, and discretization schemes. The chapter also investigates the effect of turbulence intensity on the VAWT performance and compares it with experimental data. The results show how the turbulence intensity affects the VAWT behavior in different ways.

The aim of Chapter 3 is to explore how different turbine arrangements can affect the power generation of VAWT farms, using two-dimensional CFD models based on the Star CCM+ package. The focus is on very large turbines, which have higher performance and power coefficients than small turbines. The CFD models can accurately simulate the behavior of wind turbines in farms with multiple VAWTs. The results show that the wake effect is significant when a second rotor is placed less than 10 turbine diameters downstream of the first rotor. Moreover, a specific farm configuration with five VAWTs is examined and demonstrates a 20% increase in power output compared with the same number of isolated turbines.

In Chapter 4, the wake of a two-straight-bladed vertical axis wind turbine (VAWT) with three different sizes is analyzed both to understand the flow but also to evaluate if the two-dimensional modeling provides useful and accurate information of the performance of the second turbines in comparison to the full three-dimensional CFD simulations. The near and far wake velocity fields and turbulence fields at 2.5 and 10 turbine diameters (2.5D to 10D) between the two turbines downstream of each other are investigated. Both the transition shear stress transport (SST) and the unsteady Reynolds-averaged Navier-Stokes (URANS) models were used. The CFD models were validated with wind tunnel tests and field measurement results from the literature. Grid independence verification was performed for specifically the wake using a coarse, medium, and fine mesh between the two turbines. A flow velocity correction is analyzed for the two-dimensional numerical model to evaluate this method for the performance evaluation of a downstream turbine. The near and far wakes are analysed for three types of wind turbines ranging from 0.5 m to 35 m turbine rotor diameters.

Finally, in Chapter 6, a summary of the findings and recommendations for future research are provided.

2 CHAPTER 2. ARTICLE 1: Numerical study of the effect of turbulence intensity on VAWT performance

The content of this chapter has been published as a peer-reviewed paper:
BELABES, Belkacem et PARASCHIVOIU, Marius. Numerical study of the effect of turbulence intensity on VAWT performance. Energy, 2021, vol. 233, p. 121139.

Abstract:

This paper demonstrates the capability of CFD to accurately simulate the effect of the flow turbulence intensity on the performance of vertical-axis wind turbines (VAWT). This effect is quite important as it increases the performance of small VAWTs. For this study, two and three-dimensional CFD analysis has been performed on different straight-bladed Darrieus-type rotors. Both a small and a large H-Darrieus VAWT with diameters of 0.5m and 35m respectively are investigated using NACA0018 blades. Computational results based on a commercial CFD code (Star CCM+) are compared with experimental measurements. Several simulations based on full URANS calculations are proposed. Firstly, the sensitivity of the time step, the number of iterations by time step, and discretization schemes are studied. Secondly, the effect of turbulence intensity on the VAWT performance is simulated and compared with experimental data. Finally, results reveal that the power coefficient of a small turbine is increases for higher turbulence intensity, up to 20%, but stops increasing afterward. For a small turbine H-Darrieus turbine, the power coefficient is increased by 22% when the turbulence intensity is changed from 0.7% to 20%, however, there is no increase detected in the case of a large H-Darrieus wind turbine. The impact of the turbulence intensity was assessed and a range of behaviors was identified.

2.1 Introduction

There is a growing interest in placing micro-wind turbines in urban areas, nevertheless, the high turbulence of the flow needs to be considered as it is a main feature of the flow in this environment. This turbulence is not only composed of high turbulence intensity but also of large velocity fluctuations with large vertical components due to the existence of buildings. Challenges related to rapidly changing wind direction in urban areas have been investigated [42][43] and show

that these large variations in the wind affect negatively the performance of all types of wind turbines. Other devices have been proposed to harvest wind energy from highly fluctuating winds [43], such as beam vibration driven by the wind [45][46]. Different flow-induced vibrations devices to improve the performance of harvesters were reviewed by Wang et al. [46]. More recently a technic named the hybrid piezoelectric wind energy scavenger was developed and studied by Wang et al. [47]. It showed promising results as the efficiency increased by 71%.

Nevertheless, recent work on VAWT indicates that the performance of this type of turbine increases with higher turbulent intensity for a homogeneous isotropic turbulent flow and may be a better alternative to conventional horizontal-axis wind turbines (HAWT) in urban applications [27], [28]. Therefore, this work focuses on studying high homogeneous isotropic turbulence through the turbulence intensity parameter and analyzing this effect on the performance of VAWTs. It is found in the literature that the authors Lee et al. [48] studied the influence of the skewed wind and wind direction on the power output of a small vertical-axis wind turbine installed on the rooftop of a building. The performance was investigated for a small vertical-axis wind turbine experiencing a flow with a turbulence intensity of more than 30%, and proved that the higher turbulence intensity flow increases the power output at the lower wind speed, but decreases the power output at the higher wind speed in comparison with a low turbulence intensity flow.

Experimentally the effect of turbulence intensity on H-Darrius type VAWT was studied in two different wind tunnels: the Vrije Universiteit Brussel low-speed wind tunnel located in Brussels, Belgium, and the CRIACIV wind tunnel located in Prato-Italy. These studies showed that the VAWT performance increases with increasing turbulence intensity. The measured power coefficient increases up to 20% from a smooth flow (Iu = 0.5%) to a higher turbulent flow (Iu = 14,8%), however, this improvement is only studied for low Reynolds numbers from 267,000 to 333,000 [24]. The effect of external free-stream turbulence on the aerodynamic performance of a vertical-axis wind turbine was studied by Baloutaki et al. [49]. In this study, three levels of turbulence intensity of 5%, 7.5%, and 10% were generated upstream of the vertical axis wind turbine using a grid turbulence generator. Turbulent flows generated downstream of the grid had uniform mean flow profiles, free of any wind shear effects. It is demonstrated that the turbulence generated downstream of the current grid is quasi-isotropic. It was concluded from this research that the turbine power output was substantially increased in the presence of grid turbulence, even

though the increase in turbine power coefficient due to the effect of grid turbulence was small at the same tip speed ratio. Using wind tunnel tests, the effect of turbulence length scales on the power performance of H-rotor VAWTs was investigated by Peng et al. [50]. The turbulence intensity and the length scales were generated with different wooden grids. The analysis concluded that the Power coefficient was increased significantly when increasing turbulence. However, the increase in length scale affects negatively the wind turbine performance. The small-scale vortices are more effective in energizing the boundary layer flow over the blade and delaying dynamic stall.

Another study based on an improved Delayed Detached Eddy Simulation (IDDES) numerical technique, analyzed the effect of increasing the rotational speed and turbulence intensity. It concluded that higher turbulence intensity will create stronger interaction between vortex structures and blades which may impact the life of the turbine [51]. Furthermore, by using field data and two different approaches to treat the relation between power performance and turbulence intensity for a VAWT H-rotor, it was shown that slightly higher efficiency is achieved at higher turbulence, suggesting that the H-rotors are well suited for wind sites with turbulent winds [52]. Nevertheless, some authors showed the contrary; the turbulence intensity decreases the performance of a Savonius wind turbine at Re=867000. Low-quality air flow or turbulent flow was assumed to affect the performance of wind turbines [27], [48]. The maximum averaged power coefficient decreased as the turbulence intensity increased in the air-free stream. It is noted that these studies lead to contradictory conclusions, as the effect of turbulence is not always positive. Möllerström et al. [52], proposed that the turbulent nature of the urban wind improves energy capture because of the additional energy in the wind gust. Furthermore, Berténi et al. [53] concluded that the influence of turbulence intensity on the power performance of a 200 kW VAWT is not very significant but increases slightly for higher turbulence.

On the other hand, Kooiman et al. [54] show that wind speed fluctuations with $Iu < 0.15$ lead to a minimal impact on the performance while for greater fluctuations the performance decreases linearly with increasing turbulence intensity. Furthermore, Pagnini et al. [55] performed a field analysis for two small wind turbines, one vertical axis and, one horizontal axis, with the same nominal power and placed in the same urban environment. This analysis indicated low energy production which could be linked to an inadequacy of the turbines to perform well at high

turbulence rates. Indeed, turbulence is of great importance as it affects the power output and causes random fluctuating loads, which stress both the turbine and turbine support (building, hills, etc.). Turbulence needs to be addressed when designing the turbine, both regarding structural excitation, maximum load, and fatigue predictions as well as power control routines [20]. In addition, the placement of wind turbines in urban areas required rigorous studies of the wind patterns based on the flow around the adjacent buildings [56].

One can also note the rapid progress in high-performance computing and the growing availability of large computational resources. CFD tools offer cost-effective, versatile, and accurate means to improve the understanding of the unsteady aerodynamics of Darrieus wind turbines. These tools offer more accurate analysis and lead to more cost-effective designs [57]. Among the largest simulations of VAWT, note the study of Darrieus rotor blades using more than 16,000 processor cores on an IBM BG/Q cluster allowing a highly refined simulation using a grid with 64 million elements [57].

In this paper, a numerical methodology using 3D URANS simulations is proposed to evaluate if a numerical model is able to adequately predict the performance of VAWT for different turbulence intensities similar to the experiments in Ref. [24]. Afterward, the numerical approach is used to study the effect of the turbulence intensity on the performance of the turbine. The work in Ref. [24] is continued numerically by investigating a small turbine and a large turbine for a large range of turbulent intensities. The objective is to understand the turbulence intensity effects on VAWT power generation and to identify the range of this effect. The structure of this article is organized as follows, after the introduction, section 2 presents the models used and the turbines studied. In Section 3, a description of the computational domain and the solver settings are presented. A description of the validation of cases is presented in Section 4, followed by the numerical investigation of two H-Darrius VAWTs. Finally, the main conclusions of the current work are summarized in Section 5.

2.2 Wind Turbine Simulation Models

First, common parameters in the field of wind turbines are reviewed. The power available from the wind for a cross-section area (A_s) is given by:

$$P_{wind} = 0.5\,\rho\,A_s U^3 \tag{2-1}$$

where ρ is the density of the air and U the wind speed.

For an H-type vertical axis wind turbine, the swept area (A_s) is a rectangle, calculated as the turbine diameter multiplied by the blade length. The power coefficient is a measure of the wind turbine's ability to convert wind energy to mechanical energy which is defined as:

$$p = \frac{P_{wind\ turbine}}{P_{wind}} \tag{2-2}$$

where $P_{wind\ turbine}$ is the aerodynamic power output.

The power coefficient depends on the tip speed ratio TSR or λ, which is the ratio between the velocity of the blade and the wind speed, thus calculated as:

$$\lambda = \frac{\omega R}{U} \tag{2-3}$$

where ω is the angular velocity of the turbine and R is the turbine radius.

Second, the turbulence intensity is defined. Turbulence intensity is a measure of the wind turbulence and thus also the tendency of the wind to alter speed. The turbulence intensity (Iu) is defined by the ratio of the vector norm of the fluctuating part (u') and the average of the mean velocity (U), as defined in equations (2-4)(2-5) and (2-6), respectively:

$$\text{Iu} = \frac{u'}{U} \tag{2-4}$$

$$u' = \sqrt{\frac{1}{3}({u'_x}^2 + {u'_y}^2 + {u'_z}^2)} \tag{2-5}$$

$$U = \sqrt{\bar{u}_x^2 + \bar{u}_y^2 + \bar{u}_z^2} \tag{2-6}$$

where $\bar{u}_x$ is the wind speed along the x-axis; $\bar{u}_y$ is the wind speed along the y-axis; $\bar{u}_z$ is the wind speed along the z-axis. In this definition, the time period used must be longer than the turbulent fluctuations but shorter than periods associated with long-term wind speed variations such as diurnal effects [20].

Third, the SST k–ω turbulence model selected for this simulation is reviewed. This selection is adopted according to the literature review [57]. It is found that the SST K-ω model is more accurate to capture the results near the wall of the wind turbine and its numerical results compared favorably to experimental data. The k-ω turbulence model was first postulated by Kolmogorov in

1942 [58], and later independently by Saffman in 1970 and Spalding in 1969 [59]. It has been under continuous development by Wilcox for many years and was described in detail by Wilcox [60] in 1998. The model solves two turbulence transport equations for the turbulent kinetic energy k and the specific dissipation rate ω. The model has a basic formulation for fully turbulent flows that satisfy the law of the wall without knowledge of the distance to the wall or complicated near-wall damping terms. There is also a low-Reynolds-number formulation used for modeling transition [61]. Boundary conditions can be specified to simulate mass injection or surface roughness.

In this study, there are two solution domains: fixed and rotating parts, so inertial coordination needs to be considered when the airflow passes through the fixed part.

The Navier-Stokes equations in the case of the system rotate at the fixed angular velocity written as follows:

$$\rho \frac{D\vec{v}}{Dt} = -\nabla p + \mu \nabla^2 \vec{v} - \rho[2\omega \times W + \omega \times \omega \times r] \tag{2-7}$$

where v is the velocity vector,

$W = \sqrt{V_c^2 + V_n^2}$, which: V_c, V_n are the Chord and vertical components of the velocity respectively.

The term $2\omega \times W$ is the Coriolis acceleration, and the term $\omega \times \omega \times r$ is centrifugal acceleration. As can be seen, the associated terms with Coriolis acceleration and centrifugal acceleration due to the rotation of the system are added to Navier-Stokes equations.

In the vertical axis wind turbine fields, the wind passing through the wind turbine is considered an inertial system, where it is included continuity equation and momentum conservation, as are respectively defined below:

$$\nabla . \vec{v} = 0 \tag{2-8}$$

$$\rho \left(\frac{D\vec{v}}{Dt} \right) = -\nabla p + \nabla . \tau \tag{2-9}$$

And the SST k–ω turbulence model was developed by Menter [40] as follows:

Transport equations of k:

$$\frac{\partial}{\partial t}(\rho k) + \frac{\partial}{\partial x_i}(\rho k u_i) = \frac{\partial}{\partial x_i}\left(\Gamma_k \frac{\partial k}{\partial x_j}\right) + G_k - Y_k + S_k + G_b \tag{2-10}$$

and transport equations of ω:

$$\frac{\partial}{\partial t}(\rho \omega) + \frac{\partial}{\partial x_i}(\rho \omega u_i) = \frac{\partial}{\partial x_i}\left(\Gamma_\omega \frac{\partial \omega}{\partial x_j}\right) + G_\omega - Y_\omega + S_\omega + G_{\omega b} \tag{2-11}$$

where ρ is the fluid density, p is the mean pressure, $\Gamma_U, \Gamma_k, and\ \Gamma_\omega$ are the effective diffusivities of the mean fluid speed U (V or W), turbulence kinetic energy k, and specific dissipation rate ω, respectively, which are expressed as:

$$\Gamma_U = \mu + \mu_t \tag{2-12}$$

$$\Gamma_k = \mu + \frac{\mu_t}{\sigma_k} \tag{2-13}$$

$$\Gamma_\omega = \mu + \frac{\mu_t}{\sigma_\omega} \tag{2-14}$$

and μ_t is the turbulent viscosity, which is defined as follows:

$$\mu_t = \frac{\rho k}{\omega} \frac{1}{max\left[\frac{1}{\alpha^*}, \frac{SF_2}{\alpha_1 \omega}\right]} \tag{2-15}$$

In these equations:

G_k represents the generation of turbulence kinetic energy due to mean velocity gradients.

G_ω represents the generation of ω.

$Y_k\ and\ Y\omega$ represent the effective diffusivity of k and ω due to turbulence.

All the above terms are calculated as described below.

$S_k\ and\ S\omega$ are user-defined source terms.

$G_b\ and\ G_{\omega b}$ account for buoyancy terms as described in Effects of Buoyancy on Turbulence in the k-ω models.

While the original model formulation has largely stayed unchanged from the formulation given by Menter [40], there have been several areas of improvement carried out within the small

modifications of the SST Model, the complete formulation of the SST model is given, with the limited number of modifications [41]:

$$\frac{\partial(\rho k)}{\partial t}+\frac{\partial(\rho U_i k)}{\partial x_i}=\tilde{P}_k-\beta^*\rho k\omega+\frac{\partial}{\partial x_i}\left[(\mu+\sigma_k\mu_t)\frac{\partial k}{\partial x_i}\right] \tag{2-16}$$

$$\frac{\partial(\rho\omega)}{\partial t}+\frac{\partial(\rho U_i\omega)}{\partial x_i}=\alpha\rho S^2-\beta\rho\omega^2+\frac{\partial}{\partial x_i}\left[(\mu+\sigma_\omega\mu_t)\frac{\partial\omega}{\partial x_i}\right]+2(1-F_1)\rho\sigma_{w2}\frac{1}{\omega}\frac{\partial k}{\partial x_i}\frac{\partial\omega}{\partial x_i} \tag{2-17}$$

where the blending function F1 is defined by:

$$F_1=tanh\left\{\left\{min\left[max\left(\frac{\sqrt{K}}{\beta^*\omega y},\frac{500v}{y^2\omega}\right),\frac{4\rho\sigma_{\omega2}k}{CD_{k\omega}y^2}\right]\right\}^4\right\} \tag{2-18}$$

with $CD_{k\omega}=max\left(2\rho\sigma_{\omega2}\frac{1}{\omega}\frac{\partial k}{\partial x_i}\frac{\partial\omega}{\partial x_i},10^{-10}\right)$ and y is the distance to the nearest wall.

F_1 is equal to zero away from the surface (k-ε model) and switches over to one inside the boundary layer (k-ω model).

The turbulent eddy viscosity is defined as follows:

$$v_t=\frac{a_1k}{max(a_1\omega,SF_2)} \tag{2-19}$$

where S is the invariant measure of the strain rate and F_2 is a second blending function defined by:

$$F_2=tanh\left[\left[max\left(\frac{2\sqrt{k}}{\beta^*\omega y},\frac{500v}{y^2\omega}\right)\right]^2\right] \tag{2-20}$$

A production limiter is used in the SST model to prevent the build-up of turbulence in stagnation regions:

$$P_k=\mu_t\frac{\partial U_i}{\partial x_j}\left(\frac{\partial U_i}{\partial x_j}+\frac{\partial U_j}{\partial x_i}\right)\rightarrow\tilde{P}_k=\min(P_k,10.\beta^*\rho k\omega) \tag{2-21}$$

All constants are computed by a blend from the corresponding constants of the k-ε and the k-ω model via: $\alpha=\alpha1F+\alpha2\,(1-F)$ etc...

The constants for this model are:$\beta^* = 0.09, \alpha_1 = \frac{5}{9}, \beta_1 = \frac{3}{4}, \sigma_{k1} = 0.85, \sigma_{k\omega 1} = 0.5, \alpha_2 = 0.44$ $\beta_2 = 0.0828, \sigma_{k2} = 1, \sigma_{k\omega 2} = 0.856.$

The only modifications from the original formulation are the use of the strain rate S, instead of the vorticity in equation (2-21), and the use of factor 10 in the production limiter, instead of 20 as proposed by Menter [42].

In this work a Reynold number based on the turbine diameter is used:

$$Re = \frac{\rho U D}{\mu} \tag{2-22}$$

where ρ is the air density and μ the air dynamic viscosity.

Lastly, in this work two turbines are studied and presented below.

2.2.1 Turbine 1: Large Wind Turbine

A two-blade 500 kW H-Type vertical axis wind turbine is considered for the proper selection of the simulation parameters of the URANS 2D CFD and then later for analyzing the turbulence intensity effect on a large turbine in 3D. This configuration was chosen because it is a large turbine and the Reynolds number for a wind speed of 10 m/s is 23,340,000. Furthermore, the rotor only has two blades which reduces the number of elements in the mesh and therefore reduces the computational time. The rotor geometrical specifications are reported in Table 2-1, while a picture of the installation is shown in Figure 2-1. The experimental activity recorded the power production at a fixed rotational speed of 13.62 rpm: the same condition is applied in the simulations.

Table 2-1: Main geometrical features of the large wind turbine [62].

Blade profile	NACA 0018
Blade number	2
Rotor diameter	35 m
Blade length	24.3 m
Mean chord	1.75 m
Blade taper	25%
Rotor solidity	0.10

Figure 2-1: A two-bladed Darrieus wind turbine installation of 500kw (From: [63]).

2.2.2 Turbine 2: Small Wind Turbine

This turbine is also studied for the turbulence intensity based on a full 3D simulation. A two-bladed H-type Darrieus turbine with a NACA0018 profile as shown in Figure 2-2, and detailed in Table 2-2 and Table 2-5, is used. The angular speed used is high (around 1200 rpm). The Reynolds number based on a wind speed of 10 m/s is 333,000 which is much less than the large turbine 1.

Table 2-2: Main geometrical features of the small wind turbine [24].

Blade profile	NACA 0018
Blade Number	2
Rotor diameter	0.5 m
Mean chord (c)	0.05 m
Swept area	0.4 m^2

Figure 2-2 : Set-up at the VUB wind tunnel, with turbine and hot-wire to control free flow speed [24].

2.3 Numerical Methodology

An unsteady flow simulation with moving boundaries is presented. In particular, the discretization of the computational field requires two zones; a rotating zone which contains the moving rotor, and a fixed zone that models the far field as shown in Figure 2-3:

1- the rectangular outer fixed zone, determining the overall computation area, with a circular opening centered on the axis of rotation of the turbine, identified as a fixed far field flow or the Wind Tunnel subnetwork;

2- a circular inner zone, identified as a rotor sub-grid, rotating at the angular speed of the rotor.

As shown in Figure 2-3, the computational domains with boundary conditions and sizes with respect to the rotor diameter D, to scale and main dimensions of the Wind tunnel sub-grid area. To accurately capture the wake around the turbine, inlet, and outlet boundary conditions are placed respectively at 5 diameters upwind and 15 diameters downwind. The inlet was set as a velocity inlet, with a constant velocity profile, while the outlet was set as a pressure outlet. Two symmetry boundary conditions were used for the two side walls. To avoid the blockage effect, the width of the domain is set to 10 times the rotor diameter length. In both cases, 2D and 3D, the rotating domain is characterized by a sliding mesh, rotating at the same angular velocity of the turbine, and connected by the interface to the fixed mesh. In the 3D case, only half of the turbine is modeled, and a symmetry plane is used to save computational cost. As before, the geometry is divided into two regions, a static domain, and a rotating domain which is connected by the interface boundary condition to ensure the sliding mesh option in the CFD software, as shown in Figure 2-3.

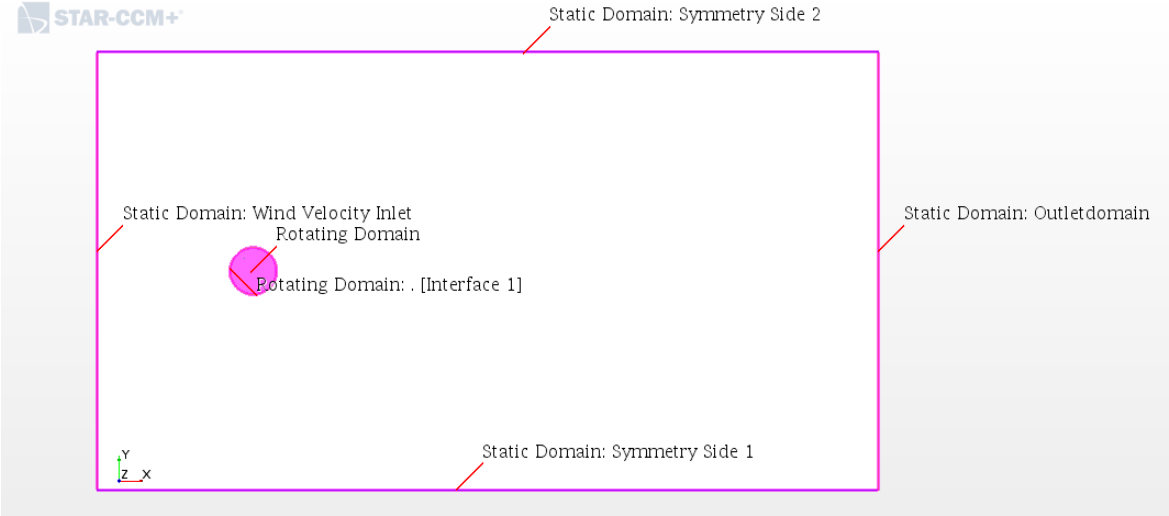
STAR-CCM+
Static Domain: Symmetry Side 2
Static Domain: Wind Velocity Inlet
Rotating Domain
Rotating Domain: . [Interface 1]
Static Domain: Outletdomain
Static Domain: Symmetry Side 1
Y
Z
X

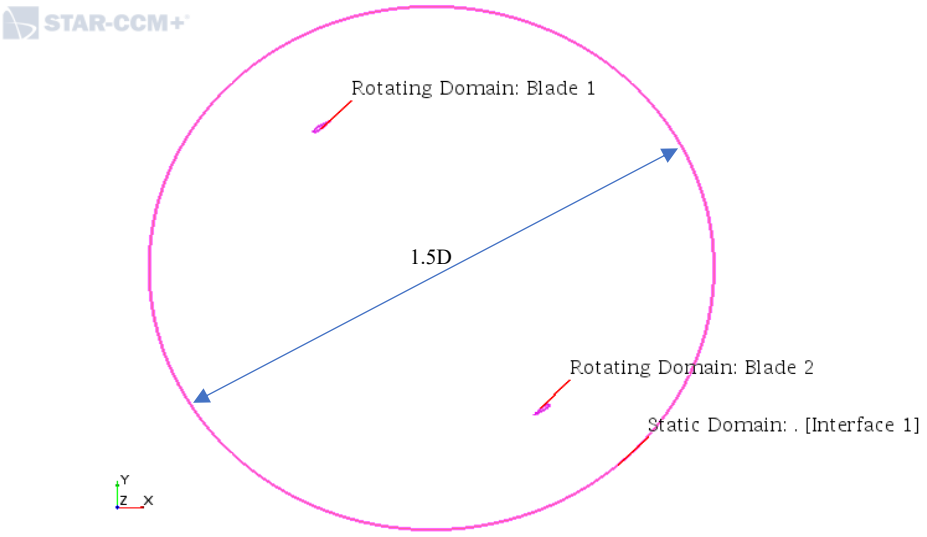
STAR-CCM+
Rotating Domain: Blade 1
1.5D
Rotating Domain: Blade 2
Static Domain: . [Interface 1]
Y
Z
X

(a)

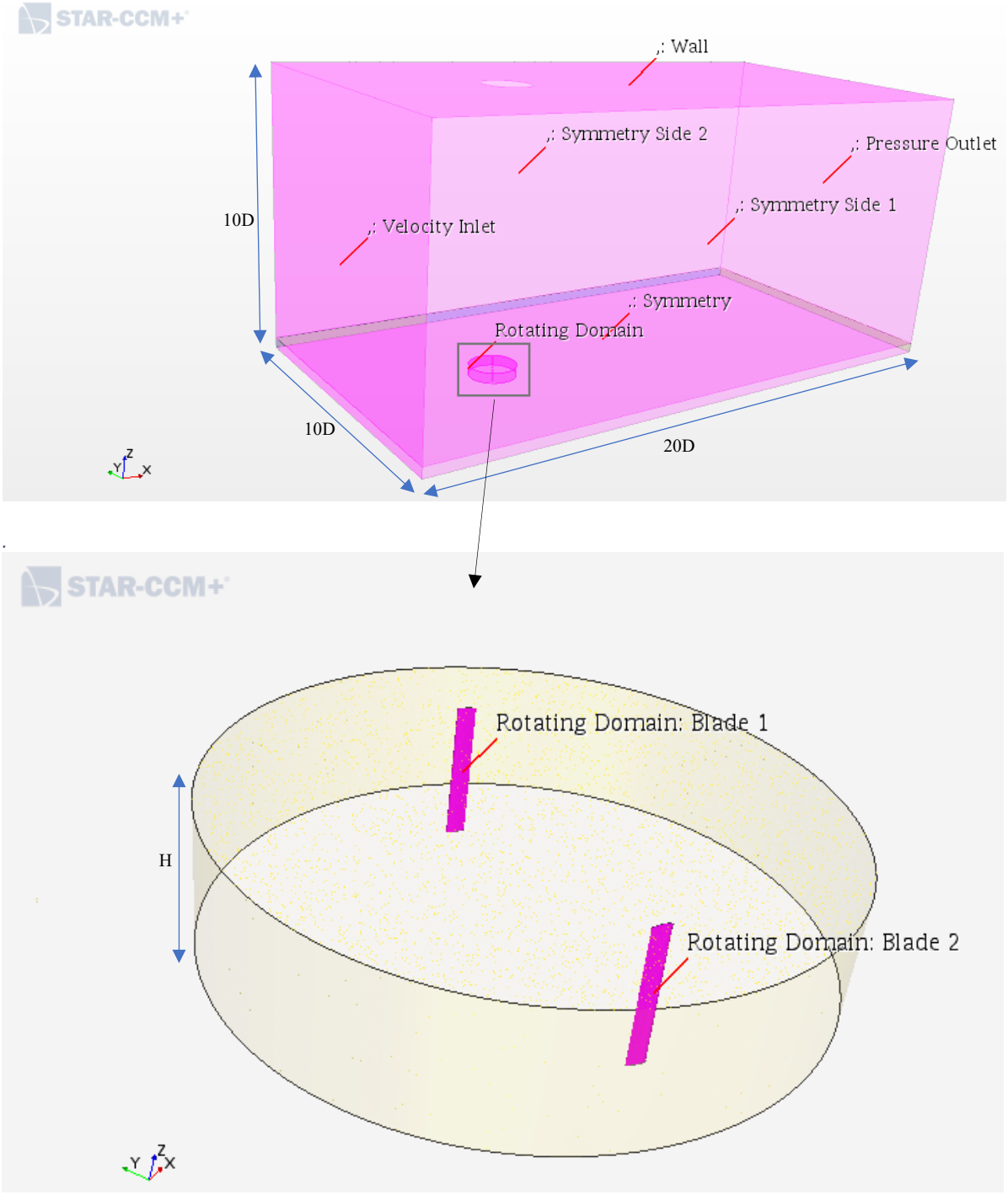

(b)

Figure 2-3 : The main dimensions of the computational domains: are (a) 2D and (b) 3D representation.

The static domain extends 10 times the rotor diameter length to the top boundary in the Z-axis from the symmetry plane. The rotating domain is basically the 2D rotating domain that is extruded at a height of H/2, where H is the height of the wind turbine.

2.3.1 Mesh topology

In Figure 2-4(a), (b), (c), and (d), both two-dimensional and three-dimensional views of the finest mesh used for the large turbine are shown. As seen in Figure 2-4(c) a finer mesh is used around the airfoil to improve the accuracy of calculating lift, drag, and flow separation.

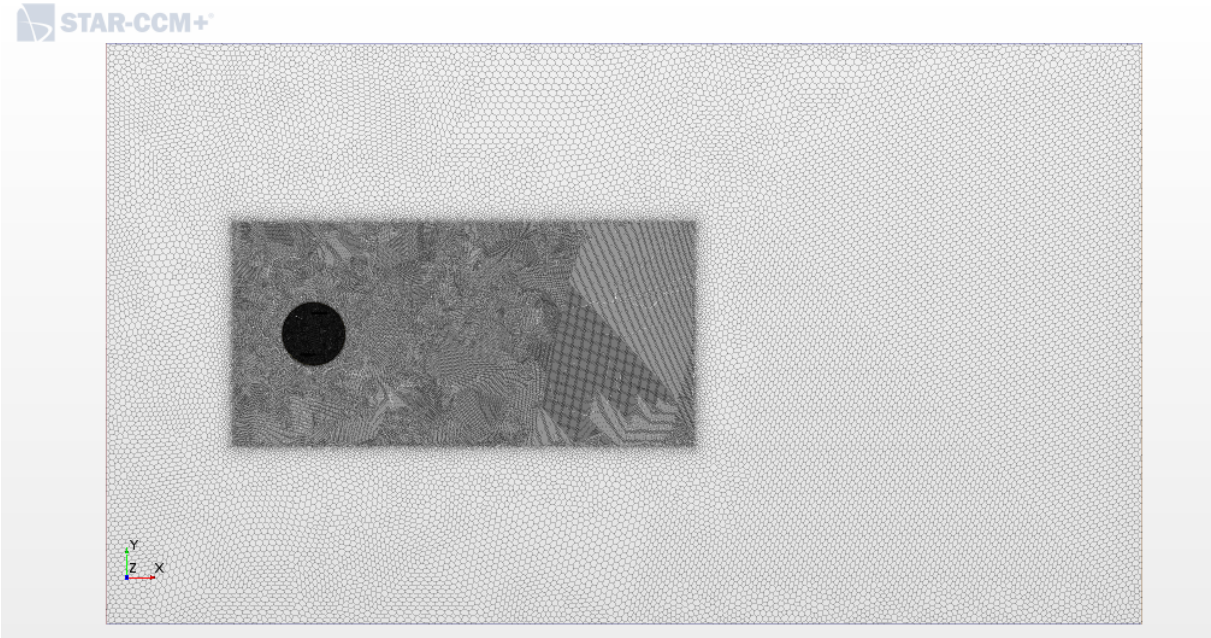

(a)

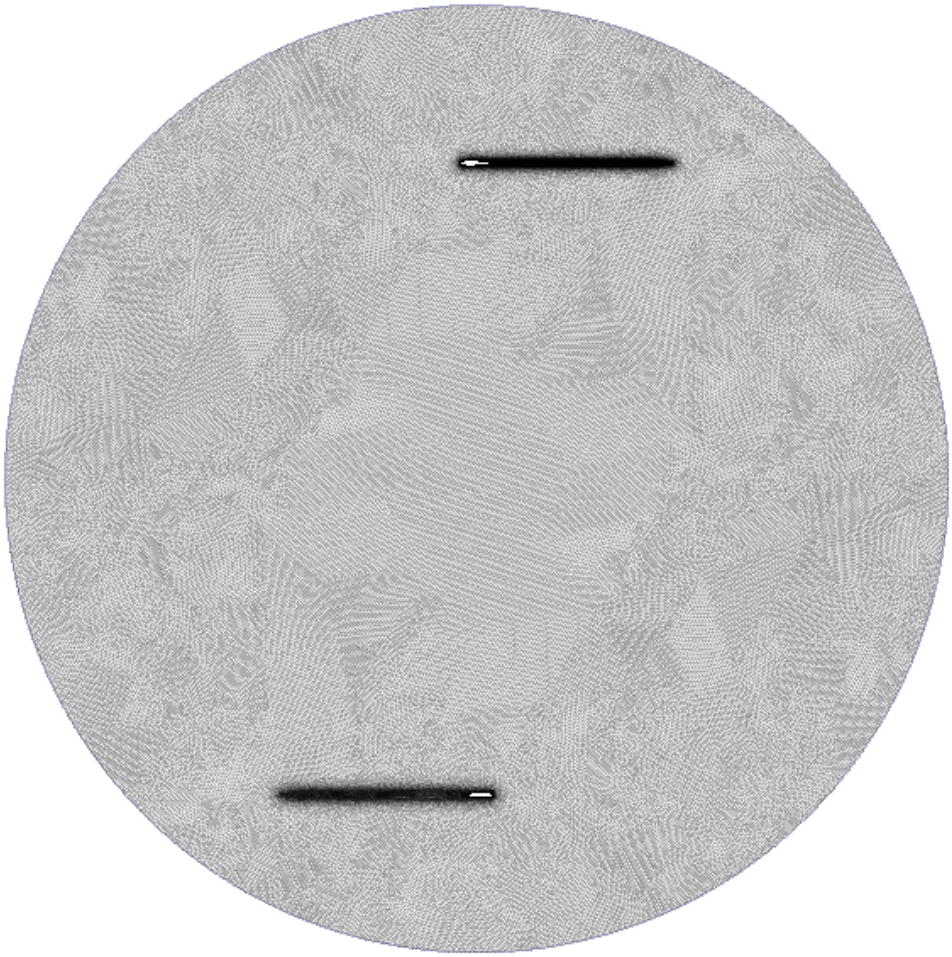

(b)

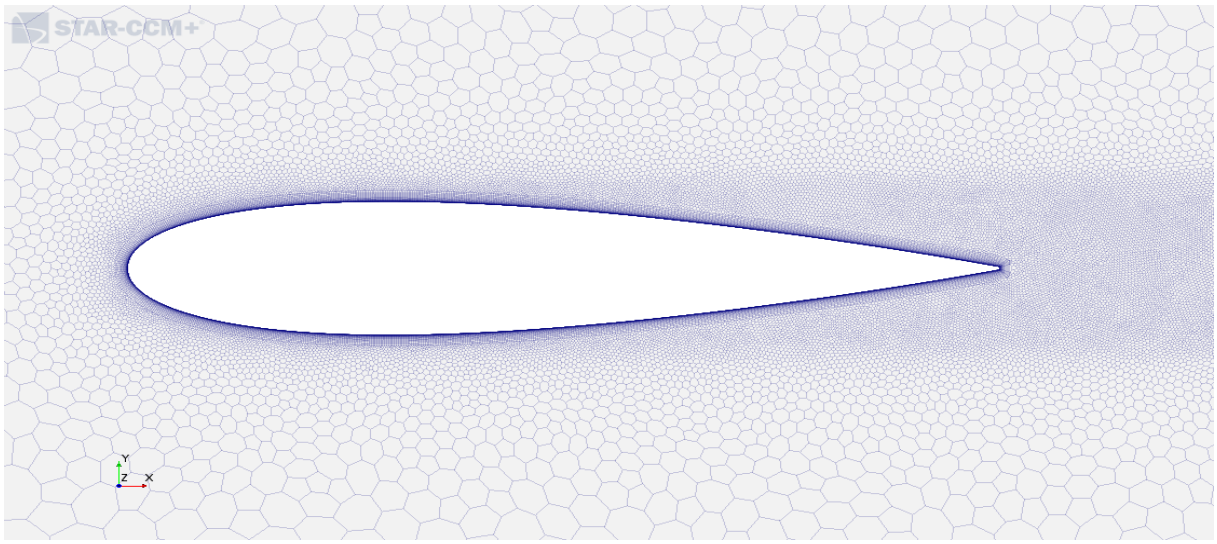

(c)

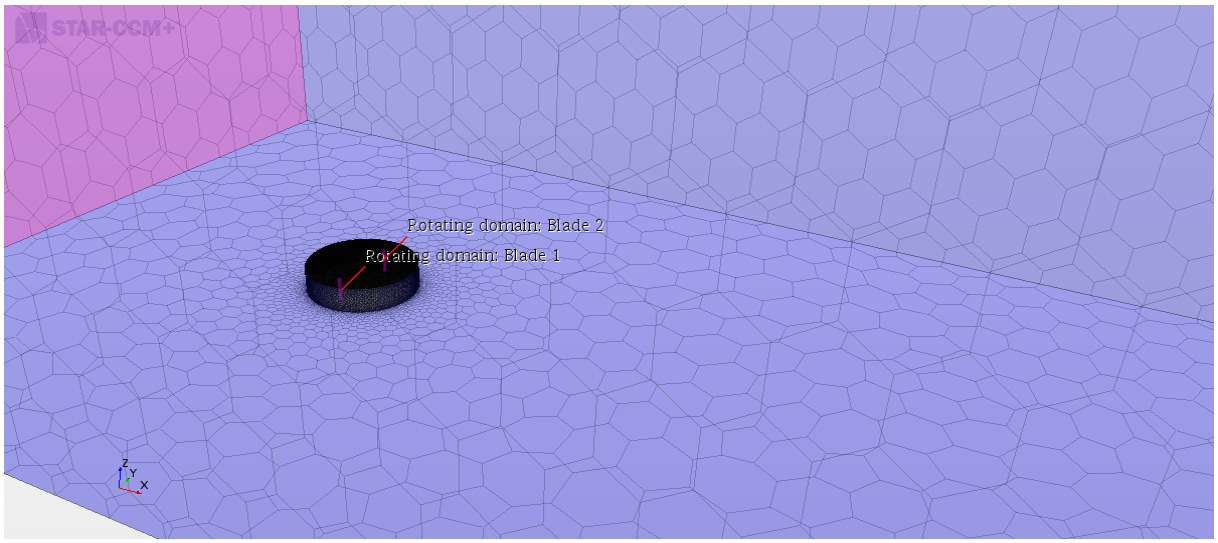

(d)

Figure 2-4: The finest mesh for the validation case: (a) Total domain 2D mesh, (b) Rotor sub-grid mesh for the bladed VAWT, (c) Airfoil mesh with 60-step boundary layer extrusion. d) 3D view.

2.3.2 Wall treatment

The dimensionless wall parameter, y^+ is an important factor describing how many cell points should be located within the wall boundary layer. For the turbulence model used in this study, the associated with the first cell should not fall outside of the log-law layer and it should not be too small that the first node is placed in the viscous sublayer of the boundary layer [64]. Therefore, the value of y^+ at the first cell center next to the wall must be below 1. The wall plot presented in Figure 2-5 shows that y^+ is between 0.14 and 0.93 for the large wind turbine for both 2D and 3D cases. These values satisfy the condition of $y^+ < 1$, which is required when using the k-ω SST turbulence model.

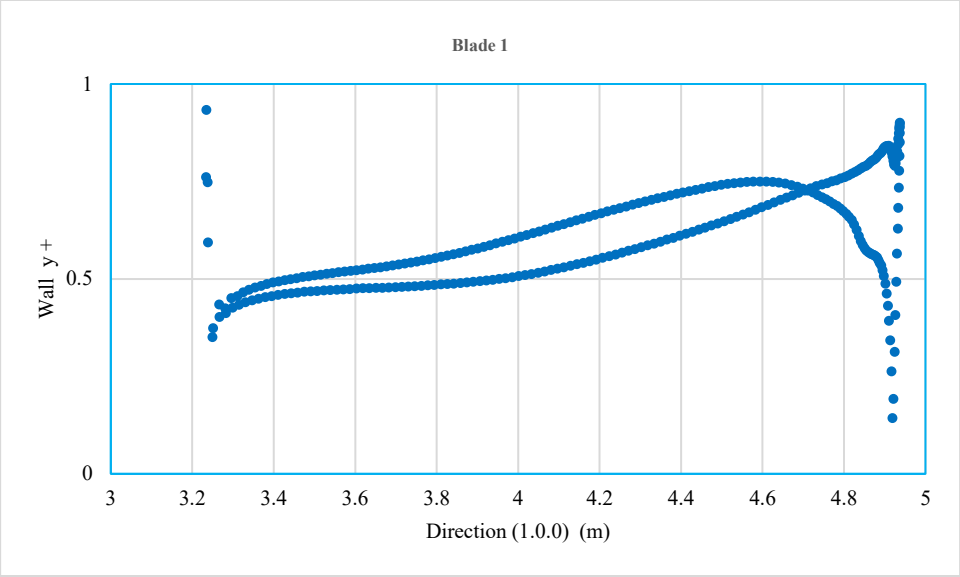

Figure 2-5: Y^+ distribution on blade 1 profile for the Large Wind Turbine on the finest mesh.

The wall treatment selected in this work is based on the specific reference velocity u^*, which is used to calculate the special value of turbulent production G_k and the special value of specific dissipation ω in the wall cell [65], where the reference velocity u^* is defined as:

$$u^* = \begin{cases} \sqrt{\beta^{*0.5}}k & ;\text{high } y^+ \\ \sqrt{gvu/y + (1-g)\beta^{*0.5}k} & ;\text{low } y^+ \\ \sqrt{gvu/y + (1-g)\beta^{*0.5}k} & ;\text{all } y^+ \end{cases} \tag{2-23}$$

Three approaches are adopted in the K-ω model, such as in the case of the high y^+, the traditional wall function is formulated, whereas in the case of the low y^+ the traditional low Reynolds number approach is used. A blending function g is defined for all y^+ formulations:

$$g = exp\left(-\frac{Re_y}{11}\right) \tag{2-24}$$

where Re_y is the wall distance based on the Reynolds number and $Re_y = \frac{\sqrt{k}y}{\nu}$.

For coarse meshes, the blending function g will be adopted if the result is not more accurate when $u^* \equiv \sqrt{\tau_w/\rho} \approx \sqrt{vu/y}$. After arrangement the Wall-Cell production term is defined as:

$$G_{k=}\begin{cases}\frac{1}{\mu}\left(\rho u^{*}\frac{u}{u^{+}}\right)^{2}\frac{\partial u^{+}}{\partial y^{+}} & ;\text{high } y^{+}\\ \mu_t S^2 & ;\text{low } y^{+}\\ g\mu_t S^2+(1-g)\frac{1}{\mu}\left(\rho\mu^{*}\frac{u}{u^{+}}\right)^{2}\frac{\partial u^{+}}{\partial y^{+}} & ;\text{all } y^{+}\end{cases} \quad (2\text{-}25)$$

And the Wall-Cell specific dissipation term is defined as:

$$\omega=\begin{cases}\frac{u^{*}}{\sqrt{\beta}ky} & ;\text{high } y^{+}\\ \frac{6v}{\beta y^{2}} & ;\text{low } y^{+}\\ g\frac{6v}{\beta y^{2}}+(1+g)\frac{u^{*}}{\sqrt{\beta}ky} & ;\text{all } y^{+}\end{cases} \quad (2\text{-}26)$$

To make sure that the mesh is fine enough in the boundary layer, the turbulence viscosity ratio is analyzed. The mesh with 60 layers closes to the blade is capable of capturing completely the boundary layer.

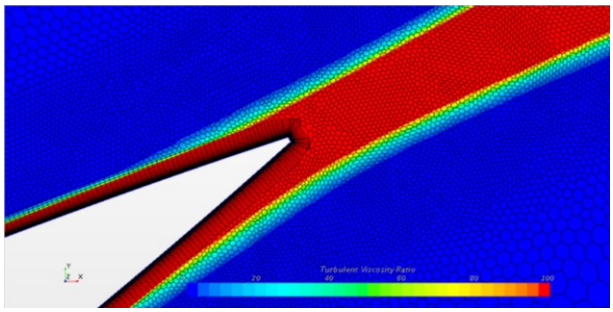

$\beta = 30°$

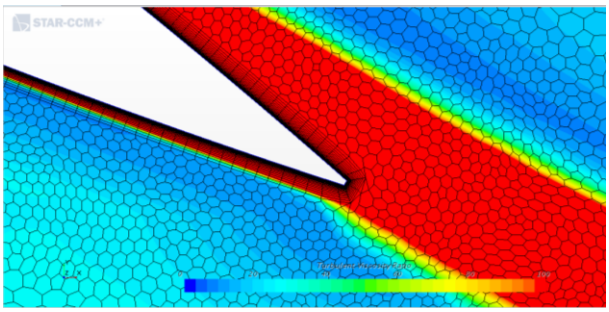

$\beta = 300°$

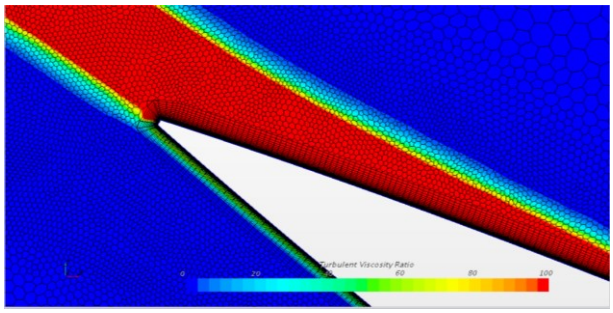

$\beta = 120°$

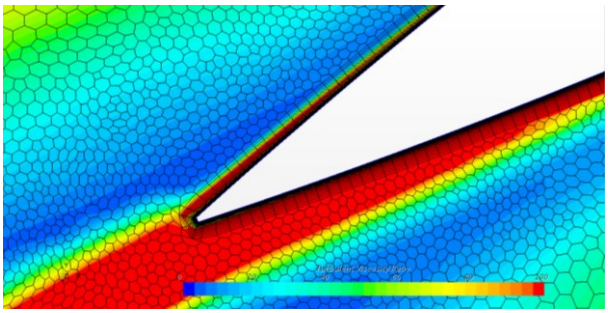

$\beta = 210°$

Figure 2-6 : Turbulent viscosity ratio near the airfoil at different azimuthal positions, λ = 4.5 for the large wind turbine.

Figure 2-6 provides an example of turbulent viscosity ratio examples for a reasonable wall function mesh for a large wind turbine. There is a good cell transition from the prisms to the free-stream polyhedral elements. One can observe that the transition in size from the final prism layer to the free stream polyhedral elements is smooth nevertheless the wake does increase due to diffusion once it reaches the coarser mesh shown in Figure 2-4.

2.3.3 Mesh independence study

The mesh size is investigated to find the mesh with the lower number of cells that provides accurate results. The accuracy is evaluated by the change in the output of interest which in this case is the moment coefficient. Four different values of the grid size are set for the 2D geometry to assess the effect of coarse, medium, and fine meshes, respectively. The main differences between the four types of meshes are the different grid sizes on the surfaces of the blades. As seen in Figure 2-7 the mesh M2 provides a value close to the finest mesh but uses fewer elements.

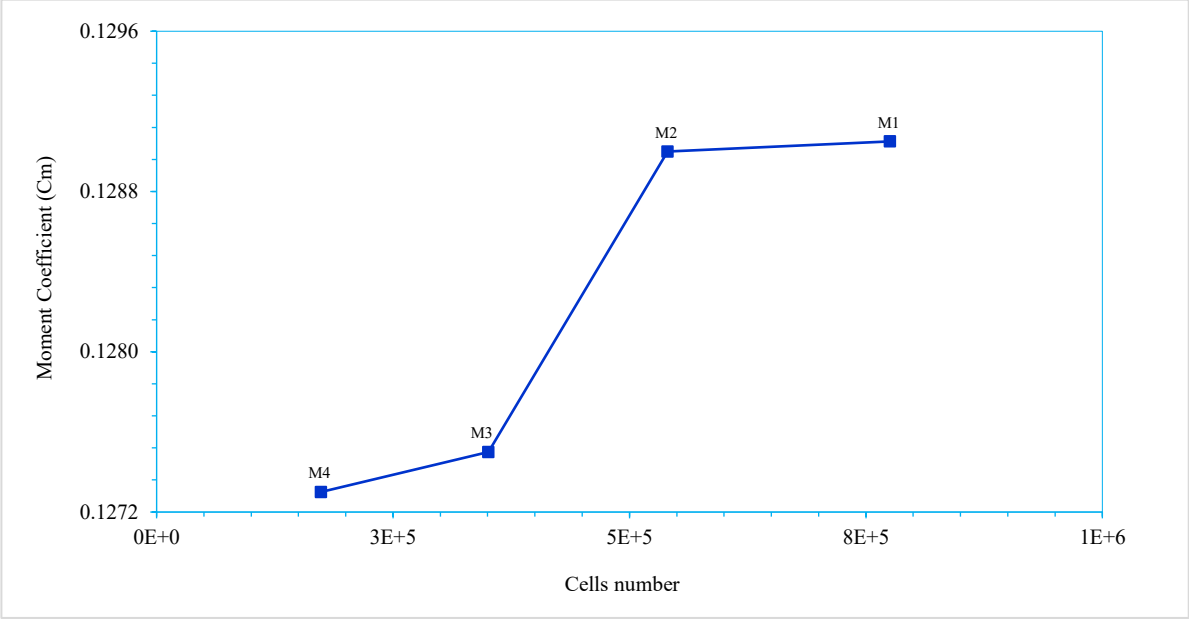

Figure 2-7: Cycle-averaged moment coefficient (Cm) for refining the mesh size.

Therefore, the mesh M2 is used for all 2D simulations. For both three-dimensional geometries, and to conduct the mesh sensitivity, three different meshes have been created as reported in Table 2-3. Results are also compared with experimental data from Molina et al. [24], and Mays et al. [63] at TSR =3 and TSR = 3.5 respectively. The average moment coefficient (Cm) obtained for the three different meshes is tabulated in Table 2-3. The total number of cells,

indicated in bold, for mesh 1, mesh 2, and mesh 3 for the large turbine range from 10 million cells to 19 million cells.

Table 2-3: Sets of generated mesh for mesh sensitivity study.

	Cell quantity						
Meshes	Mesh 1		Mesh 2		Mesh 3		Mesh 4
Turbine size	0.5 m	35 m	0.5 m	35 m	0.5 m	35 m	35 m
Static Domain	177598	7190419	227279	9043512	227279	11488322	13935132
Rotating Domain	2080170	3743029	2410295	6049341	2871419	7535062	9131783
Total	**2257768**	**10933448**	**2637574**	**15092853**	**3098698**	**19023384**	**23066915**
Present 3D CFD (Cm)	0.0497	0.0774	0.0596	0.0918	0.0608	0.0934	0.0941
Experimental (Cm) [24], [63]	0.0584	0.0928	0.0584	0.0928	0.0584	0.0928	0.0928

The difference between the average coefficient of the moment for Mesh 2 and Mesh 3 is less than 1.97% and 1.71% for the small turbine and large turbine, respectively. For the small turbine, Mesh 2 has been chosen for the rest of the simulations to save time and computational cost. For the large turbine, even if the Cm for both meshes is very close at TSR 3.5, results obtained for lower TSRs do appear to be less accurate for Mesh 2 as seen in Figure 2-8. Clearly, Mesh 2 is not able to capture the dynamic stall accurately. Mesh 3 is therefore used for turbulence intensity analysis and Mesh 4 is added to confirm that grids with higher density provide similar results. Note that two additional values computed on Mesh 4 at TSR 2.5 and 3.5 are added to Fig.8 and these values overlap with Mesh 3 values.

2.3.4 Time step independence study

To analyze the time step, five different time steps are studied for the same tip speed ratio (λ=3) for the large wind turbine. A maximum of 20 iterations per time step are used. The results obtained from this test are shown in Table 2-4 and Figure 2-9, where the means of the torque coefficient as a function of the time step is reported. One can notice that there is no difference between the values obtained for the first three smaller time steps, whereas the values equivalent to 1 and 2 degrees (equivalent to 0.01223691 s and 0.02447382 s per time step respectively) show a relatively larger difference compared to other cases. In order to accelerate the simulations with

acceptable accuracy, the angle increment of 0.5 degrees per time step, equivalent to 0.00611845 s, is used for the rest of the calculations.

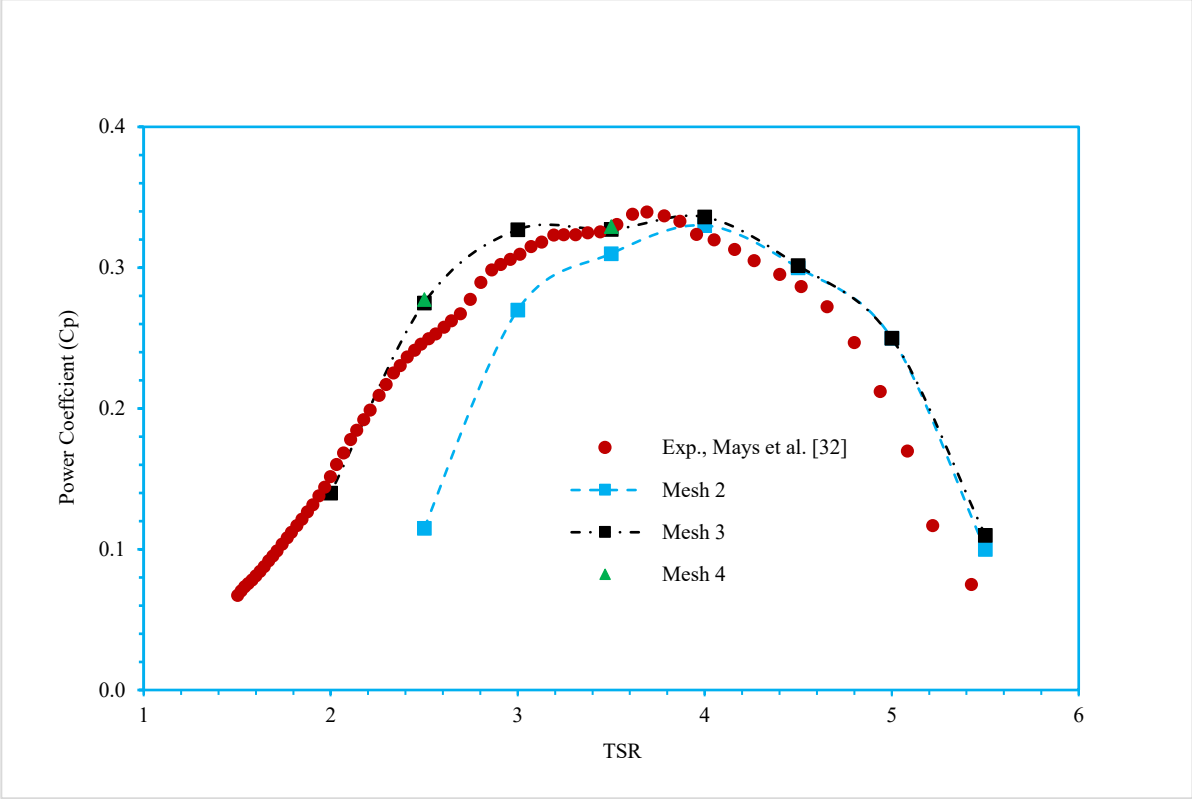

Figure 2-8: Validation of the results against experimental results for the large H-Darrieus VAWT (D=35m).

Table 2-4: Coefficient of moment as a function of Time step for the large wind turbine.

Time step (s)	Time step (°)	Cm
0.00122369	0.10	0.088010
0.00305880	0.25	0.088000
0.00611845	0.50	0.088020
0.01223691	1.00	0.087091
0.02447382	2.00	0.086010

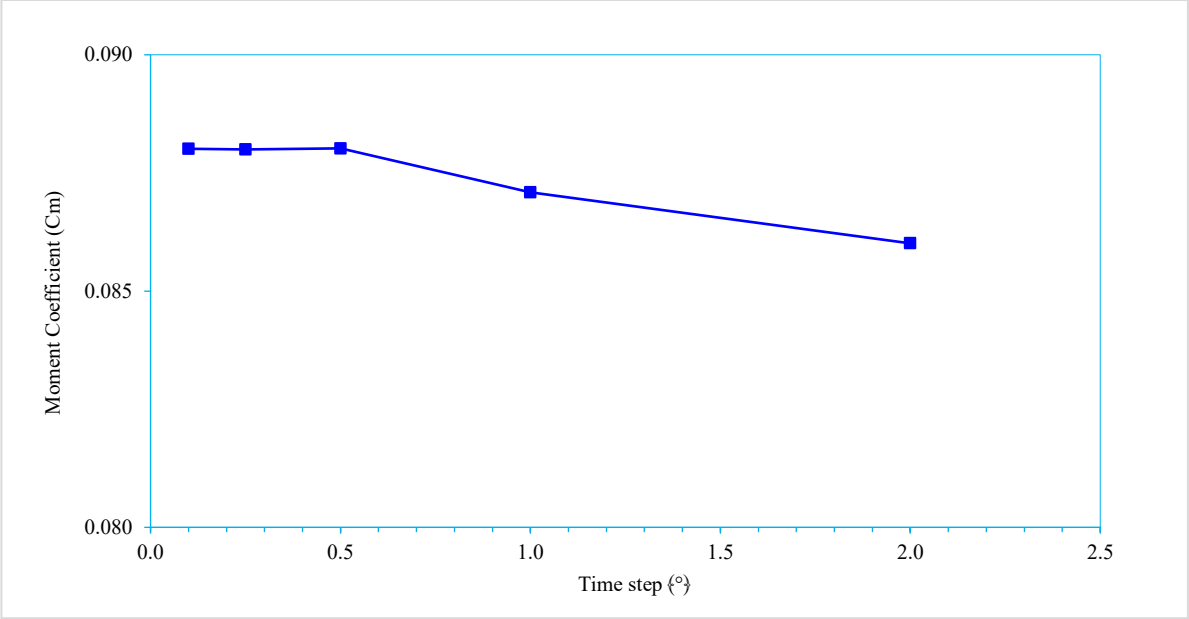

Figure 2-9: Cycle-averaged coefficient of moment (Cm) against various time steps for the large wind turbine.

2.3.5 Influence of temporal scheme parameters

Firstly, for the two-dimensional flow around the large wind turbine, the sensitivity of the temporal scheme parameters such as the number of iterations per time step is analyzed. Several simulations are performed using first and second-order schemes and 3, 5, and 7 iterations per time step were tested. The comparisons between all cases focus on the calculation of the moment coefficient, power coefficient, and time of calculation.

Table 2-6 summarizes the results of three different time steps of 0.1°, 0.5°, and 1°. The operating parameters and machine characteristics are listed in Table 2-5.

Table 2-5: The main parameters used in 2D and 3D simulations.

	NACA0018 0.5m	NACA0018 35m
Velocity Inlet	9 m/s	6.23 m/s
TSR	3.5	4
ω	1200 (rpm)	13.62 (rpm)
D	0.5 (m)	35 (m)
R	0.25 (m)	17.5 (m)
Computer type	i7, Ram 16 Go	i7, Ram 16 Go

As seen in Table 2-6, the computational time increases as the number of iterations per time step increases. The Cp values indicate that at least 5 iterations are needed and that the 2nd-order accurate scheme is a requirement. Note that the computational cost is the same for a 0.5-degree or a 1-degree rotational increment but is 4.14 times faster than the 0.1-degree rational increment. Figure 2-10 shows the instantaneous moment coefficient (Cm) for all 15 revolutions versus physical time for a Tip speed ratio of 4. For the highest time step the difference between the results is high, while for a time step of 0.1, the results seem very close together, especially in the last revolution. Based on these results, it is selected a time step related to 0.5-degree rotational increment and 5 iterations per time step for subsequent calculations.

Table 2-6: Influence of different parameter on Time step.

2D Simulation, λ=4, 15 Revolutions.

	Time step														
	0.1°					0.5°					1°				
	Scheme		Iteration/Time step			Scheme		Iteration/Time step			Scheme		Iteration/Time step		
	1st order	2nd order	3	5	7	1st order	2nd order	3	5	7	1st order	2nd order	3	5	7
Cm	0.1358	0.1305	0.1446	0.1305	0.1324	0.1342	0.1336	0.1369	0.1336	0.1302	0.1329	0.1288	0.1423	0.1288	0.1279
Cp	0.5432	0.5220	0.5784	0.5220	0.5296	0.5368	0.5344	0.5476	0.5344	0.5208	0.5316	0.5152	0.5692	0.5152	0.5116
Total CPU Time (Second)	572741	507624	432386	507624	622812	148202	122633	72580	122633	167051	137770	129613	82265	129613	176493
Total CPU Time (Hour)	159	141	120	141	173	41	34	20	34	46	38	36	23	36	49

2.3.6 Solver settings

The commercial CFD solver STAR-CCM+ is used to perform all simulations in this paper. The solution methods used for this software are set as follows: the implicit unsteady segregated flow method with the linkage between continuity and momentum equations using a predictor-corrector approach. The SIMPLE algorithm is selected for coupling the pressure-velocity equation and the SST k-Omega turbulence model. In the current research, a second-order upwind scheme is set up for the convection terms. The calculation of 15 revolutions of the VAWT will be performed while the Cp values are calculated from the last 2 cycles.

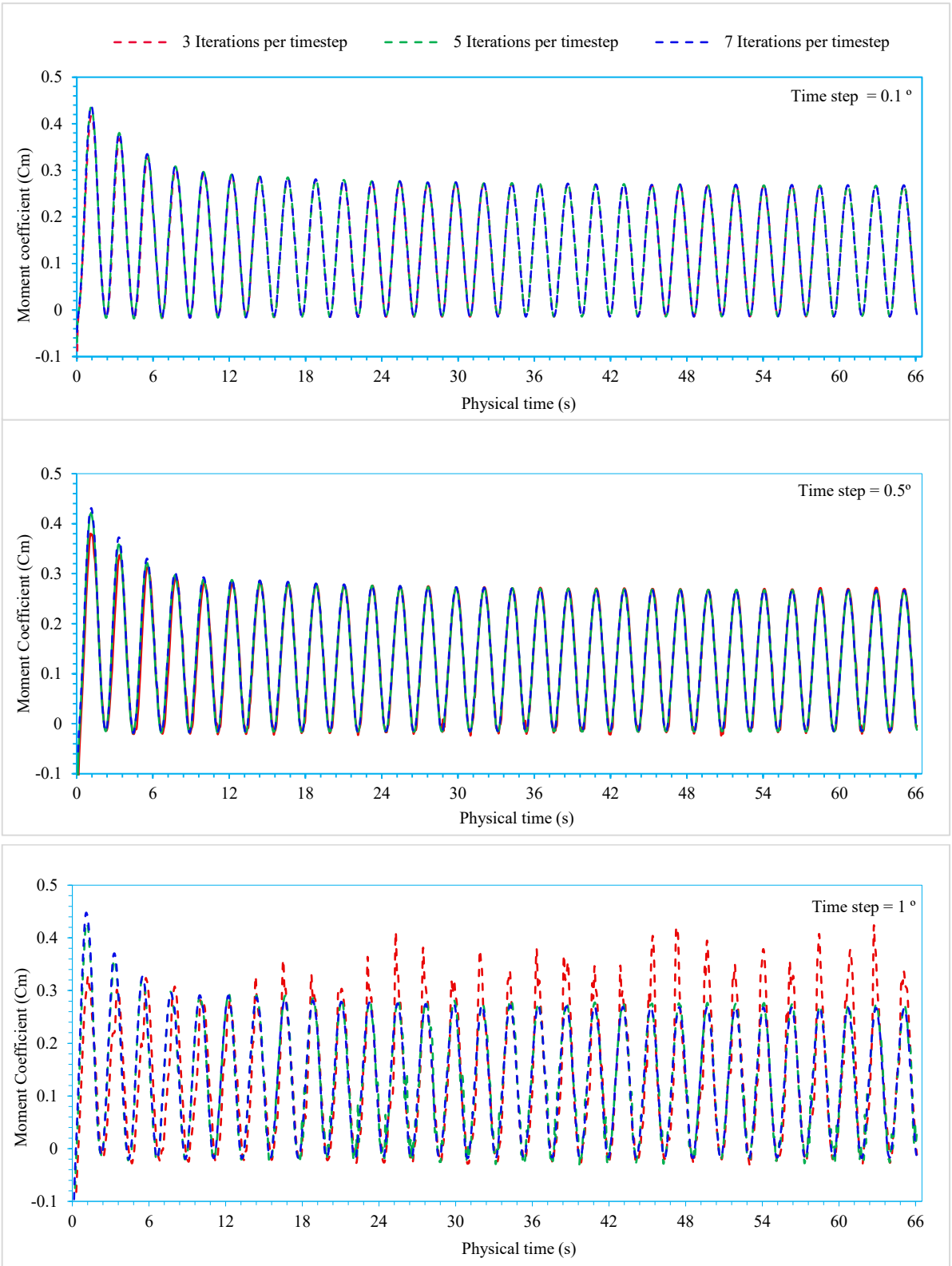

Figure 2-10: Instantaneous moment coefficient for the full 15 turbine revolution for different number of iterations by time step.

2.4 Model validation and analysis

2.4.1 Model validation

Using the selected parameters as identified in the previous section, such as a time step of 0.5 degrees and 5 iterations for the time step, the power coefficient (Cp) curve is compared with experimental data obtained for an H-Darrieus wind turbine by Mays et al. [63], Bedon et al. [62] and Molina et al. [24]. Both 2D and 3D simulation results are compared in Figure 2-11 and Figure 2-12. As expected the numerical values are higher for 2D results as the wind tip effects are not captured with the 2D model. In Figure 2-12, 3D simulation results for the large turbine show a good agreement for all TSRs when using the very fine Mesh 3. Similarly, the 3D results for the small turbine compare well with the results obtained by Molina et al. [24]. Therefore, the computational modeling strategy presented can be used to calculate the power coefficient for H-Darrieus rotors.

2.4.2 Effect of turbulence intensity

2.4.2.1 Small H-Darrieus VAWT (D=0.5m)

As indicated by Molina et al. [24], the effect of turbulence intensity and the scale length on the power coefficient are important. Their work investigated different turbulent intensities 0.7%, 9.2%, and 14.8%, in a wind tunnel. Here the same turbulence intensities are simulated to evaluate if the CFD code can capture the same behavior. Two different types of CRI and VUB wind tunnels were used to test the influence of turbulence intensity on the performance of the H-Darrieus turbine. The results obtained by the CRI wind tunnel were chosen to compare with our simulation results since the latter gave a higher power coefficient. However, a fixed value of scale length Lux=0.09m is taken for all our calculations because it corresponds to the maximum Cp obtained by the higher Turbulence intensity Iu = 14.8% as shown in Ref. [24].

In order to test the influence of the Reynolds number on the performance of the H-Darrieus turbine, four Reynolds number values: Re = 267000, Re = 300000, Re = 333000, and Re = 367000 are chosen. Figure 2-13 shows the Cp values obtained from the simulations performed by the STAR CCM+ software and compares with the power coefficient Cp obtained experimentally for Re = 267000 with the turbulent intensity of 0.7%, and Re = 300000, Re = 333000 with turbulent intensities of 9.2% and 14.8%. Simulation results show a good comparison at Re = 333000 but some discrepancies are observed for Re = 300000.

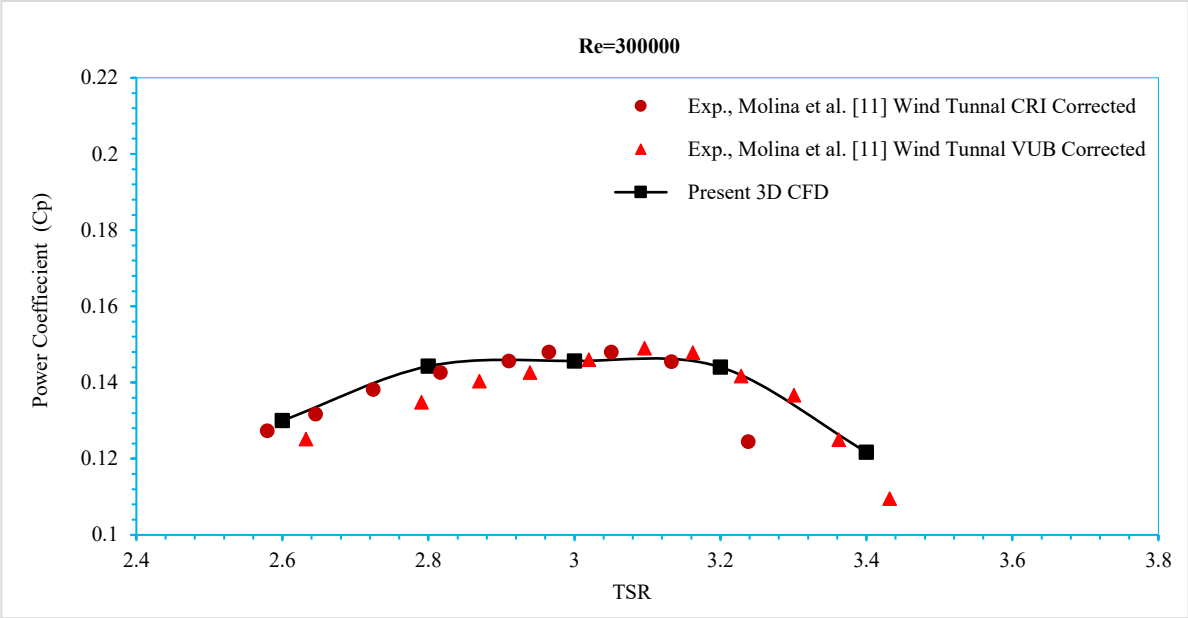

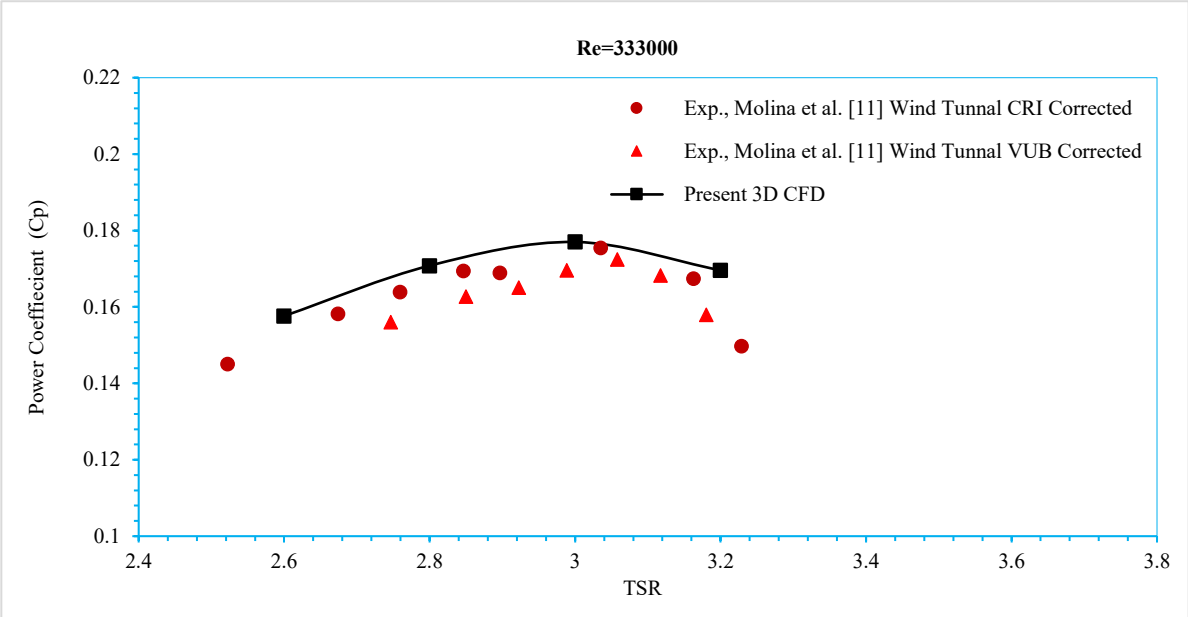

Figure 2-11: 3D Validation of present computational model for the small H-Darrieus VAWT (D=0.5m). Compared to experimental data [24].

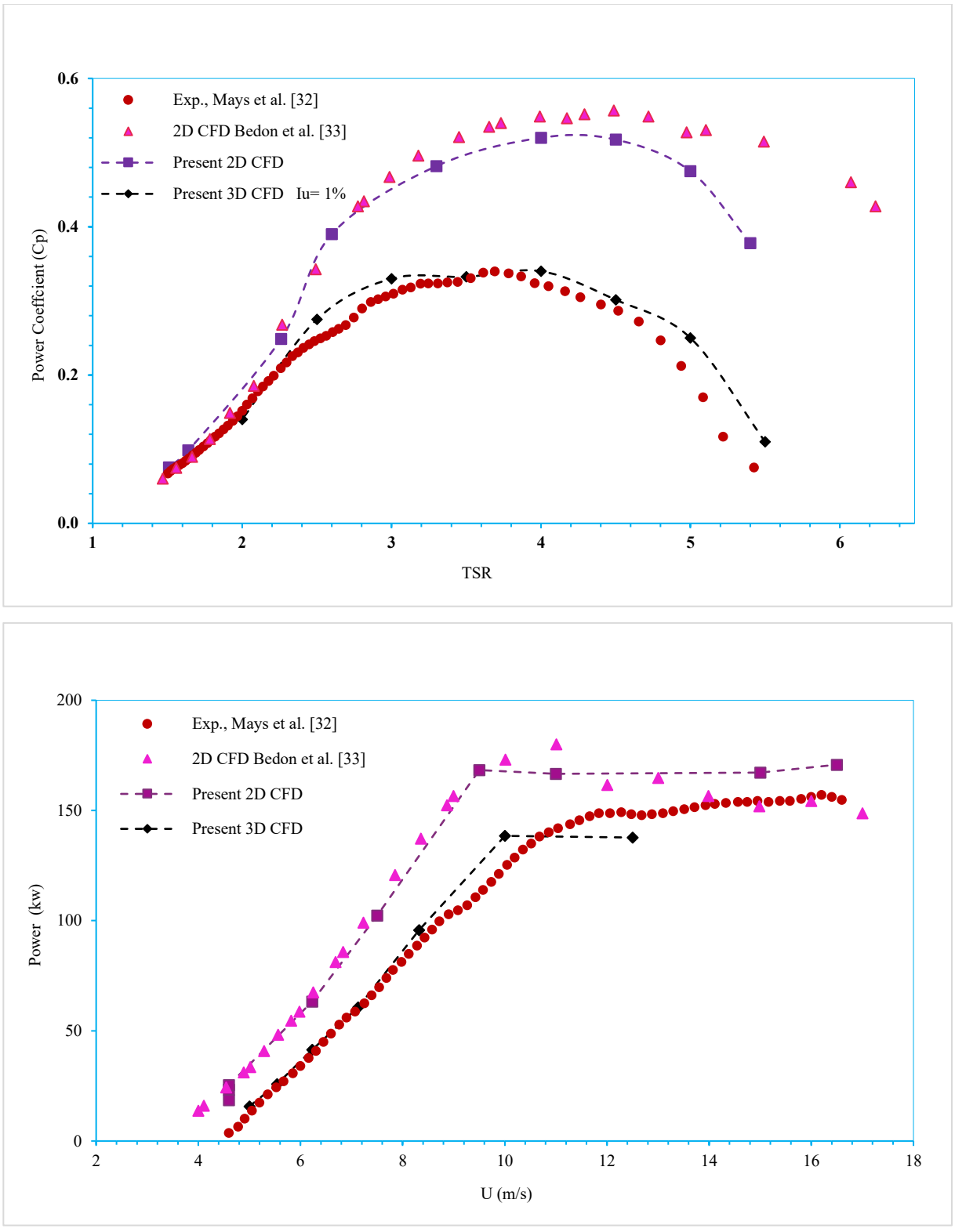

Figure 2-12: Validation of present computational model for the big H-Darrieus VAWT (D=35m). Compared to experimental data [63] and simulation of [62].

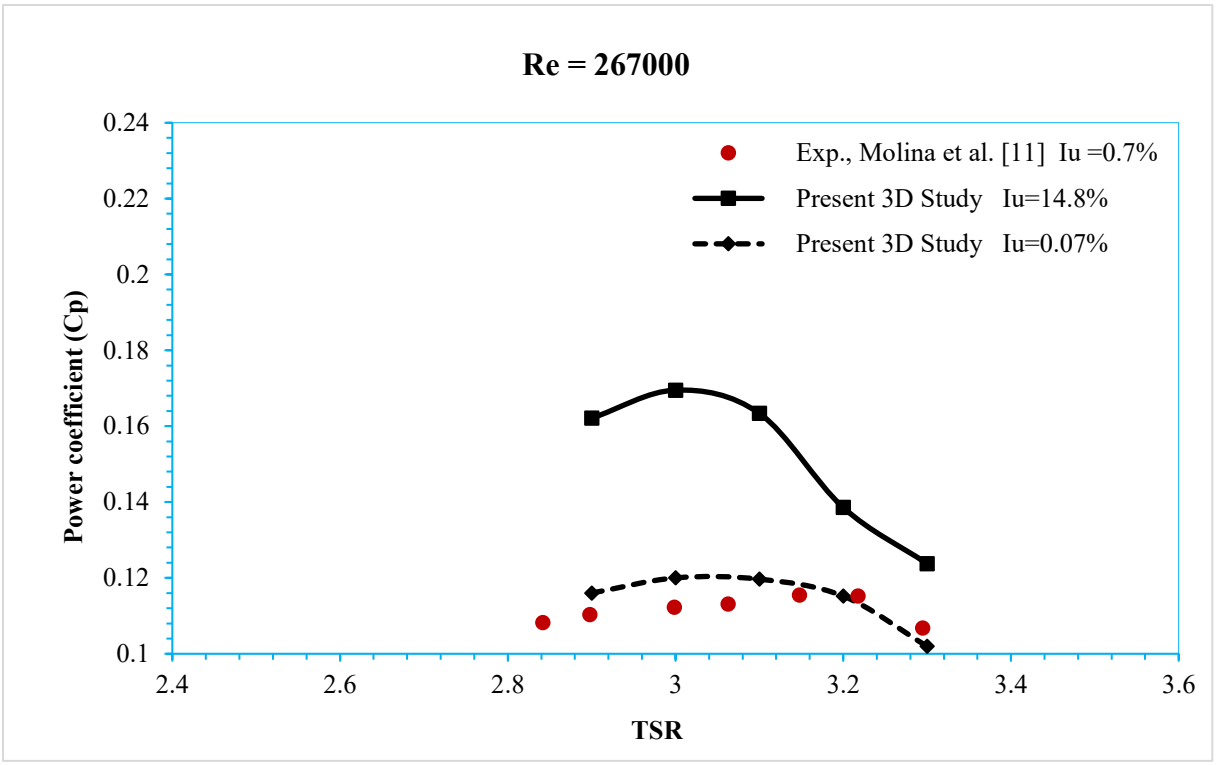
Re = 267000
Power coefficient (Cp)
TSR
Exp., Molina et al. [11] Iu =0.7%
Present 3D Study Iu=14.8%
Present 3D Study Iu=0.07%
0.24
0.22
0.2
0.18
0.16
0.14
0.12
0.1
2.4
2.6
2.8
3
3.2
3.4
3.6

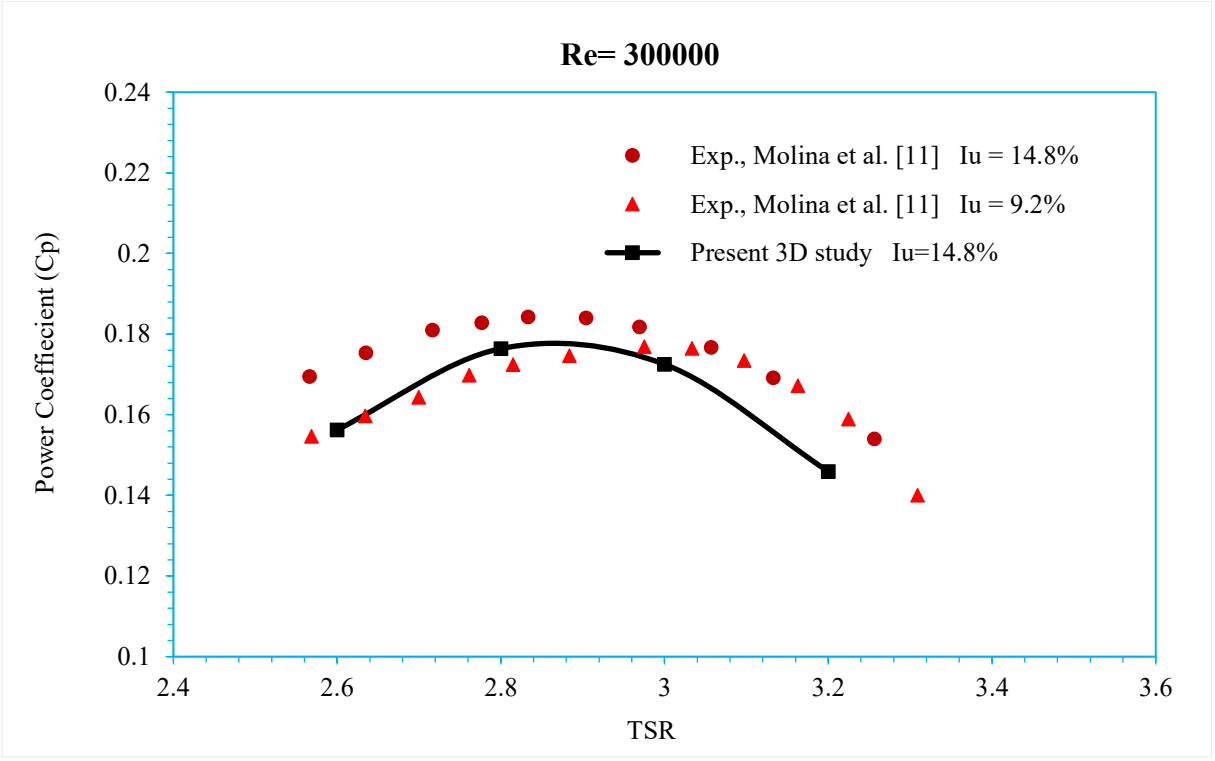
Re= 300000
Power Coeffiecient (Cp)
TSR
Exp., Molina et al. [11] Iu = 14.8%
Exp., Molina et al. [11] Iu = 9.2%
Present 3D study Iu=14.8%
0.24
0.22
0.2
0.18
0.16
0.14
0.12
0.1
2.4
2.6
2.8
3
3.2
3.4
3.6

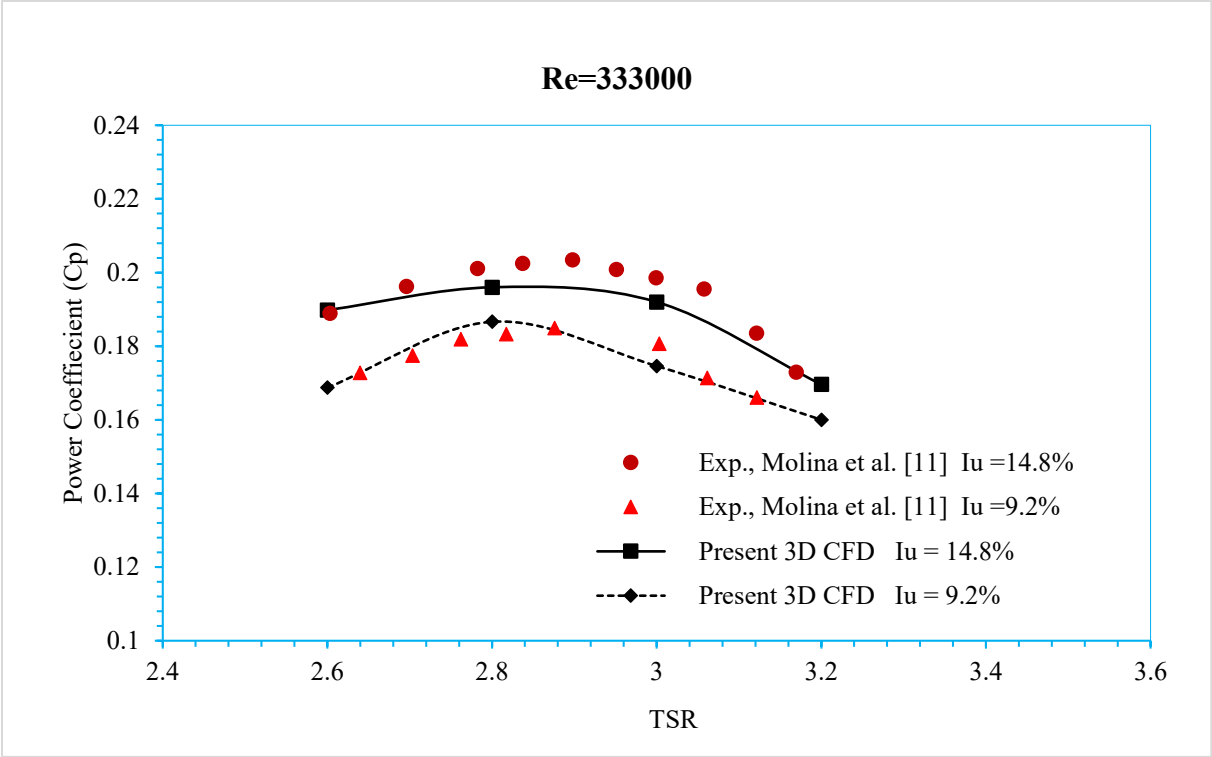

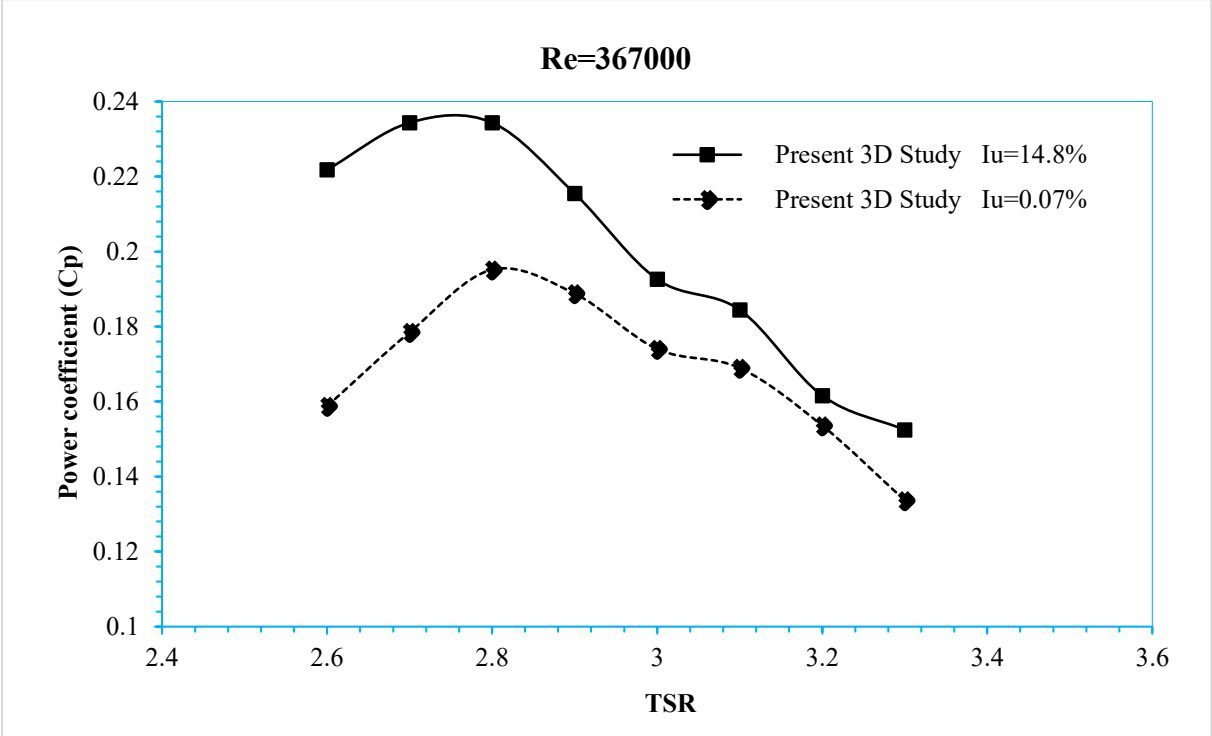

Figure 2-13: Power coefficient curves compared against the corrected curve obtained at the CRIACIV wind tunnel, at a Re = 267K, Re = 300K, Re = 333K, and Re = 367K.

These discrepancies are not explained at this point; therefore, further analysis focuses on results from Re =333000. Furthermore, using the same value of turbulence intensities, the study is extended for Reynold numbers 267000 and 367000, to prove that the increase of turbulence intensity enhances the performance of the vertical axis wind turbines.

It is clearer from Figure 2-13 that the power coefficient values are higher by increasing the turbulence intensity for the four cases of Reynold numbers investigated. This improvement is due to the significant delay of dynamic stall of the turbine blades as suggested in [66], [67]. The higher Cp values appear to be higher, especially at a low tip speed ratio where the dynamic stall is more dominant. As well, Dabiri et al. [15] and Molina et al. [24] report that the turbulence phenomenon could also improve the recovery of the wake, reducing the negative influence of the upstream blade on the downstream one, which in fact can reduce the performance of the wind turbine, the latter, is more relevant for small-scale wind turbines with high rotational speed and small diameter (ω = 1200 rpm, D = 0.5).

To illustrate the improvement of the performance of the small wind turbine NACA0018-0.5m, the moment coefficient versus azimuth angle for the two last cycles (one blade and two blades) are plotted. Figure 2-14 shows the instantaneous moment coefficient for the last two revolutions for different turbulence intensities Iu=0.7% and Iu=14.8%. The curve representing the moment coefficient obtained with Iu=14.8% is higher than that obtained by Iu=0.7% mainly after a 90-degree azimuthal angle which indicates that the boundary layer is more attached to the airfoil. By comparing both curves, note the difference in the negative values of the moment coefficient at a 150-degree azimuthal angle which indicates a less severe separation of the boundary layer.

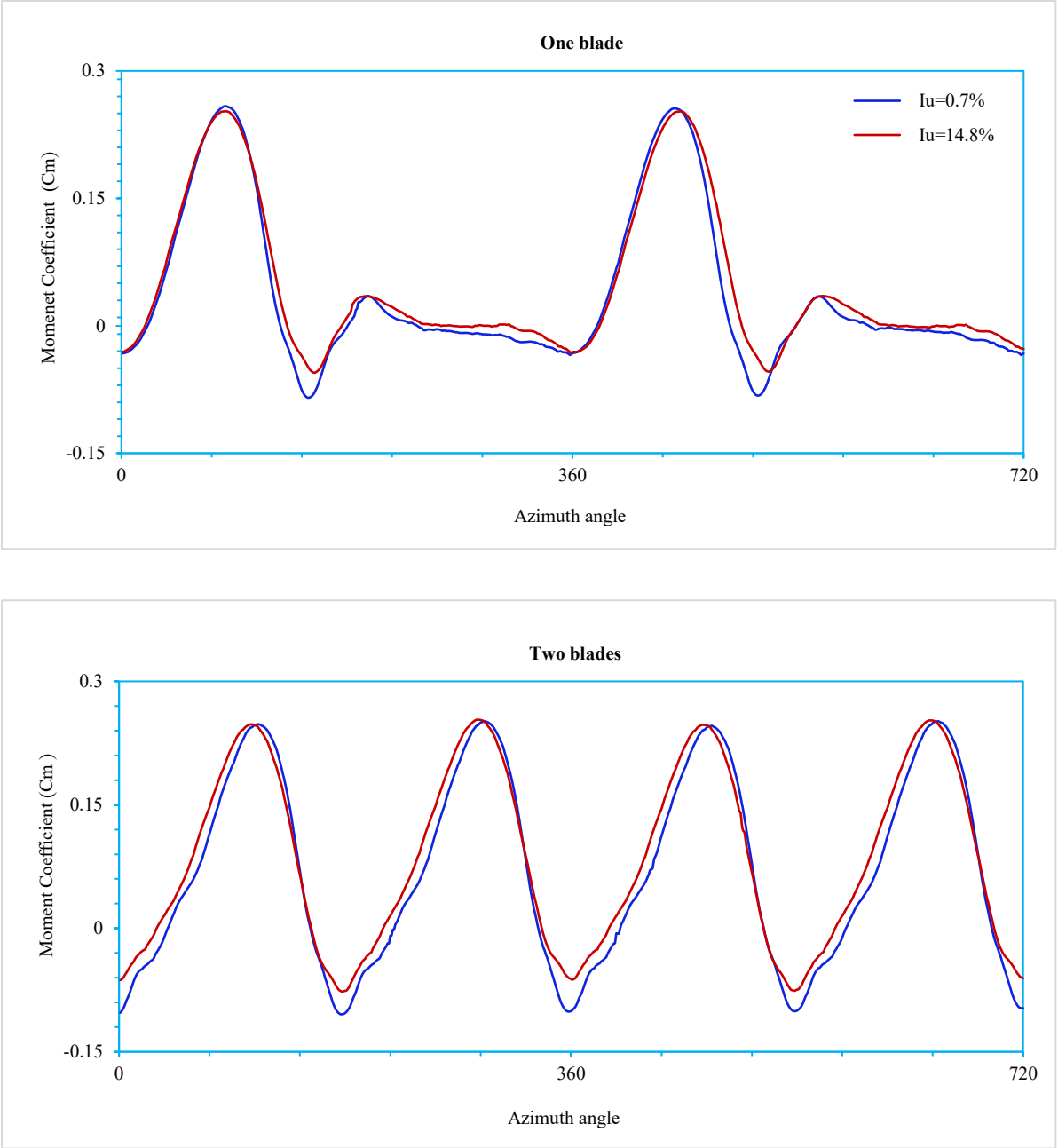

Figure 2-14: Instantaneous moment coefficient versus azimuth angle for 2 turbine revolutions for one blade and two blades.

In Figure 2-15, a very clear increase in the peak power coefficient is noted as turbulence intensity is increased. The numerical simulation results are also in very good agreement with those obtained experimentally for both Reynolds number cases. The numerical results confirm the same trend as the experimental data which is the increase of performance of the H-Darrieus turbine by

increasing the turbulence intensity up to 15% intensity. There is no large difference between the experimental data and those obtained from simulations. Furthermore, the value obtained in the PoliMi wind tunnel [68] seems to correspond to the observed trends for the same Reynolds number. All experimental and numerical values of the power coefficient increase linearly with the increase of the level of the intensity of the turbulence to reach a Cp = 0.22. But this increase stops when the turbulence intensity reaches 20%, as shown in Figure 2-15 as no considerable improvement in Cp is observed when the intensity increases from 20% to 40%. This effect can be linked to the fact that turbulence intensity higher than 20% does not improve the stall characteristics of the blades.

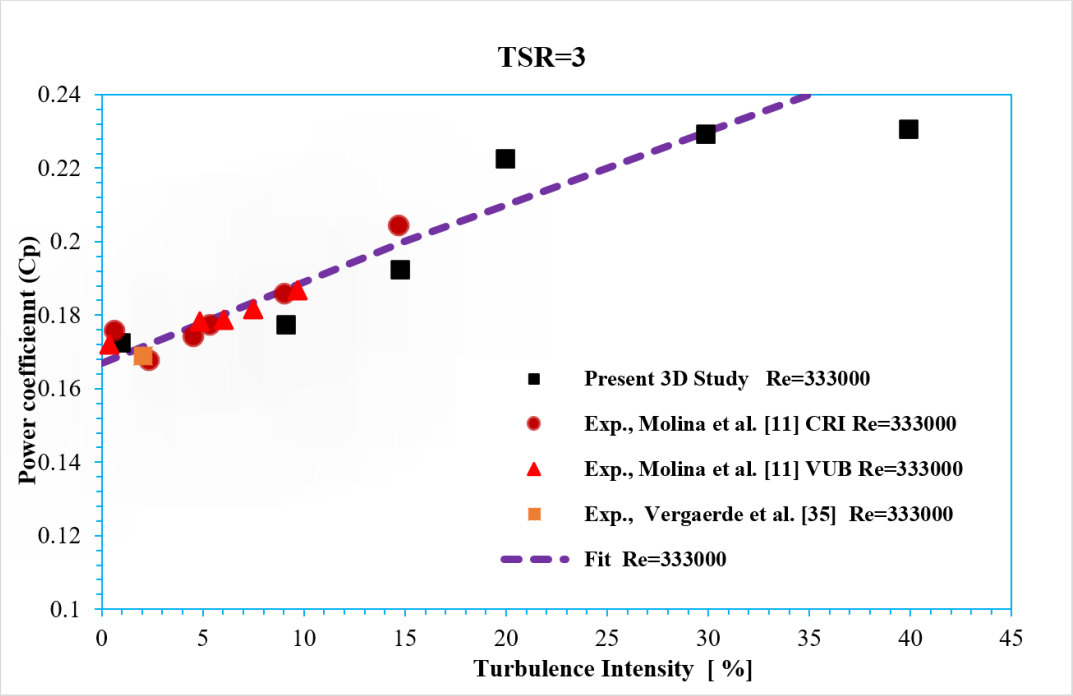

Figure 2-15: Power coefficient obtained by present simulations against different intensity turbulence levels.

2.4.2.2 Large H-Darrieus VAWT (D=35m)

In this section, the influence of turbulence intensity on the performance of a large wind turbine is analyzed. The same simulation model used above is used on an H-Darrieus vertical axis wind turbine (Diameter = 35m). Note that, the same parameters and boundary conditions are used for the validation case. Power Coefficient computed values are reported in Figure 2-16 for 3 turbulence intensities: 1%, 15%, and 30%. Note that the simulation geometry has no axial column

which may explain the small difference between the experimental data and the CFD results. Nevertheless, previous sections show that the CFD methodology can capture the effect of the turbulence intensity therefore there is very little uncertainty with respect to the turbulence intensity effect. The curves do overlap because the physics of the flow is such that the turbulence intensity does not change the flow over the blade. Therefore, for the large-scale wind turbine studied herein, the turbulence intensity appears to have no effect. More studies should be performed to confirm this conclusion for a larger set of wind turbines.

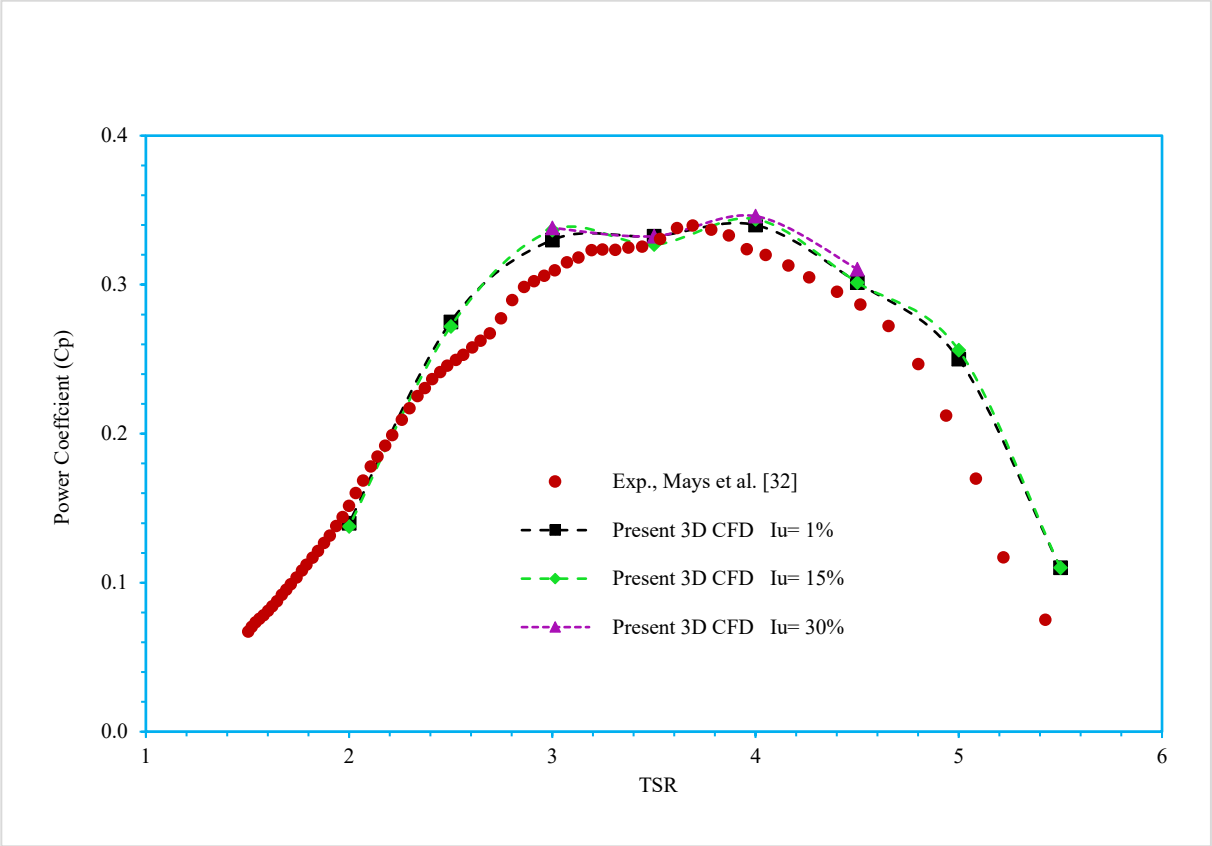

Figure 2-16: Power coefficient curves for different turbulent intensities compared against experiment data.

2.4.2.3 Comparison of the flow between the two turbines

To understand these flows, the velocity contours, the pressure contours, and the vorticity amplitudes along the horizontal plane, at the same azimuth angle $\theta = 150°$ and the same turbulence intensity of 14.8% for both wind turbines are presented in Figure 2-17 and Figure 2-18. Note that the Reynolds numbers calculated on the basis of the diameter and a fixed input wind speed of 10

m/s for the small and large wind turbines are: 333,000 and 23,340,000 respectively. This azimuth angle is selected because it is just before the region with the highest Cp difference between the turbulence intensities of the smaller turbine.

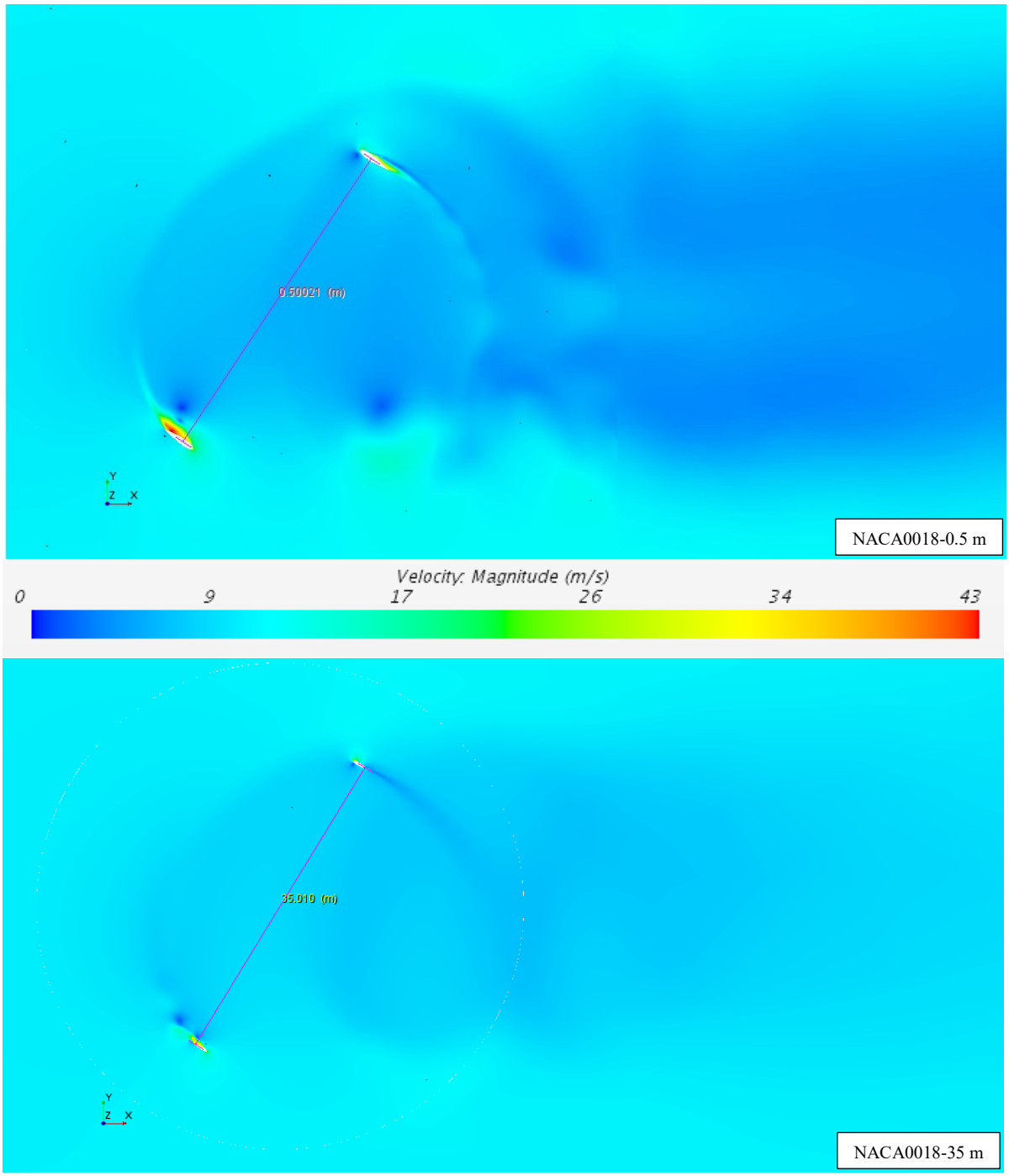

(a) Velocity

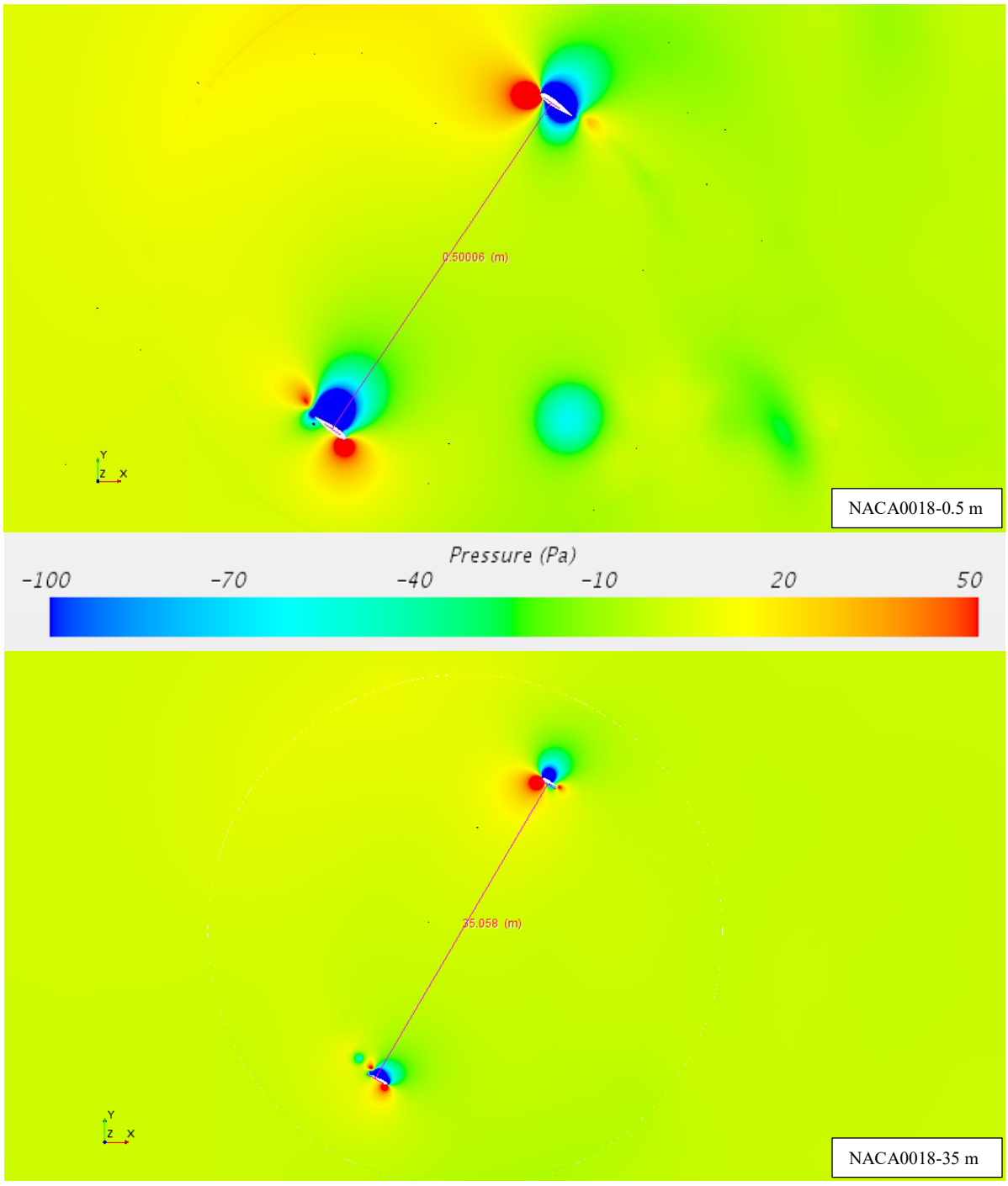

(b) Pressure

Figure 2-17: Instantaneous velocity (a) and pressure (b) contours around the blades for NACA0018-0.5m and NACA0018-35m with turbulence intensity of Iu=14.8 % at θ = 150°.

As shown in Figure 2-17, the small wind turbine creates a zone of lower velocity around and behind the turbine which implies that the turbine creates a larger wake. On the other hand, the larger wind turbine only generates a weak wake. Clearly, the higher solidity of the small turbine slows down the wind, not only in the wake but also as it approaches the turbine. This is also a reason why the Cp for the small wind turbine is smaller than the large wind turbine as the smaller turbine effectively sees a slower wind velocity. When analyzing the vorticity in Figure 2-18(b) and (d), the vorticity over the blade of the smallest turbine is much higher than the vorticity seen over the blade of the larger turbine.

Note that the chord length for the large turbine is 35 times the chord length of the small turbine. Figure 2-19 shows the vorticity at azimuthal angle $\theta = 168°$. For the large turbine, a vortex is attached to the trailing edge of the blade at both $\theta = 150°$ and $\theta = 168°$ but for the smaller turbine, the vortex only appears at $\theta = 168°$.

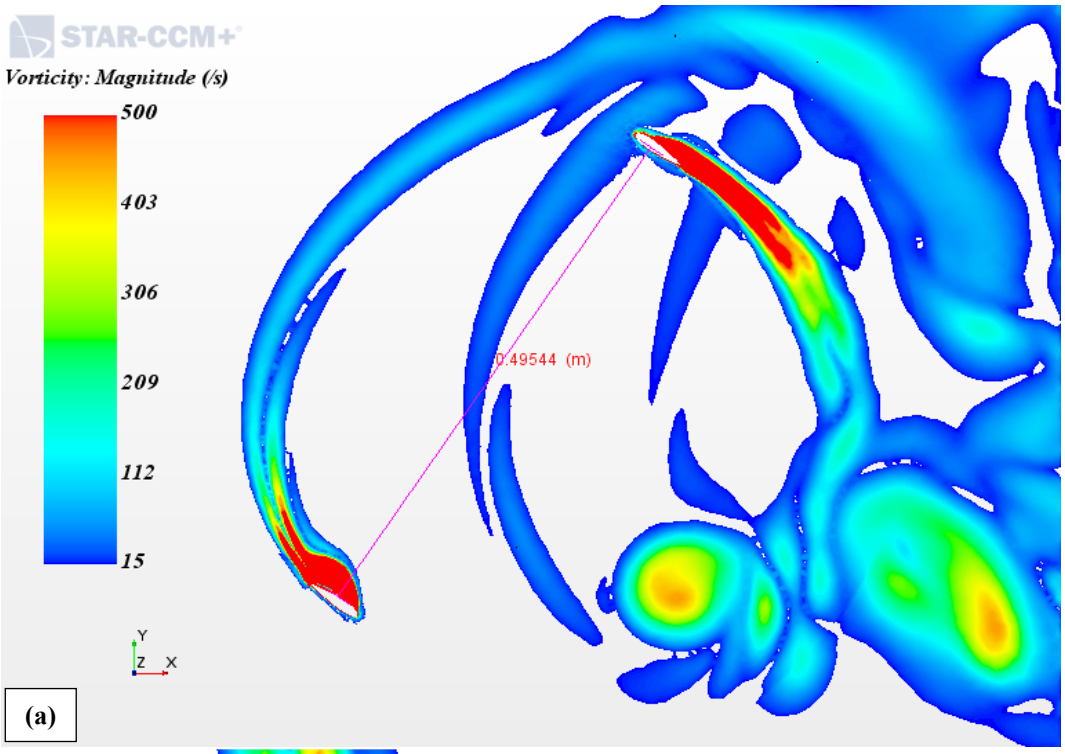

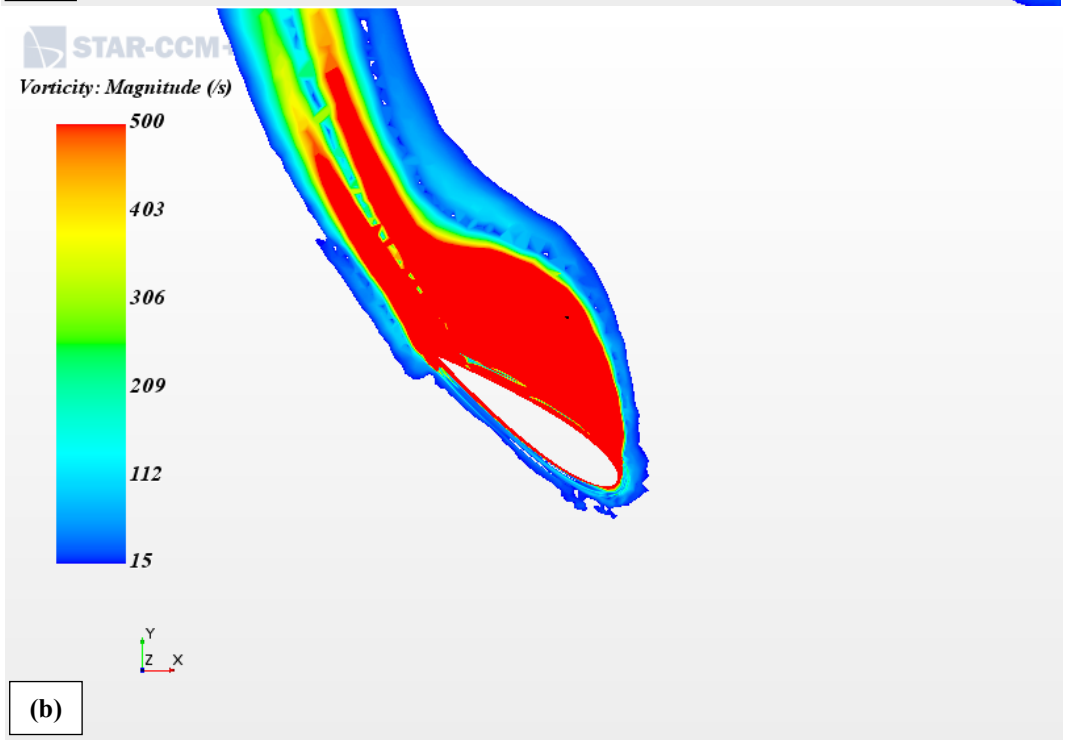

NACA0018-0.5 m

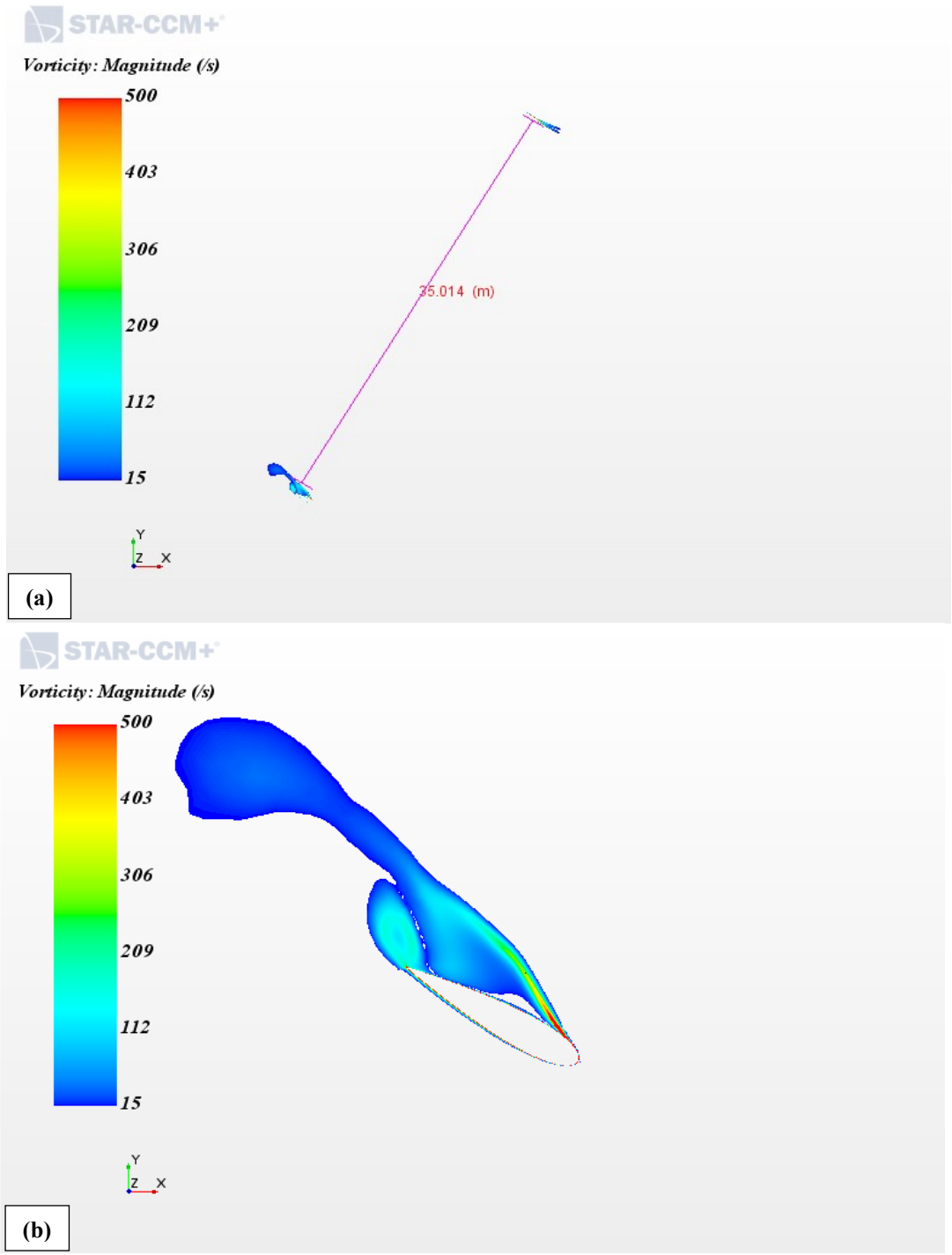

NACA0018-35 m

Figure 2-18: Instantaneous vorticity magnitude contours around the blade for NACA0018-0.5m and NACA0018-35m with turbulence intensity of Iu=14.8 % at θ = 150°. (a) Top view of 2 blades, (b) Zoom on one blade.

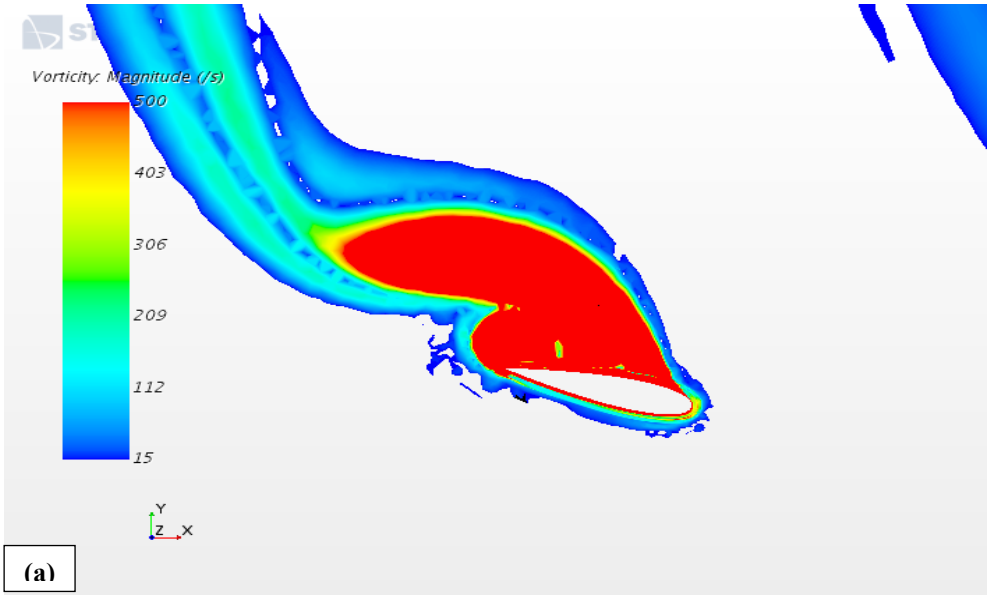

NACA0018-0.5 m

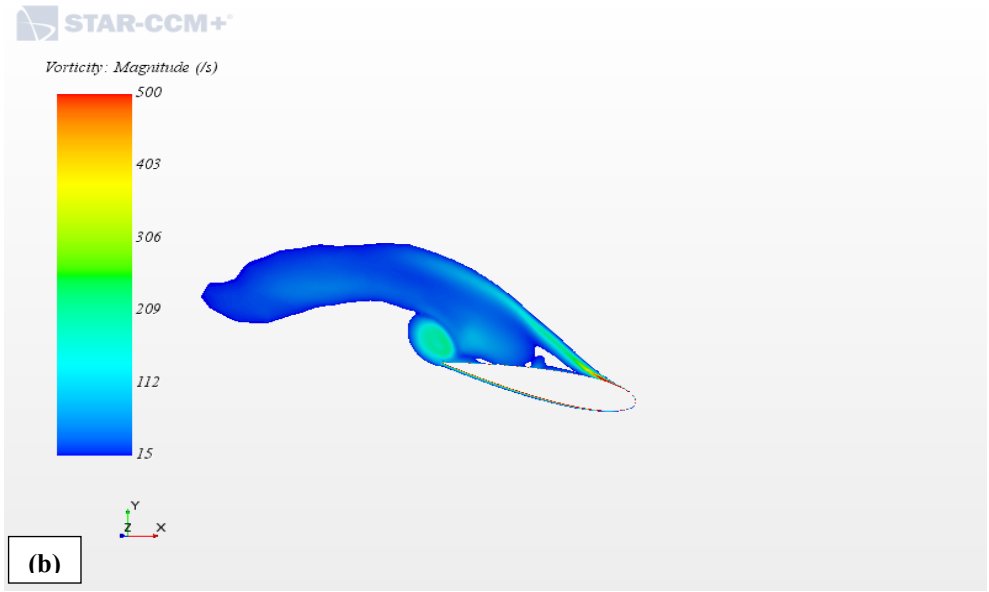

NACA0018-35 m

Figure 2-19: Instantaneous vorticity magnitude contours around the blade turbulence intensity of Iu=14.8 % at θ = 168°. (a) NACA0018-0.5m, (b) NACA0018-35m.

This vortex does not exist for a turbulence intensity of 0.07% as shown by the vorticity iso-contours in Figure 2-20 for the small wind turbine blade at azimuthal angle θ = 168°. This vortex only appears when the turbulence intensity is increased because the flow has more energy, also, as in three-dimensional flows, such as two-dimensional vortex loses its coherence when the flow

presents strong background turbulence. This vortex increases the turbine moment generated by the blade and therefore the performance of the turbine. The dynamic stall feature is only observed for the small turbine as the flow over the blade of the large turbine did not change with increased turbulence intensity. Note that the effect of blade tip vortices on the downstream blades is captured by the simulation, however, no major effect is observed, where the vortex doesn't improve the dynamic stall of the blades of the large wind turbine which leads to no increase in the generated moment coefficient.

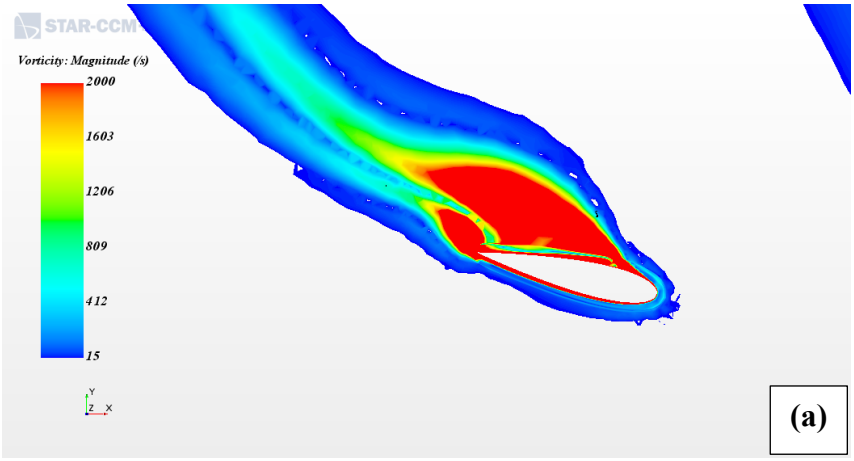

Iu= 0.07%

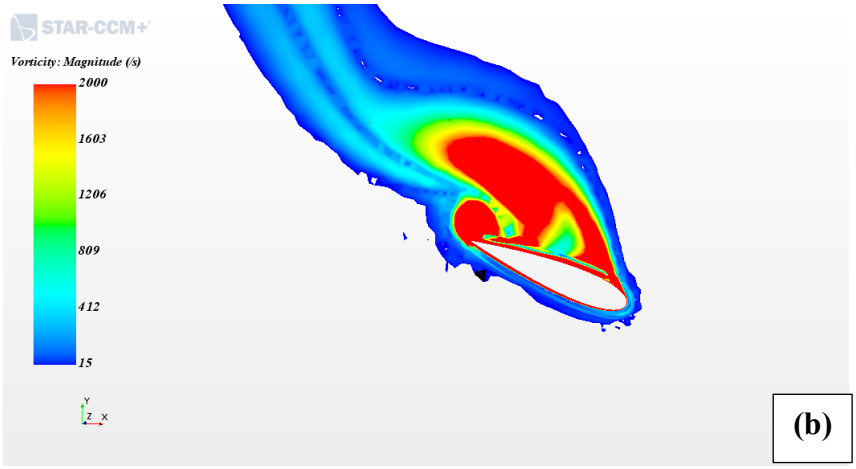

Iu= 14.8%

Figure 2-20: Instantaneous vorticity magnitude contours around the small turbine blade at θ = 168°. (a) Iu=0.07 %, (b) Iu=14.8 %.

2.5 Conclusions

The main purpose of the present work is to show that the effect of turbulence intensity can be captured with CFD and that this effect is limited to small-scale turbines. Two H-Type Darrieus vertical axis wind turbines were used for validation based on experimental data found in the literature. Details of the simulation setup, meshing methodology, and time step selection are reported in the paper. The influence of the time step, the number of iterations per time step, and the type of discretization schemes on the calculation of the coefficient moment is studied. It was found that a time step equivalent to 0.5° of blade rotation with 5 iterations per time step, and a second-order discretization scheme were more appropriate to use in the setting parameters in STAR CCM+.

The influence of turbulence intensity on the power performance of a small H-Darrieus Vertical Axis Wind Turbine is considerable but limited, such that the power coefficient is improved by 22 % when the turbulence intensity is increased from 0.7% to 20% but stops increasing after this value. When the turbine size was studied, the turbulence intensity had no effect on the performance of a large wind turbine. This effect can be linked to the fact that the large-scale turbine has a blade Reynolds number about 40 times higher than the Reynolds number of the flow on the blade of the small wind turbine. This result confirms that the dynamic stall is influenced by turbulence intensity but this influence decreases as the Reynolds number of the flow over the blade increases. In this work, the impact of the turbulence intensity has been assessed and a range of behaviors has been identified.

3 CHAPTER 3. ARTICLE 2: CFD modeling of Vertical Axis Wind Turbine Wake Interaction

The content of this chapter has been published as a peer-reviewed paper:
BELABES, Belkacem et PARASCHIVOIU, Marius. CFD modeling of vertical-axis wind turbine wake interaction. Transactions of the Canadian Society for Mechanical Engineering, 2023.

Abstract:
Since wind turbines placed in wind farms need to minimize their footprint on the ground, the effects of the wake must be considered. Placement optimization, turbine spacing, and direction of rotation are known to affect the performance of vertical-axis wind turbines (VAWTs). However, rigorous numerical modeling methodologies that investigate the influence of these characteristics are lacking, especially in the case of large wind turbines. The goal of this study is to analyze turbine configurations that might enhance the power production of VAWT farms using 2-dimensional CFD models based on the Star CCM+ package. The novelty of this work is to analyze wind farm configurations for very large turbines. This is important because large turbines are much more performant than small turbines and have a high value of the power coefficient. Results show that CFD simulations capture adequately the performance of wind turbines in farms with multiple VAWTs. In general, if a second rotor is spaced more than 10 turbine diameters downstream of the first rotor, the effect of the wake is less significant. Furthermore, a specific farm configuration with 5 VAWTs is investigated and shows a 20% increase in power output compared to the same number of turbines operating in isolation.

3.1 Introduction

Due to the depletion of fossil fuels and rising energy needs, wind energy offers clean, plentiful, renewable energy. Wind energy has been the fastest-growing energy source in recent years [50]. Wind turbines, which are the most prevalent equipment for harvesting wind energy, are divided into two types based on the direction of the rotating axis: vertical axis wind turbines (VAWTs) and horizontal axis wind turbines (HAWTs) [69].

Two pairs of counter-rotating and co-rotating vertical axis wind turbines were tested by Baloutaki et al. [49] for a free-stream wind perpendicular to the two side-by-side turbines. When

compared to the isolated situation, the counter-rotating setup improved each turbine's aerodynamic performance, while the co-rotating installation may slightly reduce the turbine performance. A vertical axis wind turbine operating downstream of a counter-rotating pair, perpendicular to the free-stream wind, was also investigated for different placements. Almost all configurations and wind speeds showed an improvement in the downstream turbine's aerodynamic performance.

The use of counter-rotating vertical-axis wind turbines (VAWTs) in order to achieve a higher power output per unit of land area is investigated by Dabiri [15]. During the summer of 2010, a full-scale field testing of 10-meter tall VAWTs of various counter-rotating configurations was undertaken. While modern wind farms with HAWTs produce 2 to 3 watts of power per square meter of land area, these field tests show that by arranging VAWTs in specific layouts higher power output per square meter is achieved. In conclusion, their results suggest that an alternative VAWT approach to wind farming has the potential to reduce the cost, size, and environmental impacts of wind farms.

In order to identify the main flow mechanisms contributing to the enhanced performance of a pair of turbines, [70] simulated two possible configurations of the counter-rotating VAWT pair, with various gaps between the two turbines, tip-speed ratios, and wind directions. For the case of two turbines side-by-side with respect to the incoming wind, the key mechanism identified is the change in lateral velocity in each turbine's upwind path due to the presence of the neighboring turbine, which makes the direction of local flow approaching the turbine blade more favorable to generate lift and torque. They discovered that the overall power of a staggered pair of turbines cannot exceed that of a pair of turbines placed side by side.

The investigations of numerous Darrieus VAWTs within an arrangement are summarised in Table 3-1. This table includes the following information: field observations, wind tunnel tests, low- to moderate-fidelity modeling, and high-fidelity CFD simulations have all been used in earlier studies.

Table 3-1: A summary of the research on Darrieus VAWT farms.

Author (date)	Method	No of rotor	Focus of study	Diameter (m)	Distance between rotors	Chord (m)	Solidity	Number of blade
Dabiri (2011)	Field measurement	6	Cp	1.2	14D	0.127	0.318	3
Sadra Sahebzadeh (2020)	CFD (URANS)	24	Cp	1	1.5D	0.060	0.060	1
Zanforlin et al. (2016)	CFD (URANS)	2	Cp	1.2	3D	0.128	0.320	3
Brownstein et al. (2019)	CFD (URANS)	2	Cp, wake	0.2	1.65D	0.045	0.675	3
Brownstein et al. 2016	LF (LRB)	2, 10, 18, 24	Cp, wake	0.31	6D	0.045	0.726	5
Baloutaki et al. (2016)	Wind Tunnul	2, 3	wake	0.3	3D	0.045	0.750	5
Lam & peng (2017)	Wind Tunnul	2	wake	0.3	2D	0,045	0.750	5
Chen et al. (2017)	CFD (DES)	2	Cp, wake	2.5	7D	0.400	0.480	3
Tavarnier et al. (2018)	LF (P/V)	2	Cp, wake	20	1D	1.000	0.150	3
Barnes & hughes (2018)	CFD (URANS)	5, 6, 9, 15, 16	Cp, wake	3.4	10D	0.136	0.120	3
Alexander et al. (2019)	CFD (URANS)	2	Cp, wake	1.2	1.5D	0.127	0.318	3
Peng et al. (2020)	CFD (URANS)	2	Cp	2.8	12D	0.420	0.450	3
Present study	**CFD (URANS)**	**2**	**Cp, wake**	**35**	**(2.5, 5, 10, 20, 30,40)D**	**1.750**	**0.100**	**2**

Note that the Unsteady Reynolds-Averaged Navier-Stokes (URANS) technique was widely used when utilising CFD simulations, which is mainly due to the low computational cost and good accuracy compared to other methods. Regarding the number of rotors used for the configurations, most studies have only investigated a double-rotor arrangement. However, there is a need to investigate multiple configurations such as rows of wind turbines. To this end, the behavior of VAWT in the wake of another turbine needs to be analysed, in particular for large turbine sizes. Large VAWTs are more efficient and therefore extract a significant amount of energy from the flow. Nevertheless, it is found that the studies of large VAWTs are very rare in the literature. The current research focuses on the effects of the relative distance (d) and size of the turbine measured by the diameter (D) of the turbines. Table 3-1 shows that most prior studies only considered relatively modest diameter size turbines. In the current work, a turbine with a diameter of 35m is investigated, which is about an order of magnitude larger than typical turbines studied in the literature.

The rest of the paper is organized as follows: Section 2 details the geometrical and operational characteristics of the turbines, computational domain, grid, solver settings, boundary conditions, respectively. Results and discussion follow in Section 3. Conclusions and perspectives are provided in Section 4.

3.2 Methodology

3.2.1 Turbine geometrical and operational characteristics

The turbine selected for this study is a large turbine used in the VAWT 850 demonstration project [63]. This turbine is rated as a 500-kW turbine and has a 35 m diameter. In order to reduce the computational costs, the turbine is simplified by excluding the shaft and the connecting rods from the geometry. Also, note that earlier studies have shown that these structural bodies result in a systematic drop in the turbine power performance [71], [72]. Therefore, neglecting these components is not expected to significantly influence the conclusions of this study. Note that the simulations are also performed in a 2-dimensional framework which leads to a higher power coefficient. The importance is to analyze the increase or decrease of performance related to the baseline configuration which is an isolated turbine. The simulated turbine is single-straight-bladed Darrieus H-type VAWTs, the important characteristics are reported in Table 3-2, and schematically depicted in Figure 3-1.

The geometrical and operational parameters of the turbines are provided in Table 3-2.

Table 3-2: Geometrical and operation characteristics of the turbines [63].

Parameter	Value
Number of blades, N [-]	2
Diameter, D [m]	35
Height, H [m]	24.30
Swept area, A [m^2]	850.5
Solidity, σ [-]	0.1
Airfoil chord length, c [m]	1.75
Airfoil shape [-]	NACA0018
Rotational speed, Ω [rad/s]	1.42
Freestream velocity, U∞[m/s]	10
Tip speed ratio (based on U∞), λ [-]	2.9

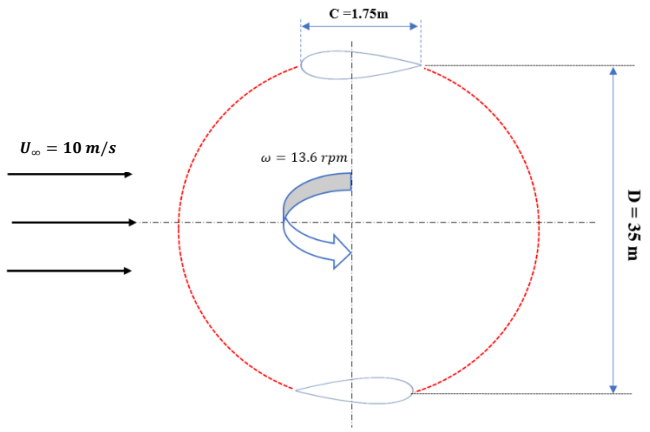

Figure 3-1: Important characteristics of the large vertical axis wind turbine selected.

3.2.2 Model set-up

To perform the simulations for this investigation, we utilized STAR CCM + version 12.06. An earlier study by [34] and [36] found that the turbulence model is essential to obtain the most accurate VAWT results when using URANS for 2-Dimensional CFD, identifying the SST k-Omega model which has become the most selected model [73]–[75]. A segregated flow-based solver was used. Boundary condition settings are as follows: at the inlet, a velocity inlet boundary condition with a velocity of 10 m/s is set. At the outlet, a pressure outlet boundary condition with a gauge pressure of 0 Pa as there is no forced pressure differential across the system is used. The

symmetry boundary condition is applied to the sides of the computational domain. The blades are modeled as walls as shown in Figure 3-1 and Figure 3-2. A time step equivalent to a one-degree rotation of the rotor is set for all cases [76]. To avoid the blockage effect, a blockage ratio ε=20 is respected as suggested by Kinsey et al. [77] for the case of 2-dimensional simulations.

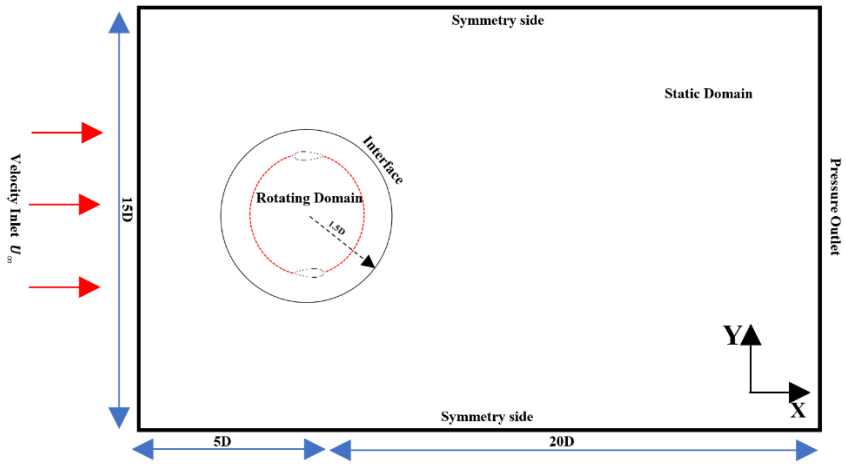

Figure 3-2: Schematic of computational domain with x and y distance indicated.

3.2.3 Computational domain

A 2-dimensional computational domain is used for this study. Note that the use of the two-dimensional domain is motivated by a lower computational cost but it is also justified by the findings of [71] in which a systematic difference between the results of the 2-dimensional and 3-Dimensional computational domains is observed.

The computational domain size is 15D × 25D (width × length). It is selected based on the best-practice guidelines for VAWT CFD simulations [71]. For all the simulations, there is a 5D distance between the upstream turbine's center and the domain inlet as shown in Figure 3-2. In addition, there is a minimum distance of 20D between the downstream turbine and the domain outlet. To guarantee the same distance between the symmetric side-boundaries and the upstream and downstream turbines, the longitudinal axis of the domain passes through the middle of the lateral distance of the two rotors. In other words, in all the simulations, ds1 = ds2. Furthermore, a minimum distance of 10D from the boundary sides of the domain is considered in all cases (ds1 = ds2 > 7.5D).

3.2.4 Mesh

The computational grid for the rotor and the arrangement in 2-Dimensional is illustrated in Figure 3-3, which consists of polyhedral cells. Considering the isolated wind turbine and the different arrangements according to various distances as shown in Figure 3-3(a), the number of cells ranges from ≈ 488 978 for the isolated case to ≈ 2357980 cells for the case of 40 rotor diameter distance between rotors. The Mesh independence study has been carried out for wind turbines studied here by [76].

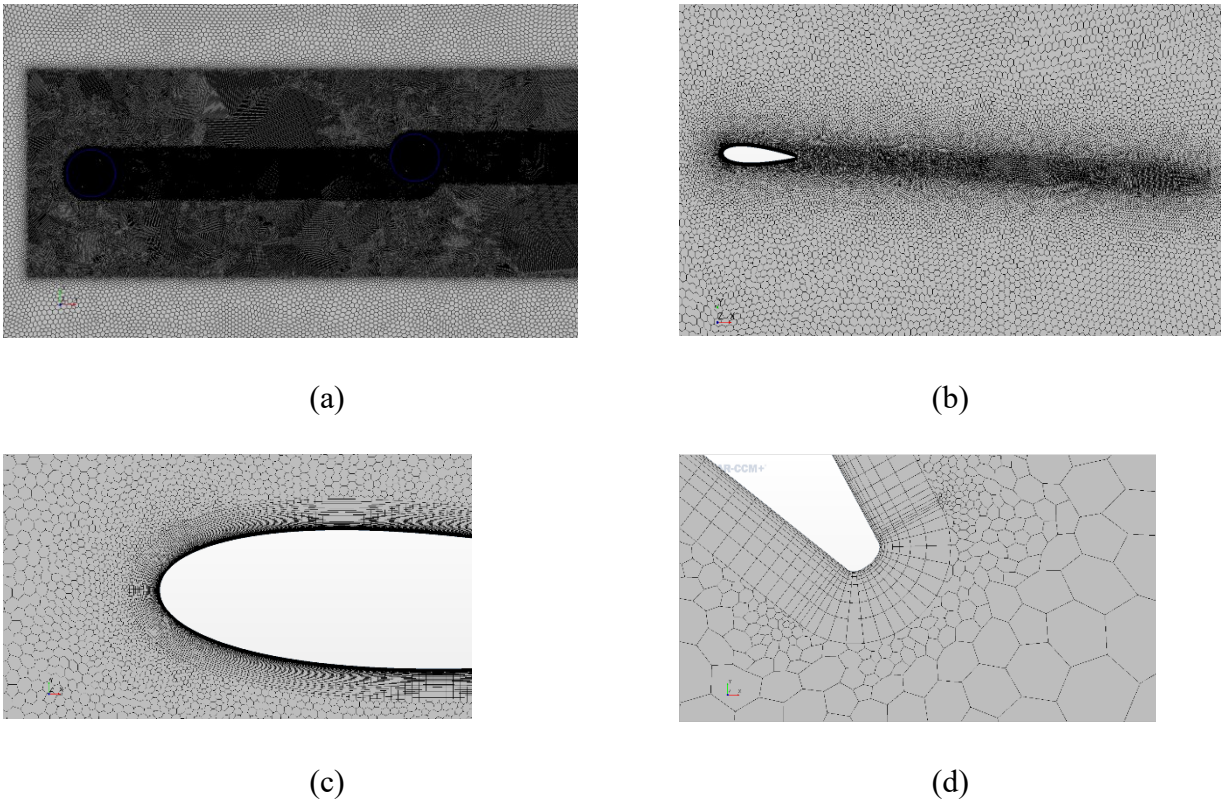

(a) (b)

(c) (d)

Figure 3-3: 2-dimensional computational grid for a sample double rotor arrangement.

To capture the boundary layer, the maximum and average Y+ on the blade of each wind turbine is less than 1 for all cases, as shown in Figure 3-4. Furthermore, for the boundary layer, 750 cells are created along the blade circumference as observed in Figure 3-4(b), (c), and (d). In addition, two types of refinement are performed, one for the wake of the blade as shown in Figure 3-3(b), and the other downstream of each wind turbine as seen in Figure 3-3(a).

To identify the mesh with the fewest cells that produce reliable results, the mesh size is examined. The change in the output of interest, in this case, the moment coefficient, is used to

measure accuracy. To evaluate the impact of coarse, medium, and fine meshes, four different grid size values are set for the 2-dimensional geometry.

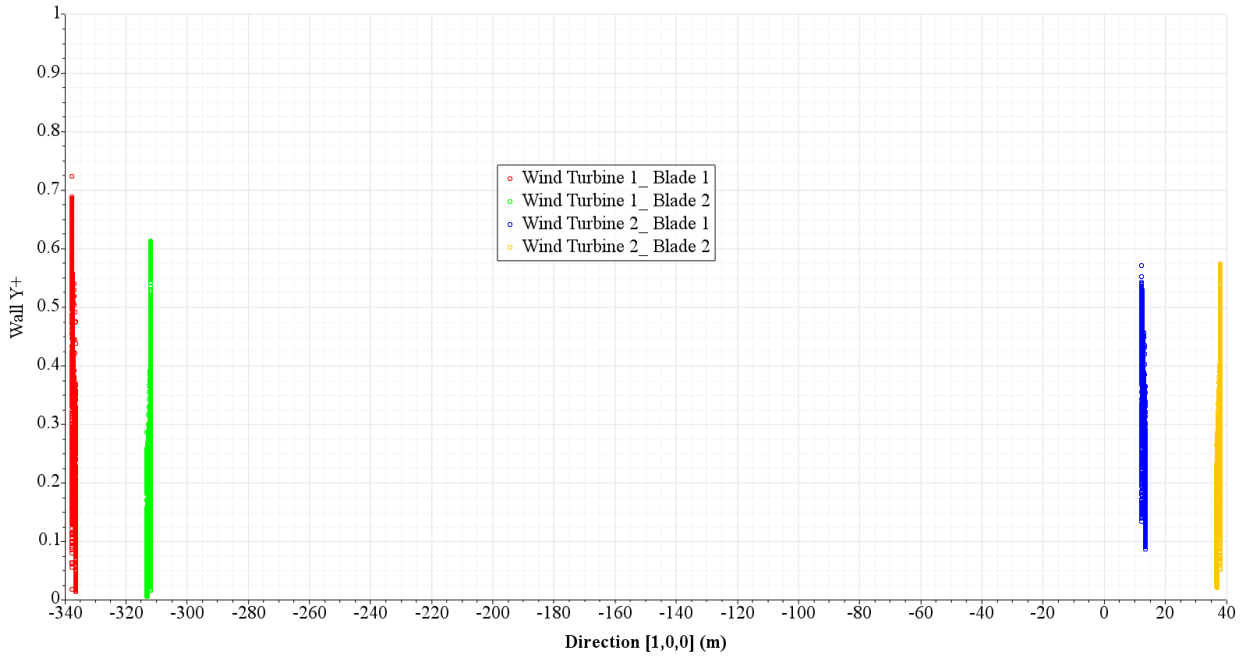

Figure 3-4: Y^+ distribution on all blade profiles for Wind Turbines on the finest mesh.

The various grid sizes on the surfaces of the blades are the primary distinctions between the four types of meshes. As seen in Table 3-3, the mesh M2 employs fewer elements while still providing a value that is comparable to the finest mesh. Therefore, for all 2-dimensional simulations, the mesh M2 is employed.

Table 3-3: Cycle-averaged moment coefficient (Cm) for refining the mesh size.

Mesh	**M4**	**M3**	**M2**	**M1**
Cell number	173784	350874	540390	775677
Moment coefficient (Cm)	0.1273	0.1275	0.12901	0.12905

The mesh size of all cases is reported in Table 3-4 and Figure 3-5, one can observe that the cell number growth is proportional to the increase in the distance between the first wind turbine and the second one, with respect to the long downstream wake refining of both rotors to ensure that the wake in these areas is well captured.

Table 3-4: Mesh detail for each distance case.

	Rotating domain	**Static domain**						
Cases	-	Isolated Turbine	2.5D	5D	10D	20D	30D	40D
Cell number	227719	261259	450600	505982	625316	1006208	1452580	1902542

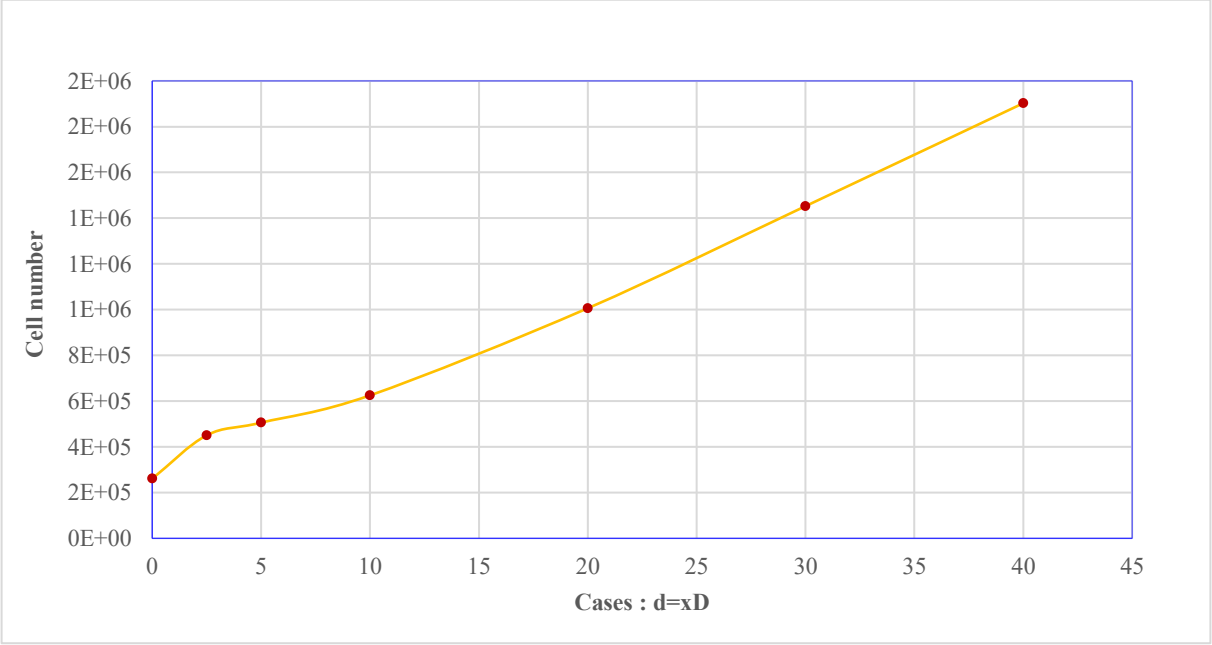

Figure 3-5: Mesh extension according to the evolution of distance.

3.3 Results and discussion

The scope of this study is to analyze a large-diameter wind turbine in different wind farm configurations. However, firstly a validation of the 2-Dimensional CFD approach is performed. Secondly, different configurations are simulated in order to analyze the wake and its effect on the performance of the huge wind turbine.

3.3.1 Validation

In this section, before the investigation of different configurations, two studies are carried out, the first type is a comparison of the present 2-dimensional and 3-dimensional CFD results by

the experimental data of [63] and the 2-dimensional numerical results of [62] respectively, the second is the relative performance of the second turbine using 2-Dimensional and 3-Dimensional simulations. For the first study, using the time step of 1º and 5 iterations for the time step as suggested in [78], after convergence of the moment coefficient of both wind turbines, the power coefficient (Cp) based on the average of the two last cycles is calculated for 2-Dimensional and 3-Dimensional models, the curves are compared with the numerical and experimental data obtained for the H-Darrieus wind turbine by [63] and [62] and presented in Figure 3-6.

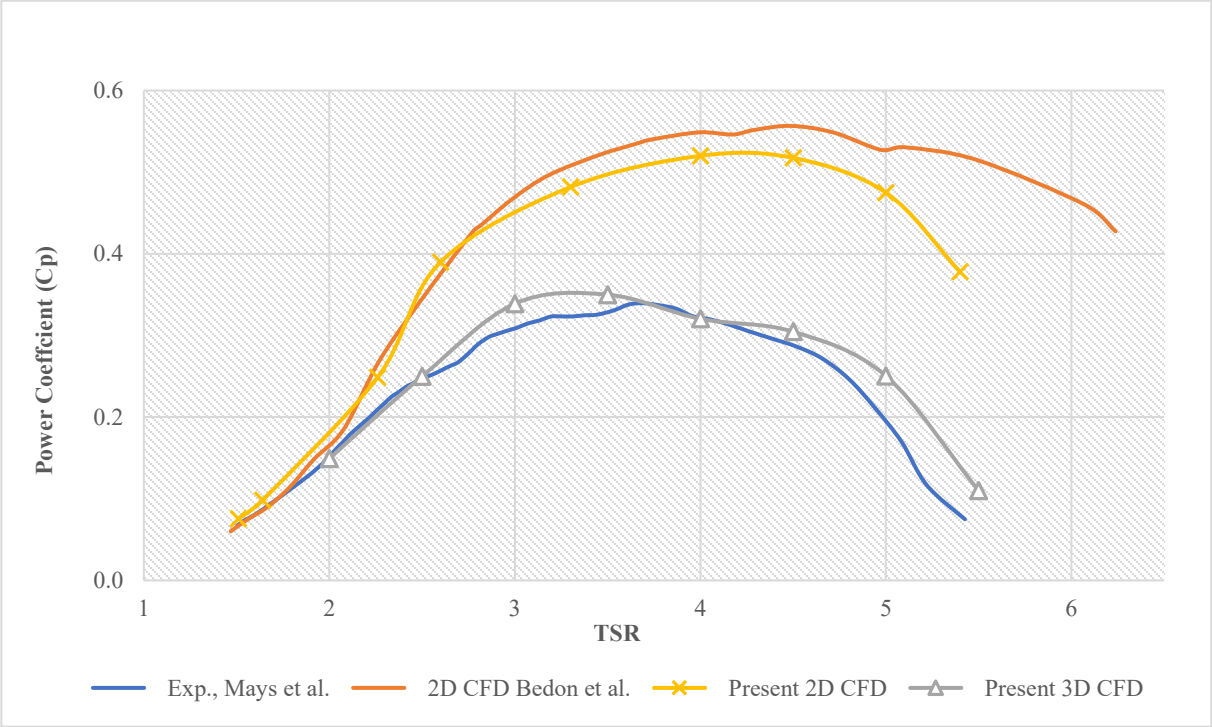

Figure 3-6: Validation of the present computational model [76].

As expected the numerical values are higher for 2-dimensional results as the wind tip effects are not captured with the 2-dimensional model. It is clear that the 3-dimensional computational modeling strategy presented provides an accurate evaluation of the power coefficient (Cp) for H-Darrieus rotors.

For the second study, aiming to validate the use of 2-Dimetional CFD modeling, the configurations of two wind turbines spaced by 2.5D are simulated using 2-dimensional and 3-dimensional models. The power coefficient (Cp) for each H-Darrieus rotor is calculated. The results are summarised in Table 3-5, for the purpose of comparing 2-dimensional and 3-

dimensional simulations regarding the precision, in particular, the ratio of $\frac{C_p2}{C_p1}$ is calculated for both cases.

Table 3-5: Comparison between 2D and 3D simulations.

	Case of 2.5D	
	2D Simulation	**3D Simulation**
Power coefficient of Wind turbine **1** (*Cp*1)	0.448	0.3094
Power coefficient of Wind turbine **2** (*Cp*2)	0.0325	0.0273
Ratio : $\frac{C_p2}{C_p1}$	**0.072**	**0.09**

Comparing the *Cp*2 for both cases, it is clear the second wind turbine is really affected by the wake of the first wind turbine that is due to the short distance between them. However, in terms of precision of the results, it is found that the ratio of 7.2% resulted for the case of the 2-dimensional model is relatively close to the ratio of 9% for the 3-dimensional model, therefore, it is concluded that using a 2-Dimensional simulation provides a good estimate of the interactions of the two turbines at a significant cost reduction.

3.3.2 Effect of different configurations

Different configurations with different numbers of wind turbines and positions are considered, in order to study the effect of the wake on the performance of the wind turbine downstream. This study firstly analyzes the effect of the downstream wake on the second turbine, and secondly, analyzes the wake downstream on rows of turbines.

3.3.2.1 Effect of the downstream wake on the second turbine

A series of simulations are performed to investigate the effect of the downstream wake of a large wind turbine with a diameter of 35 m. The first turbine was fixed and the second one was placed downstream at 2.5 times the diameter and as far as 40 times the diameter. According to the

rotation direction, the wake generated by the first wind turbine is different on each side, which led to the study of two different configurations. In the first configuration, the second wind turbine is installed on the starboard side of the first wind turbine in the direction of the wind, and in the second configuration, it is installed on the port side.

3.3.2.1.1 The second turbine installed on the starboard side of the first turbine:

To understand the effect of the spacing between vertical wind turbines on their performance, the power coefficient of each wind turbine is calculated and compared to the result of the isolated wind turbine. Note that two values of turbulence intensity are used for all cases. The power coefficient is shown in Figure 3-7 for different x-positions of the second wind turbine.

One can observe a minimal effect of the turbulence intensity on these results. For this large turbine, it is concluded that the turbulence intensity does not improve the dynamic stall characteristics of the turbine blades. It is also confirmed by [76]; however, a significant improvement is found in the case of small wind turbines. The overall power coefficient for the second wind turbine is decreased by about 60% compared to the isolated wind turbine. This diminution is maintained from d=2.5D until d=10D. After that, the Cp increases proportionally with increasing distance between the wind turbines. The wake of the first wind turbine creates a velocity deficit with significant vorticity, as shown in Figure 3-8.

In this Figure, the vorticity contours are presented for all cases identified as 2.5D to 40D, and the vortex is captured between vorticity values above 0.1 s^{-1} and under 1.0 s^{-1} for all cases. These contours show the shape of the wake downstream for both wind turbines and the interaction of the wake between them. This graphic depicts the wake's flow arrangement more clearly. For all the cases, the wake flow is divided into three sections, as seen in this picture. The predominant wake flow is on the upper and lower portions; however, it is weak in the center, this latest is created due to the large diameter of the rotor. The vortex' intensity is depicted by the color. Red indicates a higher vortex revolving until it turns blue or where the weaker vortex eventually loses strength. As an example, the wake strength disappears starting in the case of 20D and above, where the shape of the wake begins oscillating, knowing that at that stage, it lessens the impact on the second turbine, so the second wind turbine starts recovering its normal power coefficient. Note that initially the upper and lower parts of the vortex stream in a straight line with a relative mixing with the middle of the wake. At this point, both vorteces began to weaken, and the middle vortex either mixed with the second turbine's vortex or until it disappeared altogether. The overall view

illustrated in Figure 3-8 shows that the second wind turbine rotates entirely in the heart of the wake of the first wind turbine until d=30D, where afterward the second wind turbine starts interacting with large eddies only. After d=30D, the second wind turbine starts to receive a uniform flow gradually until a distance superior to d=40D, when it produces the same power coefficient (Cp) as the first wind turbine.

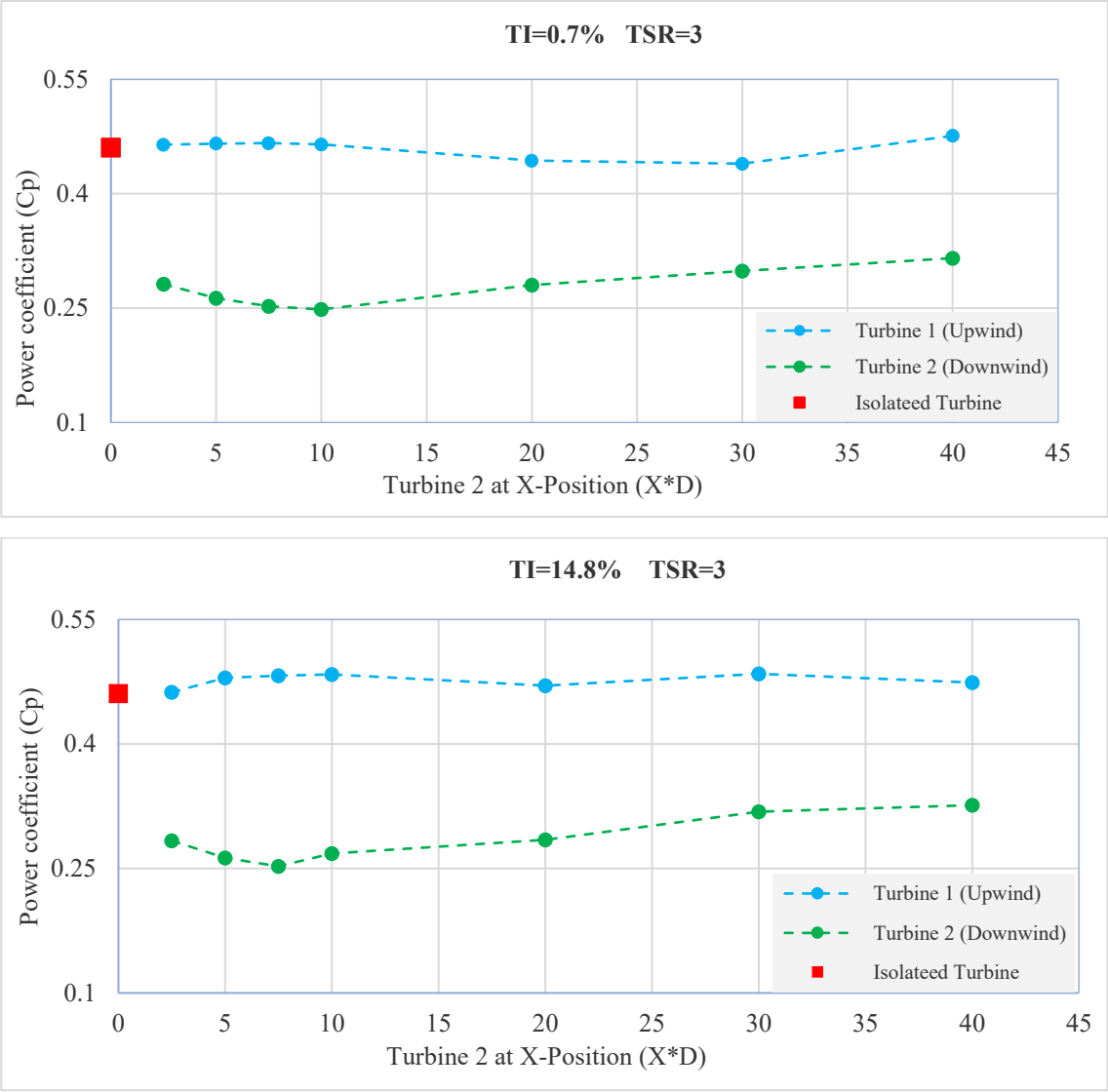

Figure 3-7: The power coefficient against the different positions of turbines 2. **Turbine 2 at Y= - R (Starboard side).**

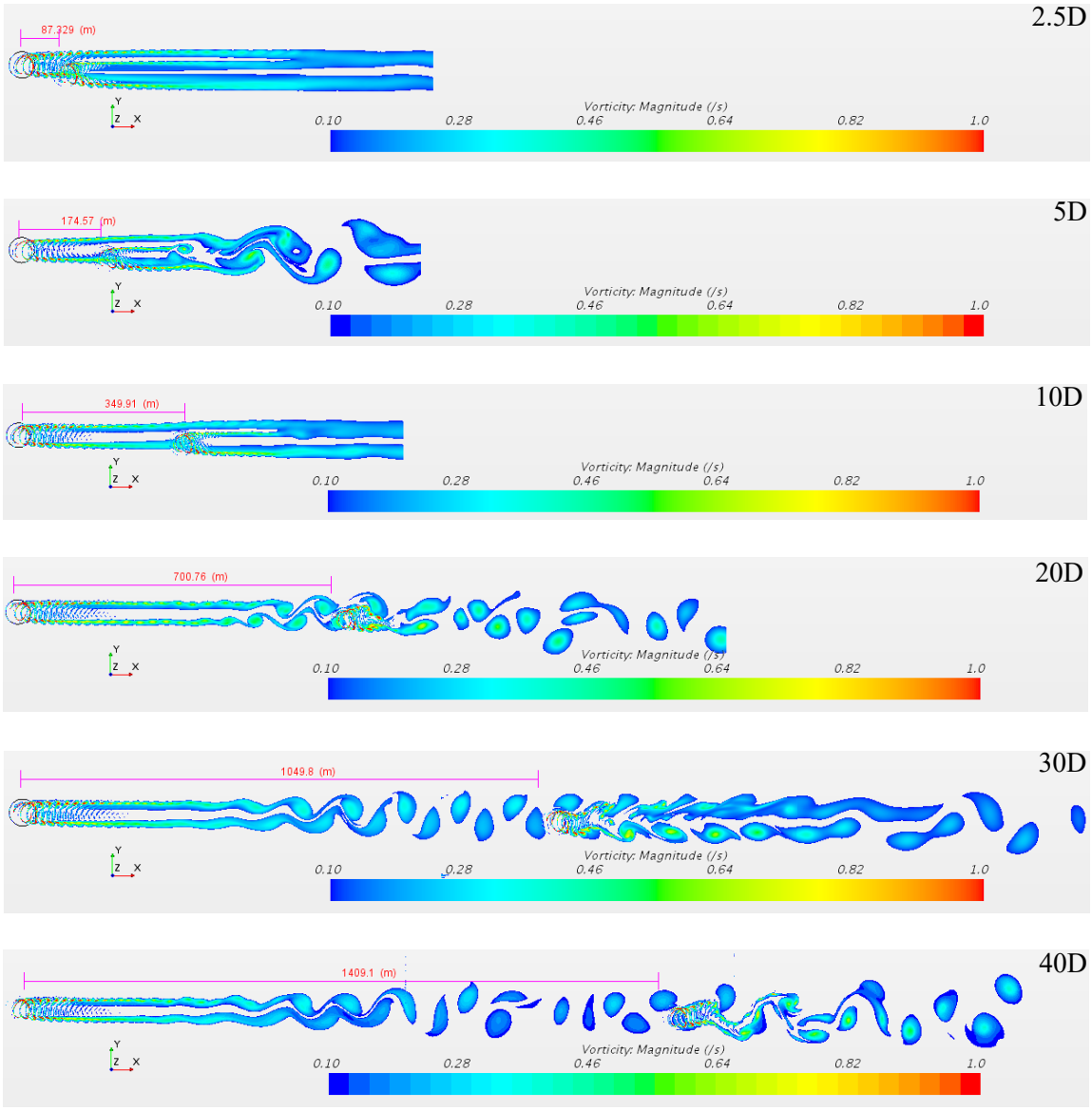

Figure 3-8: Vorticity distribution downstream of the VAWTs for different distances TI=14.8% **(Starboard side).**

3.3.2.1.2 The second turbine installed on the port side of the first turbine:

In this simulation, the second wind turbine is placed on the port side at different distances, and the power coefficient (Cp) of all cases is presented in Figure 3-9. To start, from the overall look of Figure 3-9, one can note that the second turbine performs better on the port side. Furthermore, the performance is better for the low turbulence intensity simulations, particularly after a distance greater than 20D. Lastly, the second wind turbine has a good performance when placed very close to a distance of 2.5D. Maybe that is due to the blade orientation of the second

wind turbine during the rotation, which coincides with the flow direction generated by the wake of the first wind turbine. Afterward, a significant decrease in the power coefficient of the second wind turbine is observed between the placements of d=2.5D to d=5D as shown in Figure 3-9. There is a remarkable difference between results obtained with TI=0.07% and TI=14.8%. In the case of TI=0.07%, the Cp recovers the value of the isolated turbine rapidly; compared with the case of TI=14.8%. This phenomenon may be explained by the fact that the high turbulence intensity delays the dissipation of the wake generated by the first wind turbine, as one can see in Figure 3-10.

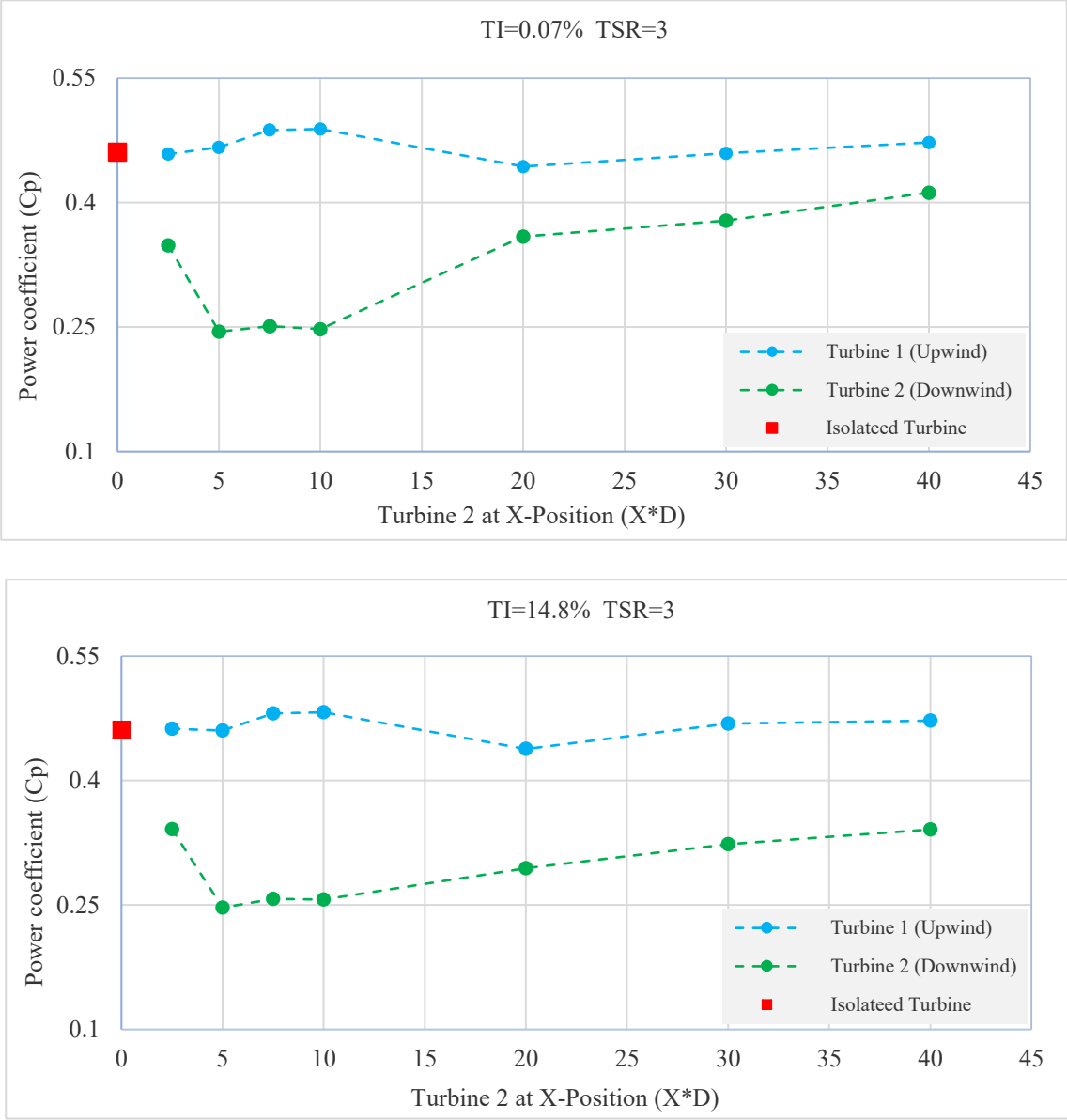

Figure 3-9: The power coefficient against the different positions of turbines 2. **Turbine 2 at Y=R (Port side).**

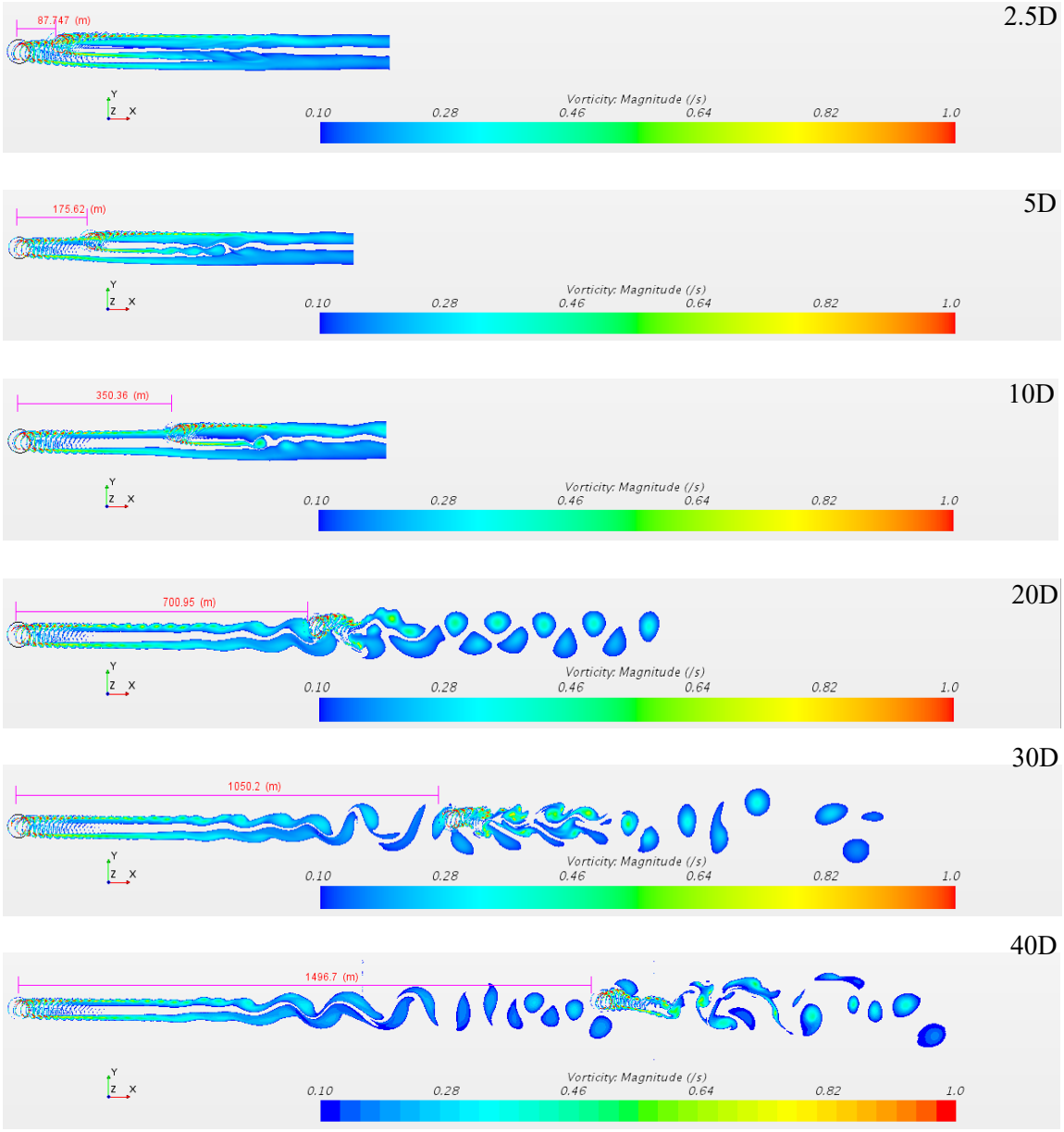

Figure 3-10: Vorticity distribution downstream of the VAWTs for different distances at TI=14.8% (**Port side**).

3.3.2.2 Effect of the wake downstream on rows of turbines

To further analyse the interaction of wind turbines, two configurations are simulated, the first farm contains 3 wind turbines, and the second farm with 5 wind turbines. For the configuration of 3 wind turbines, the first wind turbine (1) is placed at the origin of the coordinate system, and the wind turbines (2) and (3) are placed at the coordinates of (5D, 1.5D) and (5D, -1.5D) respectively, as shown in Figure 3-11. For the configuration with 5 wind turbines, turbines 4 and

5 are added to the farm of 3 wind turbines at the coordinates of (10D, 3D) and (10D, -3D) respectively as shown in Figure 3-12

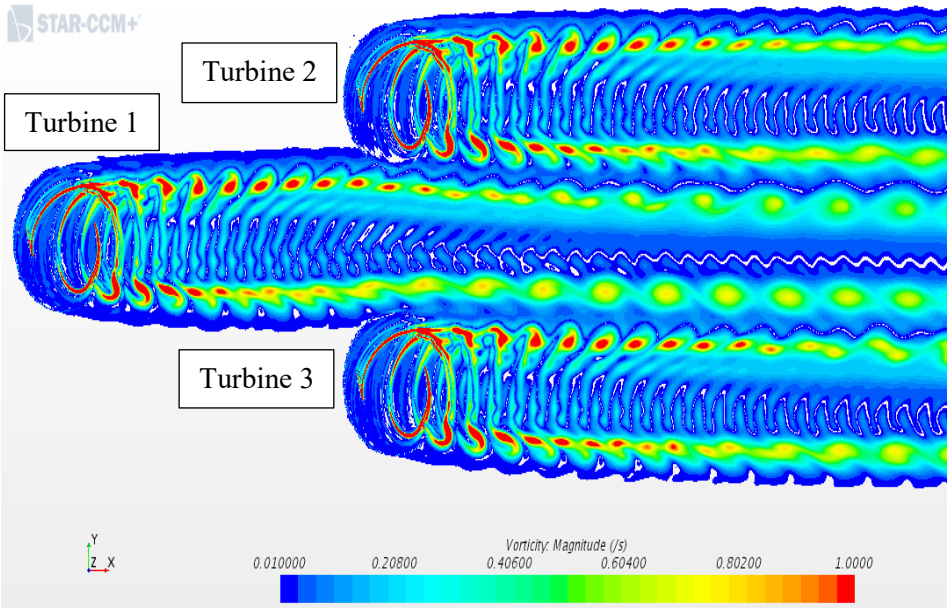

Figure 3-11: Vorticity contours for an array of 3 turbines (TI=14.8%).

A. Farm with 3 vertical axis wind turbines:

The power coefficient (Cp) for each wind turbine is calculated and compared to the power coefficient (Cp) of the isolated wind turbine. The results are presented in Table 3-6. This figure presents the power coefficient (Cp) against the position of each wind turbine. In the case of turbulence intensity set at 0.07%, improvements are seen for turbine 3. It is clear from this graph that turbine 3 extracts more energy than wind turbine 1, the isolated turbine, and turbine 2. This increase in Cp is due to the fact that turbine 3 turns in the same direction as the wake of the first turbine, so turbine 3 benefits from the acceleration of the flow resulting from this wake and the blockage between turbines 2 and 3.

Table 3-6: The power coefficient (Cp) against the different positions of turbines. (3 Turbines)

	Isolated Turbine	Turbine 1	Turbine 2	Turbine 3
Distances	0	0	5D	5D
Power Coefficient (Cp) TI=0.07%	0.4606	0.4605	0.4587	0.5408
Power Coefficient (Cp) TI=14.8%	0.4606	0.4605	0.5124	0.5414

In the case of turbulence intensity set at 14.8%, the performance of turbine 2 approaches turbine 3, because the increased turbulence intensity offers turbine 2 a large delay of dynamic stall of the turbine blade. As we can see in Figure 3-12, in red color, the vortex created by both blades does not dissipate until it interacts with the blades of wind turbines 2 and 3. In addition, because of the short distance between turbines 1 and 3, the acceleration and strength of the wake created by turbine 1 had less time to affect turbines 2 and 3.

Comparing the extracted energy from turbines 2 and 3, and the isolated wind turbine, confirms that placing a wind turbine in this array configuration is more beneficial than an isolated wind turbine, such as a wind turbine in a farm can benefit from the wake of each other, with the respect of the coordinate position of the downstream wind turbines.

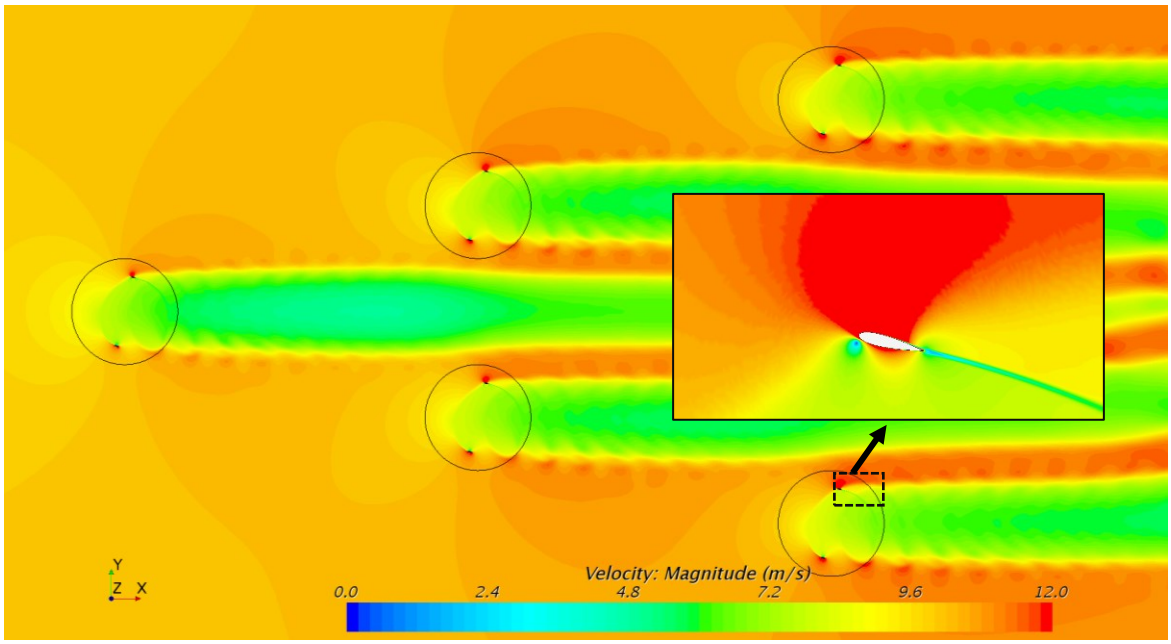

Figure 3-12: Velocity Contours for an array of 5 turbines. All Turbines have counter–clockwise directions.

B. Farm with 5 vertical axis wind turbines:

To expand the positive results of the 3 wind turbines configurations analyzed in the previous section, another case with 5 wind turbines is considered. A similar configuration is investigated as shown in Figure 3-12. The Cp of each wind turbine in this configuration is calculated and compared to the Cp of the isolated wind turbine; the results are presented in Table 3-7. This case is also simulated using two values of turbulence intensities TI=0.07% and TI=14.8%, the wake in the case of 5 wind turbines is not affected by the variation of the turbulence intensity, contrary to

the park of 3 wind turbines and more investigation is needed to understand this behavior. One can observe in Table 3-7 a linear increase in Cp from turbine 1 to turbines 2 and 3 to turbines 4 and 5. The Cp of turbines 4 and 5 is relatively higher than the Cp of turbines 2 and 3. It appears that each row of turbines increases the velocity around it. Therefore the velocity reaching turbines 2 and 3 is higher than turbine 1 while the wake of turbine 1 is passing between the two turbines. As seen in Figure 3-12, the flow accelerates on both sides of the rotor. The flow velocity is higher when the blade is facing the flow or in the opposite direction. This higher velocity appears in red and represents a significant increase in the incoming wind speed. The wake of each rotor appears in green a represents a significant velocity deficit. Overall this triangular configuration forces the flow to accelerate on both sides, therefore, providing the turbines downstream with higher incoming velocities.

Table 3-7: The power coefficient against the different positions of turbines. (5 Turbines)

	Isolated Turbine	Turbine 1	Turbine 2	Turbine 3	Turbine 4	Turbine 5
Distances	0	0	5D	5D	10D	10D
Power Coefficient (Cp) TI=0.07%	0.4606	0.4605	0.4932	0.5095	0.5251	0.5347
Power Coefficient (Cp) TI=14.8%	0.4606	0.4605	0.5054	0.4869	05229	0. 5365

The time evolution for the upper wind turbines (Wind turbines 1, 2, and 4), is shown in Figure 3-13 was the moment coefficient is shown for each turbine as a function of time. The moment coefficient oscillates between zero and a peak value between 0.32 and 0.38. The peak value occurs when the blade is located close to 90 degrees, that is when it is at the most forward point of the rotor. As seen this peak value increases for each downstream turbine. As discussed earlier, the increased velocity downstream increases the moment created by the blade of the downstream turbines. The lower value of the moment coefficient close to zero is not affected as this happens when the blades are on the side of the rotor and do not generate a moment.

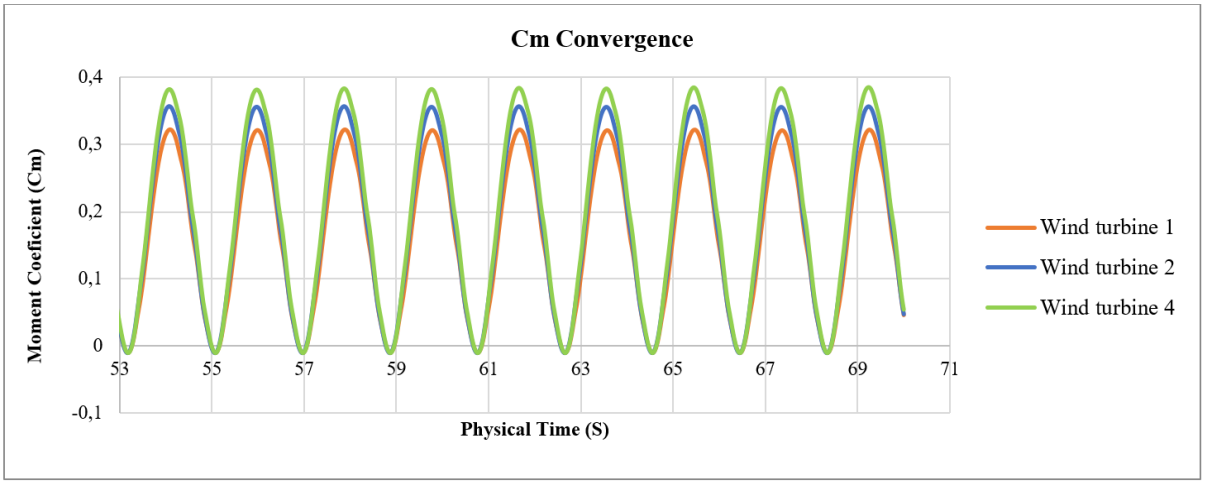

Figure 3-13: Moment convergence for wind turbines 1, 2, and 4.

Furthermore, the vorticity contours of the five wind turbines are traced in Figure 3-14, the range varies from 0.01 to 1 1/s, and the overall wake observed, looks like parallel straight lines separated by different colors, however, the blue color is the predominant. It is clear that the eddies created downstream by the treating edges of the rotor blades in red color propagated and lost their strength before reaching the blades of the rotor downstream. In the near wake, we can also clearly see the wake of each blade as it rotates cycle after cycle.

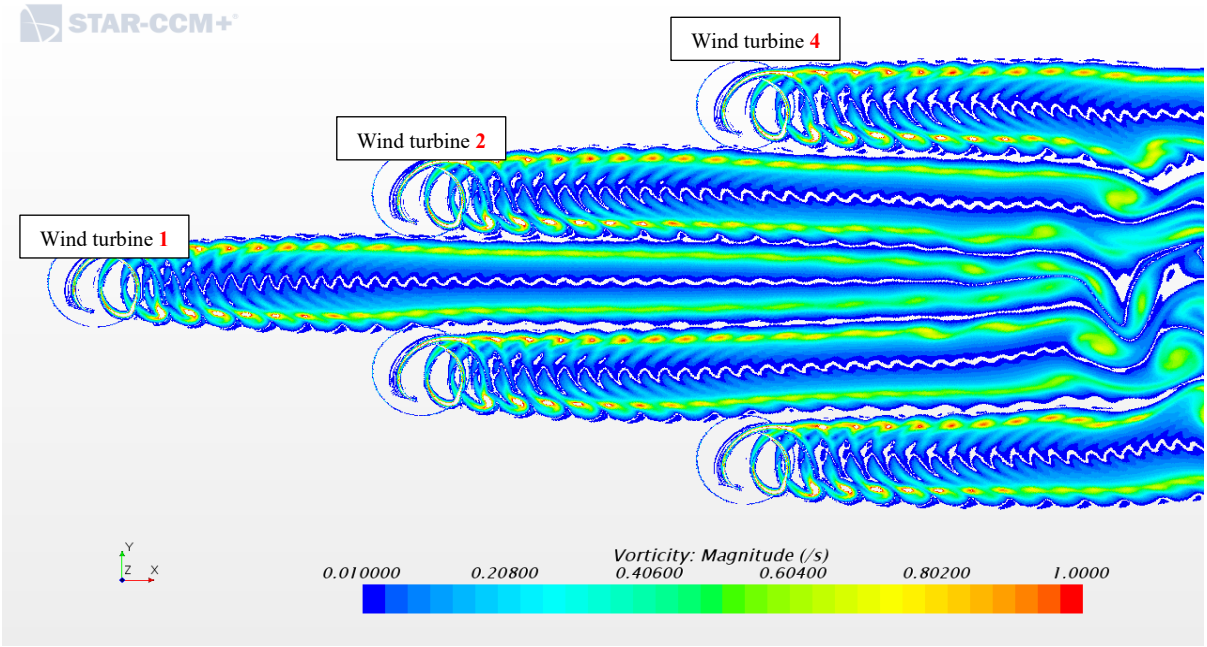

Figure 3-14: Vorticity contours for an array of 5 turbines. All Turbines have counter–clockwise directions.

3.4 Conclusion

The main purpose of the present work is to estimate the performance of large vertical-axis wind turbines when placed behind each other or in a triangular configuration facing the wind. The power coefficient is used as the main parameter of this evaluation and qualitative information with respect to the isolated turbine is presented. The following conclusions can be summarized:

- Results show that 2-dimensional CFD analysis can be used to evaluate the relative performance of the second turbine with respect to the first turbine even if the 2-dimensional modeling overestimates the Cp value of each turbine;
- The effect of the wake on the turbine downstream is high particularly when the second turbine is on the port side of the first turbine;
- The wake of the first turbine typically breaks down into larger eddies, after a distance between 10 and 20 rotor diameters;
- A proposed triangular configuration of 5 VAWTs exhibits a 20% increase in power output compared to operating the same 5 turbines in isolation.

The limitation of this study is that it provides quality information related to the performance of the downstream turbines with respect to the first turbine facing the flow. For precise quantitative results of the actual values of the downstream turbines, 3-dimensional CFD modeling needs to be performed.

4 CHAPTER 4. ARTICLE 3: CFD analysis of vertical axis wind turbine wake-rotor interaction: a comparison between 2 and 3-dimensional modeling

The content of this chapter has been submitted as a peer-reviewed paper to the Journal of Energy Resources Technology in June 2023.

Abstract:

In this study, the wake-rotor interaction for three different vertical axis wind turbines (VAWT) is analyzed. The main purpose of this work is to evaluate if the 2-dimensional modeling provides useful and accurate information on the wake-rotor interaction in comparison to the full 3-dimensional computational fluid dynamics (CFD) simulation. This study is based on the unsteady Reynolds-Averaged Navier-Stokes (URANS) equation using the transition shear stress transport (SST) model for turbulence. The CFD models used in this study are validated with wind tunnel tests and field measurement results from the literature. Grid independence verification was performed for the wake using a coarse, medium, and fine mesh ranging from 21 to 43 million cells. A flow velocity correction approach is applied to the 2-dimensional model to asses its effectiveness to calculate the power coefficient and to capture the wake between turbines. The near and far wakes are analysed for the three types of wind turbines ranging from 0.5 m to 35 m rotor diameters. This study shows that the 2-dimensional model simulation provides useful information for the performance of the second turbine when studying turbines with an aspect ratio of around 1 which have low solidity. Within these limitations, the 2-dimensional model can therefore be used to calculate the minimal distances between turbines placed in the same flow direction.

Keywords: Vertical axis wind turbine, Computational fluid dynamics, Wake-rotor Interaction, 2 or 3-dimensional modeling, correction method.

4.1 Introduction

Wind energy is the most economical renewable energy source since it is both clean and abundant [79]–[81]. The installed wind power capacity has significantly expanded during the last ten years [33], [82]–[85]. Wind energy has been harvested for many millennia by cleverly constructed wind turbines. Indeed, there exist many types, and are classified by the orientation of the rotational axis. The two primary categories of modern wind turbines are horizontal axis wind turbines (HAWTs) and vertical axis wind turbines (VAWTs).

The HAWTs have significantly advanced over the last half-century, and they now Monopolize the commercial market [86]. However, the VAWTs are able to overtake the pioneers, in particular

for off-shore locations, because of their distinct benefits, including features like omnidirectionality, simple design, and affordable putting-in and repair fees [87] [88]. The VAWTs are an attractive choice for constructing wind farms as these turbines perform better in turbulent flows [89] [88]. However, the downstream wind turbines are significantly impacted by the strong wake and a proper distance is still required between rows of turbines [90]. The wake is generally created by the strong vortex shedding from the blades which is caused by the quickly varying angle of attack. The change in the angle of attack also results in fatigue loads and very unstable lift fluctuations [91]. This phenomenon often called a dynamic stall, is distinguished by the development of vortices and their release into the wake. It greatly influences the aerodynamic performance and wake structure of VAWTs. The dynamic stall of VAWTs has been researched since the early 1980s [78].

When creating the schema of wind farms, it is crucial to consider wake interference in the turbine array, which led researchers to perform several experiments [15], [83], [92]. Similarly, numerical simulations [76], [93]–[95] were used to thoroughly study the wake of standalone wind turbines in an array. Due to dynamic stall, the wake aerodynamics of H-rotor VAWTs are significantly more complicated than those of their HAWT equivalent [78], therefore, additional work is required to create wake models appropriate for VAWTs. According to Hohman et al. [92], and Rolin et al. [95], the wake region around the wind turbines can generally be divided into two sections: the near-wake region, which enlarges approximately two times the rotor diameter downstream, and the far-wake area, which extends more than the near-wake region.

The turbulent evolution in the near wake is highly influenced by the dynamic stall and blade interference. As the blades of the wind turbine move in the downstream half-revolution, they interact with the vortices released during the upstream half-revolution, causing interference. As stated, it is impossible to directly model the intricate aerodynamics in the close wake, that's why a few studies are found in the literature, like Tescione et al. [97] which analyzed the near wake of an H-rotor VAWT using the panel approach in conjunction with a free-vortex wake. This study calculated the wake aerodynamics of a VAWT operating at a TSR of 4.5 and exhibited strong correspondence with experimental data, indicating the near-wake model captured important dynamic effects. The turbulent evolution in the immediate wake region is greatly impacted by dynamic stall and blade interference. As the wind turbine blades advance through the downstream half-revolution, they come into contact with the vortices released in the course of the upstream

half-tour, leading to interference effects. As highlighted in [78], accurately modeling the intricate aerodynamics in the close wake is exceedingly challenging, resulting in limited studies in the literature.

For instance, Tescione et al. [97] examined the near wake of an H-rotor Vertical-Axis Wind Turbine (VAWT) using a panel approach mixed with a liberated vortex wake. In their investigation, they calculated the wake aerodynamics of a VAWT functioning at a Tip-Speed Ratio (λ) of 4.5 and achieved satisfactory accordance with experimental data, demonstrating that the near-wake model captured significant dynamic effects. However, it should be noted that the model tended to overestimate horizontal and vertical expansions downstream over the wind side direction. The intricate interaction between the blade and wake, the robust shedding of tip vortices, and the occurrence of the deep dynamic stall in the near wake pose considerable challenges in attaining precise predictions.

Furthermore, Brownstein et al. [98] conducted an analysis on VAWTs, measuring performance improvement for paired turbine setups, both upstream and downstream units. The study focused on the near wake, investigating a three-dimensional model with Re=73000 and a distance comprised between 1.25 and 3 times the diameter. The findings suggest that within the paired arrays, both the upstream and downstream turbines experienced performance enhancement. Notably, the downstream turbine's performance gains were associated with bluff body accelerations around the against the current of the turbine, leading to increased incident freestream velocity at specific positions on the downstream turbine. Conversely, decreases in downstream turbine performance were linked to its placement within the wake of the upstream turbine. Overall, the more resilient array outline demonstrated an average 14% improvement in the farm performance across a wind direction span of approximately 50º.

Moreover, Alexander et al. [99] conducted an investigation using 2D CFD investigations to analyze the physical factors contributing to enhanced performance in a paired configuration of double-rotor VAWTs using a 1.5 diameter as distance. The study revealed that a single-rotor VAWT allowed more than 54% of the entering flow to bypass the VAWT's outer region. However, introducing a second rotor in the setup counteracted the cross-stream flow that would typically occur on one side by generating a contrary cross-stream flow from the second wind turbine. As a result, the primary reason for the approximately 10 improvements in the Cp for the double-rotor

VAWT was primarily attributed to a decrease in the bypass flow that circumvents the single-rotor VAWT's outer area.

An additional two-dimensional URANS CFD simulation is documented in [100], aimed at investigating how the aerodynamic performance of co-rotating Darrieus H-type vertical axis wind turbines (VAWTs) is affected by their relative distance (D/2), and angle (Θ) in double rotor configurations. The relative distance is confined between 1.25D and 10D, while the angle spans from -90◦ to +90◦. Through a comprehensive flow analysis, it was observed that the optimal spacing led to the creation of a high-velocity region in a tight passage between the two rotors, resulting in flow acceleration. The downstream turbine benefited from its blade(s) advancing through this zone, leading to increased power coefficient values. These findings validate the favorable layout design for VAWT farms and underscore the considerable potential for small VAWT farms to achieve high power densities. However, it should be noted that this study lacks three-dimensional analysis, which is essential for accurately predicting the vortices generated between both rotors and at the blade tips.

Moreover, the region situated in the downstream direction after the near-wake is referred to as the far wake. In contrary to the near wake, the far wake is more appropriate for wake modeling, and accurately representing it is crucial for mitigating mutual wake interference when designing wind farms with multiple turbines [78]. Several researchers [101]–[103] have confirmed that the far-wake flows are minimally touched by the Reynolds number and the geometrical characteristics of the turbines.

In this context, the dynamic wake impact on the downstream VAWTs is explored in [94] through the utilization of CFD simulations. The study involves raising the separation gap between two wind turbines. It is illustrated that vertical-axis wind turbines require a velocity recovery distance larger than 15D. Notably, this observation is also corroborated by Belabes et al. [76]. Furthermore, the wake flow is bifurcated into two segments near the wind turbine. The primary wake flow is situated in the upper section, exhibiting both clockwise and counterclockwise rotations. The wake flow from the wind turbine positioned before the flow direction significantly influences the downstream wind turbines through large-scale vortex shedding. However, the limitation of this investigation lies in its reliance on 2-dimensional modeling. It is evident that a considerable portion of the research focusing on wake-rotor interaction employs 2-dimensional models. While the constraints of these models are recognized, their quantification remains

unexplored. This study strives to shed light on the utility of 2-dimensional models for VAWT farm layouts, aiming to offer comprehensive insights. As per recent investigations, certain alternative VAWTs exhibit rapid wake recuperation, leading to elevated packing densities and presenting significant potential for implementation in urban setups, thereby amplifying their appeal [89]. Several researchers have studied many different factors, including Reynolds number [104], turbulence intensity [76] [105], blade shape [106], [107], rotation rates [108], and lower frequency [109], which have an impact on the dynamic stall, and subsequently on the wake.

In a related context, Huang et al. [105] delve into the impacts of open stream turbulence on aerodynamic performance. The study employs dynamic stall conditions produced by restricting gusts, which entail incoming velocity fields that undergo periodic changes. Dynamic stall analysis is conducted for angles of attack ranging from 10º to 25º. The research illustrates how higher freestream turbulence levels enhance lift at high angles of attack and delay stall occurrence. Notably, the most noticeable influence of turbulence on aerodynamic forces occurs during the lowering angle of the attack phase, where freestream turbulence facilitates the re-gluing of the boundary layer. Additionally, the approaching turbulence significantly reduces the negative damping of the moment coefficient. The findings reveal that in a turbulent flow with a turbulence intensity of 5%, freestream turbulence enhances the aerodynamic production of the wind turbine blade. However, these studies have encountered contradictions due to the use of different models and numerical or experimental approaches. The investigation's credibility may be affected by neglecting certain parameters that could influence the results.

Belabes et al. [76] conducted further examination on various straight-bladed Darrieus-type wind turbines, which involved investigating both a small and a large H-Darrieus Vertical-Axis Wind Turbine (VAWT) with diameters of 0.5m and 35m, respectively, both equipped with NACA0018 blades. The study findings reveal that for turbulence intensity up to 20%, the power coefficient of the small turbine shows an increase, but this trend levels off beyond 20% turbulence intensity. Specifically, when turbulence intensity is raised from 0.07% to 20%, there is a 22% rise in the Cp for the small H-Darrieus turbine, whereas no such increase is observed for the large H-Darrieus wind turbine.

Recent years have seen a huge rise in the amount of computing power that is accessible [110], which has made it possible to calculate VAWTs using modern CFD simulations, which is quickly emerging as a standard analysis technique for this type of device. However, these simulations have

historically prompted researchers to use simplified 2D flow models, which have a far lower processing requirement and are still incredibly expensive for design purposes. The use of a 3D CFD model is clearly more accurate but the computing cost remains a key obstacle. Comparison between 2D and 3D of the rotor performance has been well studied and the overprediction of the 2D model is well documented [64]. However, exploring the wake structure of an H-type VAWT and its impact on a downstream turbine is not as frequently encountered. This study addresses this gap by examining both 2-dimensional and 3-dimensional UNRANS CFD simulations of the wake between two turbines to assess the 2-dimensional precision. A full analysis of the wake effect on the downstream turbine is conducted, and potential corrections to the 2-dimensional model are discussed.

The current investigation aims to offer a critical understanding of the wake interaction between the two VAWTs. As such, the study examines three varying dimensions of H-type VAWTs. The contributions of this research can be distilled into two main facets:

(1) The study employs comprehensive 3-dimensional unsteady simulations to examine the interactions in the near and far wakes of two Vertical-Axis Wind Turbines (VAWTs), with the second turbine positioned in the wake of the first one

(2) Additionally, a detailed investigation is conducted using two-dimensional and three-dimensional simulations of a turbine pair, involving three different wind turbine sizes. The assessment includes both the simulation cost and the accuracy of the results, based on the power performance ratio (Cp2/Cp1) between the two wind turbines. This analysis is of critical importance in determining the suitability of 2-dimensional modeling for exploring more intricate scenarios arising when multiple turbines are placed in a wind farm.

The overarching structure of the current study is as follows: Section 2 presents the detailed geometric model geometrically for each of the three VAWTs, while Section 3 delineates the numerical approach employed. This section also discusses a comparison with a wind farm field test and the verification of accurately capturing the 3D wake. In Section 4 the comparison between 2D and 3D models is presented and a correction to the 2D model is discussed. The limits of the present work are highlighted in Section 5 along with a perspective for future research.

4.2 Geometric model

To evaluate the impact of the size, aspect ratio, and solidity on the current investigation three different turbines with rotor diameters of 35 m, 1.2 m, and 0.5 m are studied. These turbines are

shown in Figure 4-1, Figure 4-2, and Figure 4-3. These are H-type VAWTs and have been investigated experimentally in Refs. [15], [24], [63]. The main characteristics of the rotors of these turbines are summarized in Table 4-1.

Table 4-1: Geometrical and operation characteristics of the selected VAWT.

Parameters	**Large Turbine**	**Small Turbine**	
	Bedon et al. [62]	Dabiri et al. [15]	Molina et al. [24]
		Value	
Number of blades, N [-]	2	3	2
Diameter, D [m]	35	1.2	0.5
Height, H [m]	24.30	6.1	0.8
Swept area, A [m^2]	850.5	7.32	0.4
Solidity, σ [-]	0.1	0.317	0.05
Airfoil chord length, c [m]	1.75	0.127	0.05
Airfoil shape [-]	NACA0018	NACA 63-412	NACA 0018
Rotational speed, Ω [rpm]	13.62	350	1200
Freestream velocity, U∞ [m/s]	7.13	8	9
Tip speed ratio (based on U∞), λ [-]	3.5	2.75	3.0
Aspect Ration (H/D)	0.69	5.08	1.6

Figure 4-1: VAWT 850 installation [63].

Figure 4-2: The Wind turbine installed in Wind tunnel [111].

Figure 4-3: Three VAWTs at experimental wind farm [112].

The angular velocity, rotor radius, and freestream velocity are denoted as ω, R, and V_∞, respectively. The moment coefficient (Cm) and power coefficient (Cp) can be computed using the following formulas:

$$C_T = \frac{T}{0.5\rho V_\infty^2 AR} \tag{4-1}$$

$$Cp = \frac{T\omega}{0.5\rho V_\infty^3 A} \tag{4-2}$$

where T and A are the torque and flow area, respectively.

4.3 Numerical method

4.3.1 Turbulence modeling

The study presents both 2-dimensional and 3-dimensional methods to model the unsteady aerodynamics of the VAWT numerically. The solver settings used in the current investigation are listed in Table 4-2, where the URANS equations are solved using a velocity-pressure split-coupled algorithm. The software's solution methods are configured as follows: the implicit unsteady segregated flow method is utilized with a predictor-corrector approach linking the continuity and momentum equations. The coupling of the pressure-velocity equation employs the SIMPLE algorithm, and the shear stress transport k-Omega turbulence model is selected. A second-order upwind scheme is employed for convection terms in this study. The computations are conducted for 15 revolutions of the VAWT, and the reported *Cp* values are derived from the last 2 tours, following the transient analysis recommendations provided in the STAR-CCM$^+$ 12.06 User manual [65]. The numerical method's solution validation and sensitivity tests for the physical time step are documented in [76].

In this investigation, turbulence is simulated using the shear stress transport *k-ω* approach within the commercial CFD code STAR-CCM$^+$ 12.06 [65].

Table 4-2: Turbulence model and Solver settings.

Fluid flow modeling approach	**Segregated flow model**
Discretization scheme; -Time -Convection	Implicit unsteady, 2nd-order Hybrid 2nd-order upwind/bounded central-differencing
Physical time-step	1º per time step
Pressure-velocity coupling algorithm	SIMPLE
Maximum inner iteration	20
Equation of state	Constant density
Material	Air
Reynolds-Averaged Turbulence	SST k-Omega Turbulence

As prescribed in the STAR-CCM$^+$ 12.06 User manual [65] and the investigation by Shur et al. [113], the dissipation rate in the transport equations of the shear stress transport k- Omega turbulence model is substituted with $\tilde{\omega}$, which is defined as:

$$\tilde{\omega} = \frac{\sqrt{k}}{l_{hyb}\beta^* f_{\beta^*}} \tag{4-3}$$

where β^* is equal to 0.09 and f_{β^*} is the free-shear correction factor, and l_{hyb} is the length scale which is expressed as:

$$l_{hyb} = \tilde{f}_d(1 + f_e)l_{RANS} \tag{4-4}$$

$$\tilde{f}_d = \max\big((1 - f_{dt}), f_B\big) \tag{4-5}$$

$$f_{dt} = 1 - tanh[(C_{dt}r_{dt})^3] \tag{4-6}$$

$$f_B = \min[2exp(-9\alpha^2), 1]\,, \qquad \alpha = 0.25 - \frac{d_w}{h_{max}} \tag{4-7}$$

$$f_e = max[(f_{e1} - 1), 0]\, \Psi f_{e2} \tag{4-8}$$

$$f_{e1} = \begin{cases} 2exp(-11.09\alpha^2)\,, \alpha \geq 0 \\ 2exp(-9\alpha^2), \alpha < 0 \end{cases} \tag{4-9}$$

$$f_{e2} = 1 - max(f_t, f_l) \tag{4-10}$$

$$f_t = tanh[(C_t^2 r_{dt})^3] \tag{4-11}$$

$$f_l = tanh[(C_l^2 r_{dl})^{10}] \tag{4-12}$$

$$r_{dl} = \frac{v_t}{\sqrt{\nabla u : \nabla u^T k^2 d^2}}, v_t = \frac{\mu_t}{\rho} \tag{4-13}$$

$$r_{dl} = \frac{v}{\sqrt{\nabla u : \nabla u^T k^2 d^2}} \tag{4-14}$$

In the context of the given equations, $\boldsymbol{f_B}$ represents the blending function, and $\boldsymbol{f_e}$ corresponds to the elevating function, which incorporates certain wall-modeled capabilities to resolve the log layer. Here, $\boldsymbol{d_w}$signifies the wall distance, and $\boldsymbol{h_{max}}$ denotes the maximum local grid spacing. Additionally, Ψ denotes the low-Reynolds number correction function. The values of $\boldsymbol{C_{dt}}$, $\boldsymbol{C_t}$, and $\boldsymbol{C_i}$ are set to 20, 1.87, and 5, respectively. Moreover, v stands for the kinematic viscosity, $\boldsymbol{\mu_t}$ represents the turbulent eddy viscosity, and κ is the von Karman constant, assigned a value of 0.41. Lastly, $\boldsymbol{l_{RANS}}$ symbolizes the length scale.

4.3.2 Computational domain

The computational domain comprises a fixed rectangular background region and two cylindrical regions as illustrated in Figure 4-4. The dimensions of the computational domain are depicted in Figure 5. In this investigation, the distances between the rotational centers of the two wind turbines are selected as 2.5D and 10D. The separation between the inlet and outlet is 27.5D and 35D correspondingly for the cases of 2.5D and 10D. Hence, the gap from the inlet boundary to the rotational center of Wind Turbine 1 (WT1) is 5D, while the gap from the outlet boundary to the rotational center of WT2 is 20D. The gap from both boundaries to the centerline of rotation is

7.5D. Concerning the three-dimensional structure, the divide between the upper limit of the VAWT blades and the superior limit of the domain is 10D.

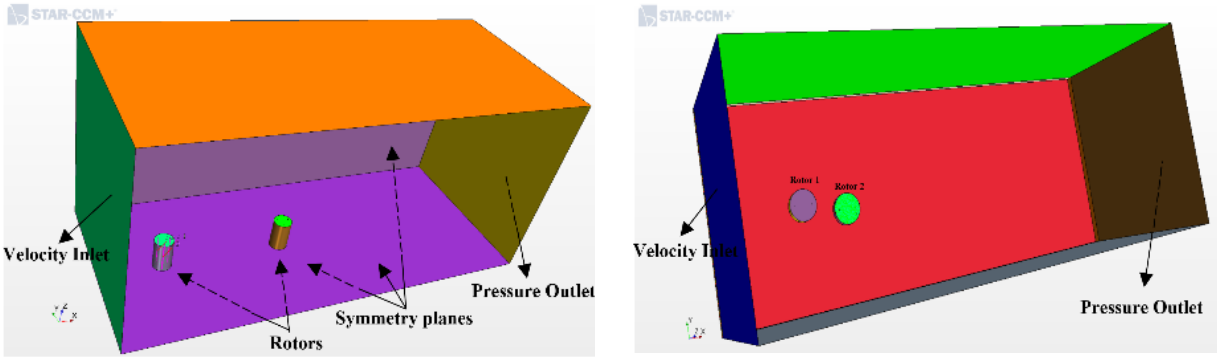

(a) (b)

Figure 4-4: Overall view schematic of the computational domain: **a)** Configuration, (D=1.2m, Ls=10D); **b)** Configuration (D=35m, Ls=2.5D).

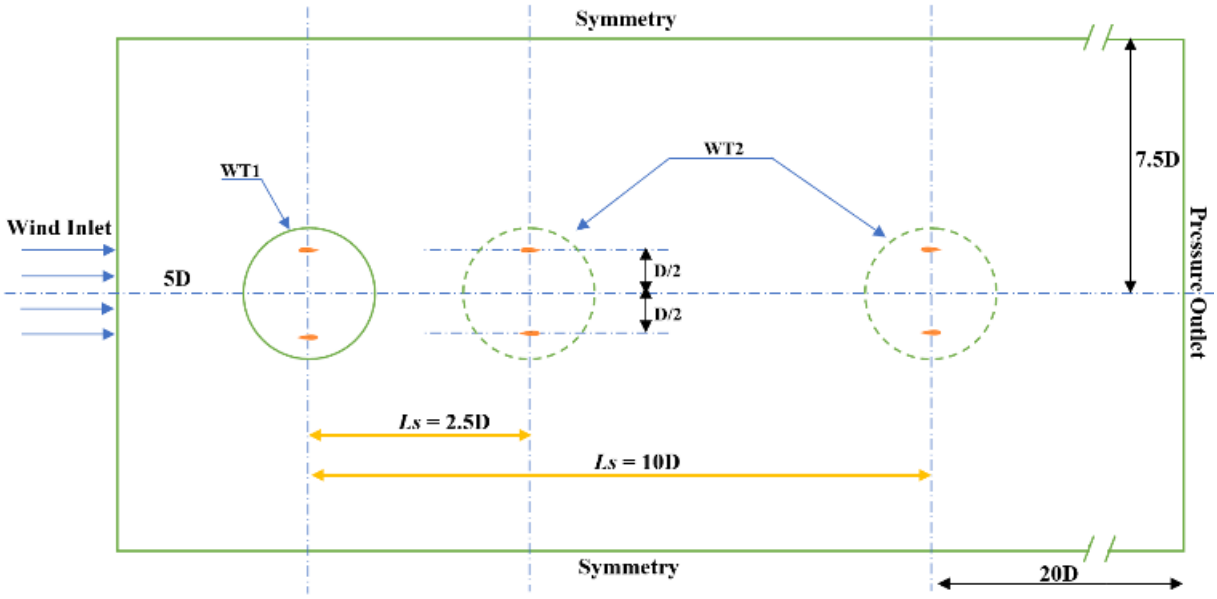

Figure 4-5: Computational domain of two wind turbines for two configurations. Configuration of (D=35m, Ls=2.5D), and Configuration (D=35m, Ls=10D).

4.3.3 Computational grids and time step settings

The computational mesh for the rotor and its layout in both 2-dimensional and 3-dimensional scenarios are depicted in Figure 4-6, comprising polyhedral cells. Concerning the lone wind turbine used for validation and the configuration based on the separation between the two VAWTs,

the cell count varies from approximately 488,978 cells for the isolated setup to 955,277 cells for the configuration with 2 VAWTs in the 2-dimensional case. As for the 3-dimensional setup, the cell count ranges from 13,932,515 for the isolated configuration to 25.5 million polyhedral cells when two VAWTs are considered. To ensure proper boundary layer capture on each blade, both the highest and the medium Y^+ values on the turbine blade are maintained below 1 for all cases. Along the blade circumference, there are 750 cells. Moreover, two types of refinement strategies are employed, one is applied after the trailing-edge side of the blade, and the other focuses on the region downstream of each wind turbine.

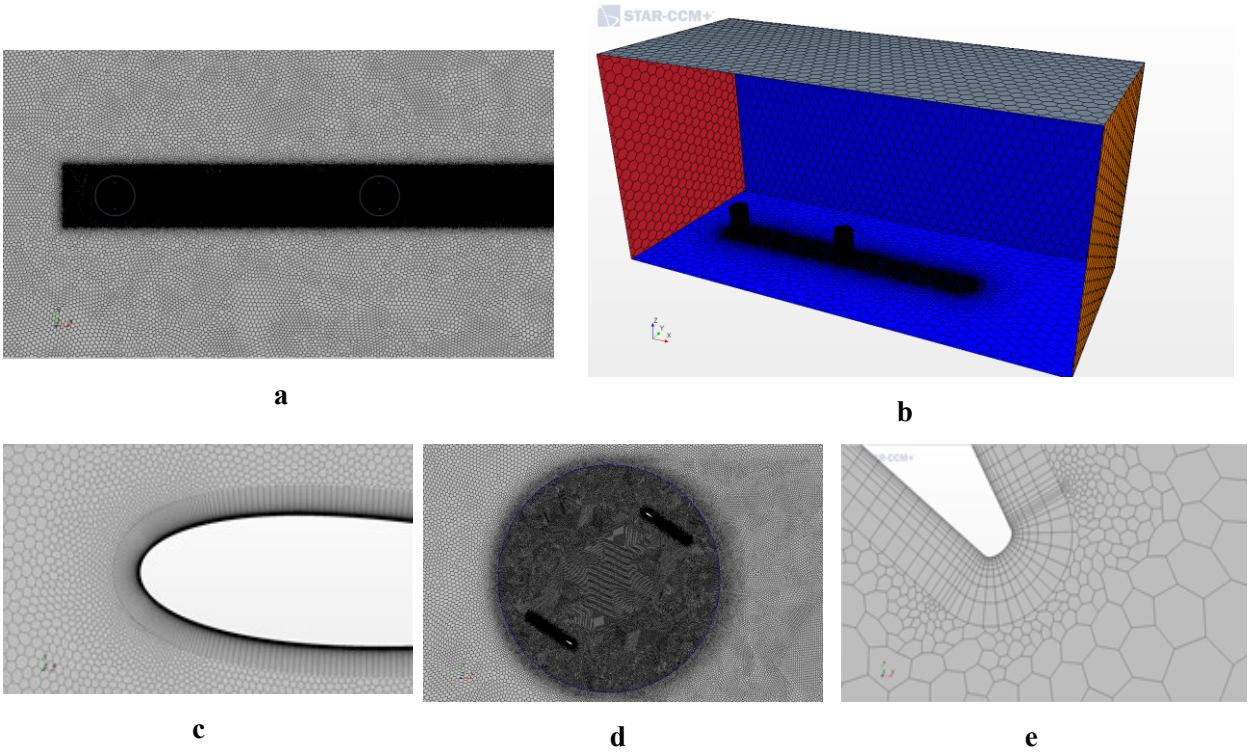

Figure 4-6: Computational grid. **a**: 2D Mesh, **b**: 3D Mesh, **c**: Leading-edge boundary layer, **d**: Trailing-edge refinement, **e**: Trailing-edge boundary layer.

4.3.1 Analysis of the computational domain size

To investigate the impact of the domain width on the wake between the two turbines, a large domain size is compared with the original domain size reported above. The new domain width extended up to 20D on each side. The Cp and the velocity iso-contours of the wake are compared between domains with a width of 7.5D on each side and with 20D. The study encompassed three different wind turbine sizes, and the Cp values calculated for each are reported

in Table 4-3 which reveals that the performance of both turbines remains unaffected by the domain width. Figure 4-7 and Figure 4-8, displaying the velocity iso-contours, demonstrate the shape of the wake for all cases is similar. This recent investigation reaffirms that, in order to minimize calculation costs, a domain width of 7.5D is adequate to mitigate any domain-related effects on wake results. This conclusion holds true across all wind turbine sizes.

Table 4-3 : Comparison between small and large domain for different wind turbines sizes.

	Small domain		**Large domain**	
	Turbine 1	**Turbine 2**	**Turbine 1**	**Turbine 2**
Case of D=1.2m	0.280	0.143	0.275	0.148
Case of D= 0.5m	0.340	-0.060	0.332	-0.060
Case of D= 35m	0.440	0.017	0.440	0.015

4.3.1 2DValidation: comparison with field data

Belabes et al. [76] validated both turbine models using 0.5m and 35m as the diameters of the rotors. Their results exhibited good agreement with the experimental data procured for an H-Darrieus wind turbine, as reported by Molina et al. [24] and Bedon et al. [62]. Furthermore, this section includes validation of the flow around multiple turbines with a diameter of 1.2m. The primary aim is to check the capability of CFD in analyzing the flow field for multiple Vertical-Axis Wind Turbines (VAWTs), with a specific focus on mean velocity and turbulent kinetic energy flows.

To simulate the field test configuration, the same setup as reported by Kinzel et al. [14] is employed, as depicted in Figure 4-9 and Figure 4-10. The turbines utilized in the simulation have a diameter of 1.2m, and at a typical input velocity of 8m/s, they function at a nominal rotation rate of 350 rpm with a Tip-Speed Ratio (TSR) of 2.75. Table 4-1 provides a summary of the wind turbine parameters.

The simulation incorporates 18 wind turbines, mimicking the field layout. Figures 11 and 12 illustrate the geometrical model and the mesh for this configuration, respectively. The mean average horizontal flow velocity at the rotor midheight is obtained by averaging velocities across seven sensor points at each measurement site.

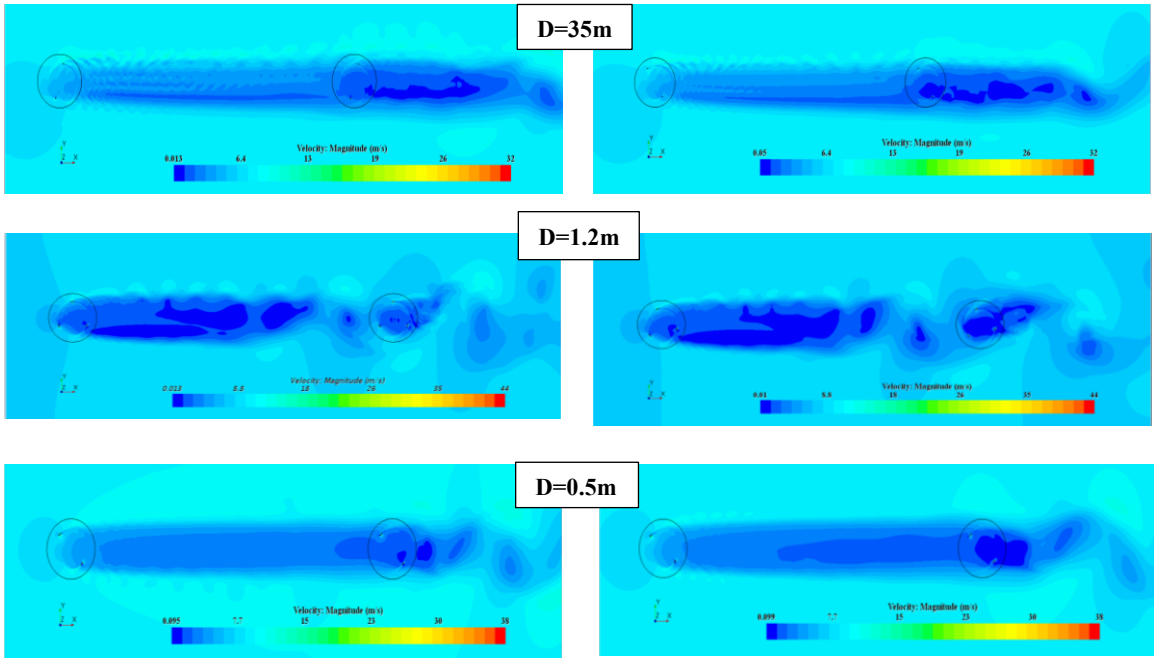

Figure 4-7: Velocity contours for simulations with a **Small Domain.**

Figure 4-8: Velocity contours for simulations with a **Large Domain.**

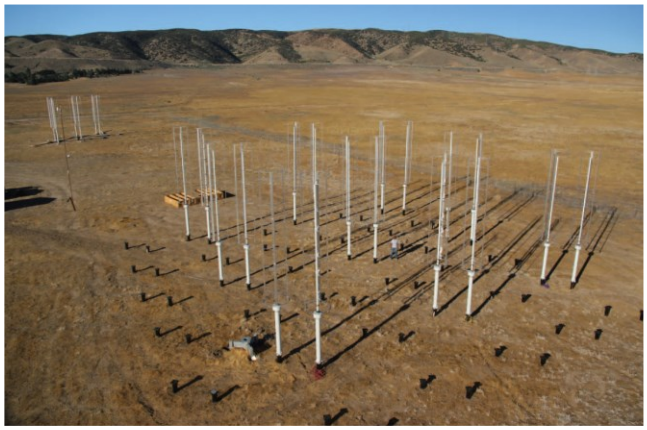

Figure 4-9: Photograph of the VAWT array [14].

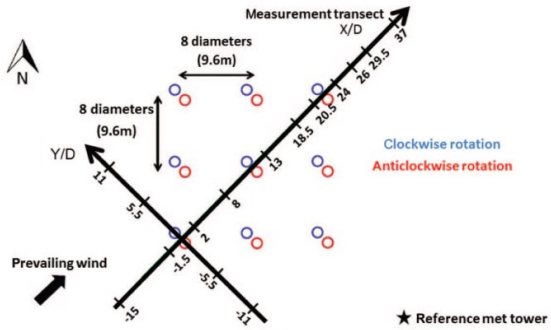

Figure 4-10: Sketch of the VAWT array [14].

Figure 13 displays the curves representing the averaged mean horizontal flow velocity along the center line of the turbine array. It is evident from Figure 13 that the CFD results, shown in red, fall within the range of the lower and higher values obtained from the field measurements. This latest can prove that the results obtained numerically have a good comparison with the field measurement data of Kinzel et al. [14].

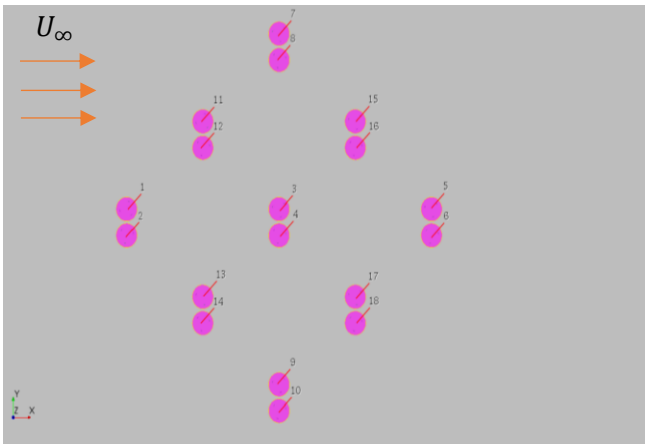

Figure 4-11: Schematic of the computational domain of 9 double rotor arrangement.

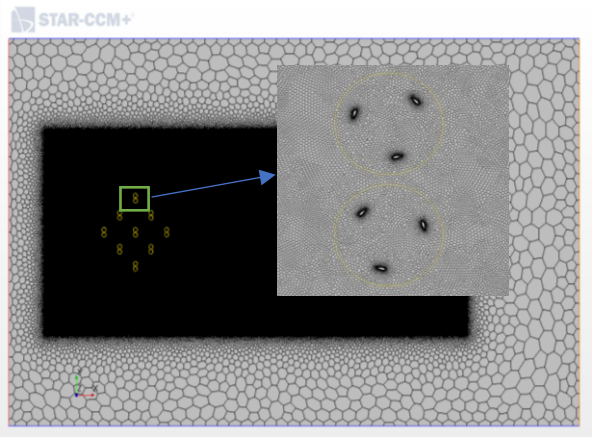

Figure 4-12: Computational grid for 9 double rotor arrangement.

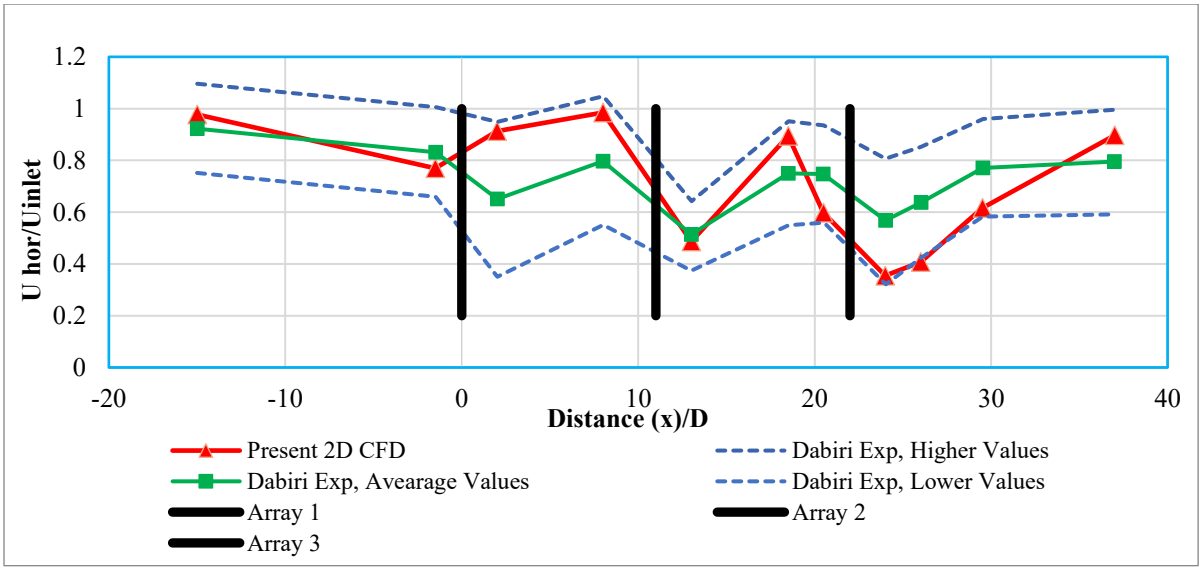

Figure 4-13: Average mean horizontal flow velocity at rotor mid-height normalized by the inflow velocity.

Figure 4-14 and Figure 4-15 display the vorticity and velocity contours of the wake produced by the array of 18 wind turbines. Examining the vorticity in Figure 4-14, it becomes evident that the wind turbines in the third, fourth, and fifth rows are fully situated within the wake of the upstream turbines.

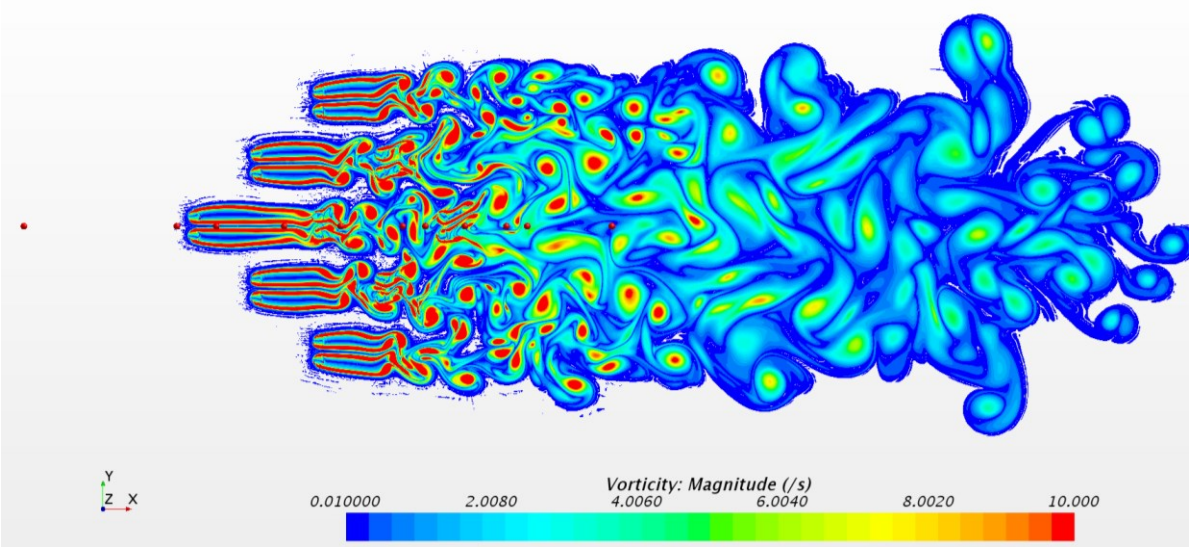

Figure 4-14: Vorticity Contour of the entire wind farm and location of the points where average velocity is collected.

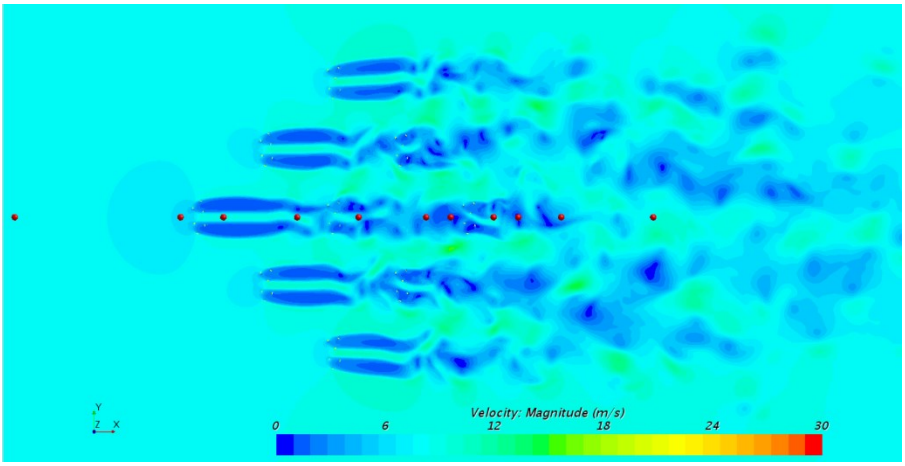

Figure 4-15: Velocity Contour of the entire wind farm.

Figure 4-15 presents the contours revealing that as the flow undergoes energy extraction by the turbines, the flow velocity decreases within the region where the turbine pairs are positioned. However, upon reaching the subsequent turbine pair, the flow velocities begin to rise again. As energy transmission from the front and sides continues to be substantial in this portion of the turbine array, flow velocities continue comparatively high beyond the first row of turbines.

Overall, there is a downstream reduction in velocity, as evident in Figure 4-15, where the velocity measures only 0.35 of the incoming wind velocity after the third row of turbines. These

findings lead to the conclusion that the CFD solution utilizing Star CCM+ effectively predicts the velocity field within a vertical-axis wind turbine array.

4.3.2 Verification: mesh refinement of the wake

Verification of grid independence is a crucial aspect of validating the computational model. In this section, we investigate the grid required to precisely capture the wake and performance of the second wind turbine. To achieve this, we select a huge wind turbine with a diameter of D=35m, and based on the grid strategy and primary grid parameters outlined in Table 4-4, we establish three sets of grids with different densities. These meshes are categorized as coarse, medium, and fine, comprising approximately 21 million, 32 million, and 43 million cells, respectively, with around 10 million cell intervals between each mesh.

The power coefficient (Cp) is employed as a parameter to assess the mesh sensitivity in this case. Figure 4-16 illustrates the variations in double-blade torque calculated using the three grids. Remarkably, even the coarse mesh demonstrates good grid quality concerning the Cp of the first wind turbine, and the results for the three sets of grids are relatively close. As we focus on the second wind turbine, the curves for the double-blade torque variation nearly coincide for the medium and fine meshes. Hence, it is confirmed that the medium grids fulfill the requirement of reliability for calculations, offering a cost-effective solution. Additionally, we analyze the wake velocity distribution for each mesh.

Table 4-4: The power coefficient obtained by the three different meshes.

		Power coefficient (Cp)	
Mesh	Cells number	Wind turbine 1	Wind turbine 2
Coarse	20 991 938	0.283	0.217
Medium	32 270 718	0.298	0.097
Fine	43 179 319	0.297	0.105

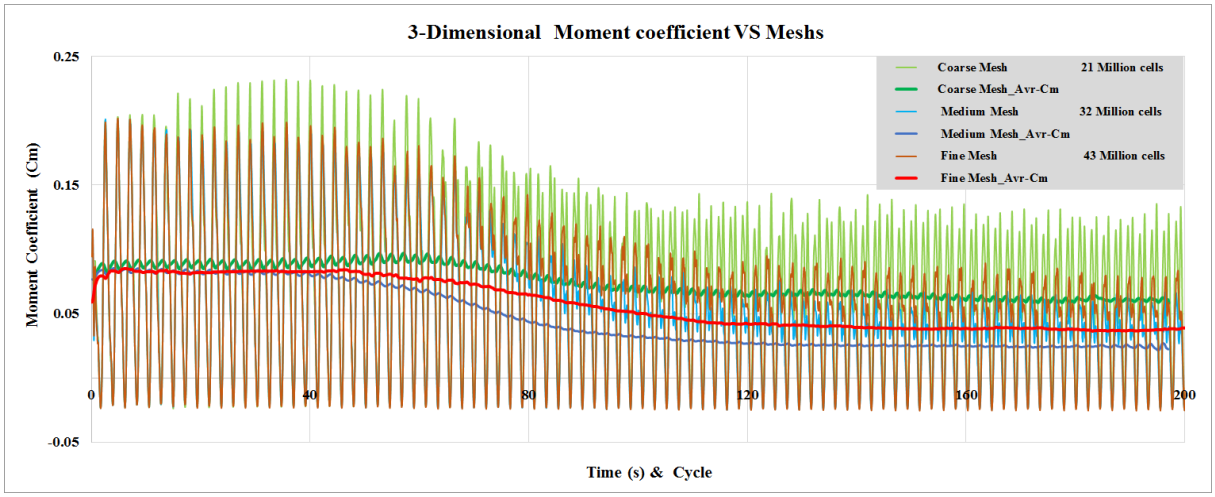

Figure 4-16: The Moment coefficient (Cm) convergence for three different meshes.

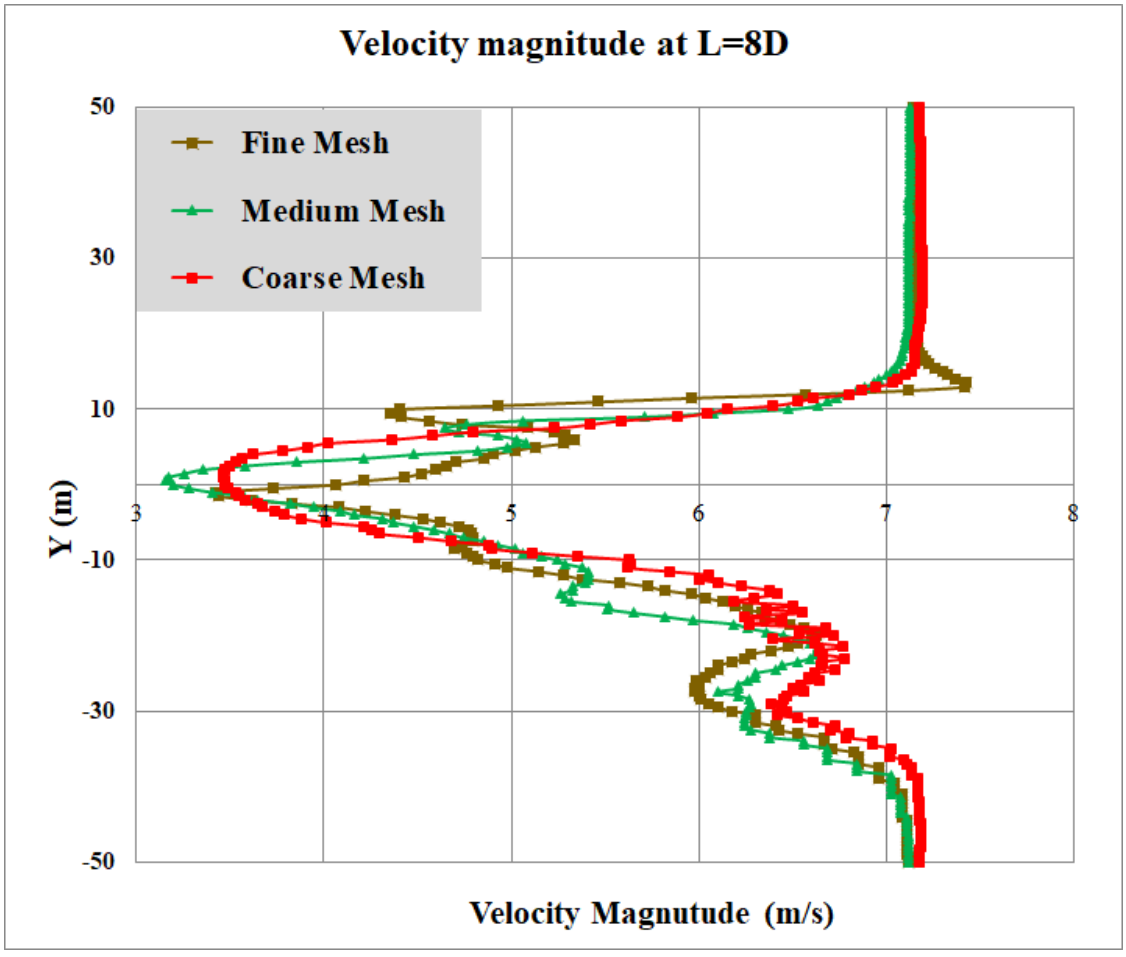

Figure 4-17: Velocity magnitude on line at L=8D.

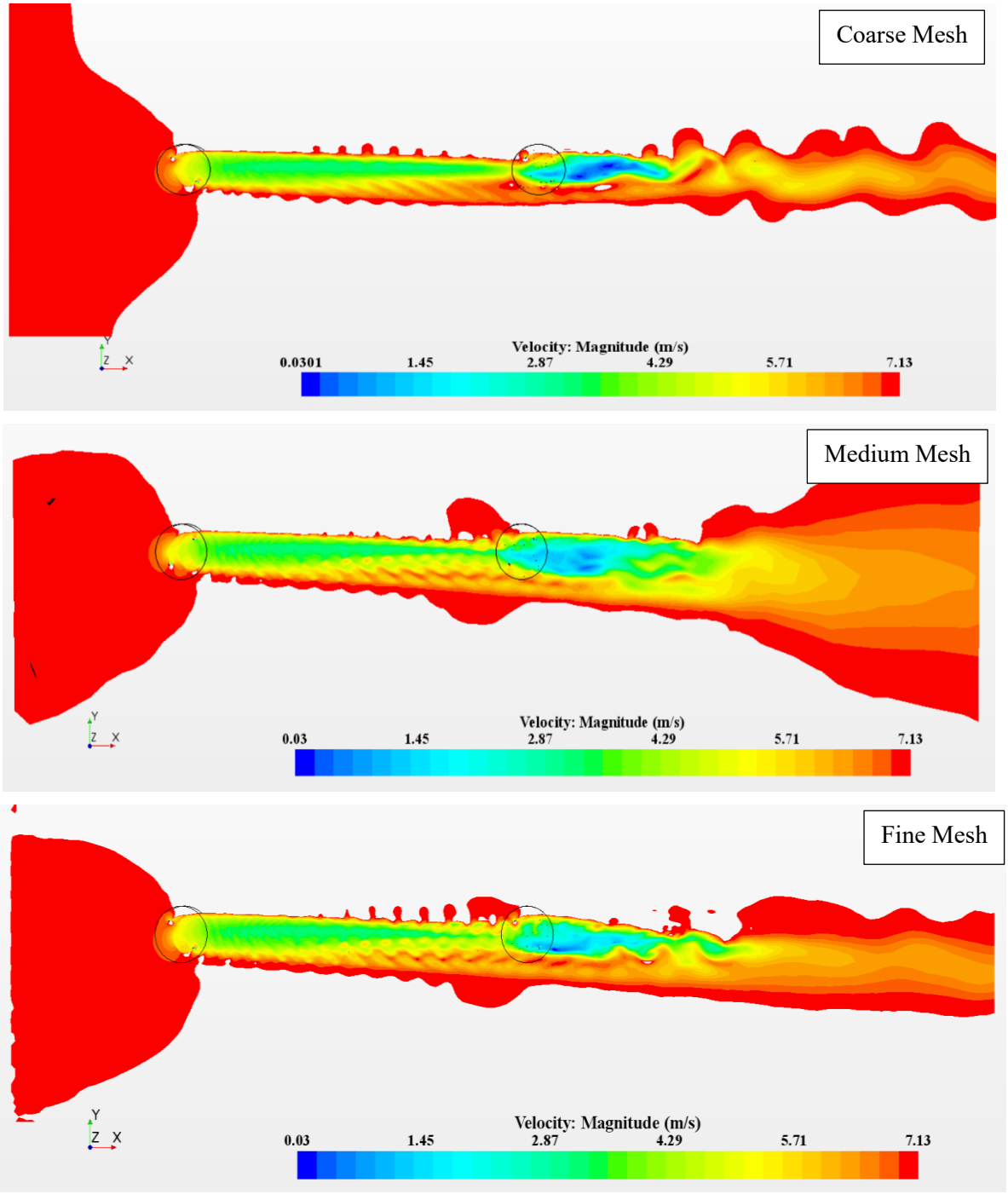

Figure 4-18: The instantaneous Velocity contours for the coarse, medium, and fine mesh after convergence.

Figure 4-17 presents the velocity wake profiles of the Vertical-Axis Wind Turbine (VAWT) on the X-Y plane along the axis of rotation. Notably, there is a significant velocity decrease at the center location of the rotor when the downstream distances of the first wind turbine are 8D.

Furthermore, the rotation of the rotor causes the wake to shift to negative Y values. All three meshes effectively capture these characteristics and show good comparability. Nevertheless, the minimum velocity is smaller for the medium and fine mesh calculations and is about 3.5 m/s for the course mesh calculation which shows a larger wake. Arguably the wake is more diffused on the coarser mesh and this leads to a higher Cp value of the second turbine.

To visualize the structure of the entire wake, Figure 4-18 presents the contours of the instantaneous normalized velocity on X-Y planes at the center of the rotor. It is noteworthy that the wake downstream of the second turbine is dissimilar when using a coarse or a fine mesh, this phenomenon occurs because, in the simulation with the coarse mesh, WT2 is harnessing a greater amount of energy from the wind. This clearly affects the wake behind the second turbine. This is indicated by the blue color in the wake region after WT2. The second difference is observed in the wake between the two turbines. The medium and fine mesh calculations capture more eddies than the coarse mesh, and are seen as a mixture of green and yellow areas close to the second turbine. In conclusion, the coarse mesh is not able to capture the wake accurately, and therefore the value of the Cp for WT2 is over-estimated.

4.4 Simulation results and analysis

4.4.1 Comparison between 2-dimensional and 3-dimensional simulations of the wake

In this section, the wake generated by an upstream turbine and its interaction with a second downstream turbine obtained from a 2-dimensional simulation is compared with results from the medium mesh used in the 3-dimensional simulation. The objective is to evaluate the potential of simulating the wake turbine interaction with a computationally faster 2-dimensional simulation to predict the realization of the second turbine and in particular the minimum distance required between turbines. To this end, the speed variation across the first wind turbine wakes in the inflow direction at a position 8D distance from the first turbine is shown in Figure 4-19, where the distance is measured between the rotation center of WT1 and WT2. The probe-line of velocity measurement is located at the middle plane of the blade (at H/2) for the three turbines with sizes: (D = 35m, H=24.5), (D=1.2m, H=6.1m), and (D=0.5m, H =0.8 m). It measures the instantaneous magnitude of the velocity.

In general, the velocity profiles for each wind turbine have similarities, in particular, the pick velocity deficit is similar for 2 and 3-dimensional simulations. In the case of the large wind turbine (D = 35m, H=24.5) the width of the wake is large for the 2-dimensional simulation. For the small

turbine (D=0.5m, H =0.8 m) and the taller wind turbine (D=1.2m, H=6.1m) the 2-dimensional wake is thinner. The wake velocity deficit is lowest for the large-diameter turbine and increases for the turbine as the diameter decreases.

To illustrate the difference between the three wind turbines, the velocity contours on a horizontal plane for the 3-dimensional and 2-dimensional cases are presented in Figure 4-20 and Figure 4-21, respectively.

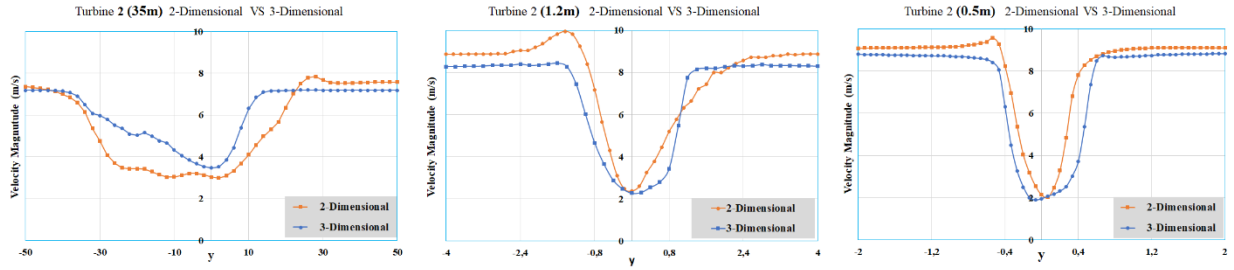

Figure 4-19: Velocity magnitude at horizontal plan of L=8D.

From Figure 4-20 note the width of the wake between the three wind turbines, where the blue color presents the lowest velocity in the wake and the red present the highest which corresponds to the freestream flow. For the three turbines, the wake is quite different between the 2-dimensional and the 3-dimensional simulations. For the largest turbines, the 3-dimensional wake is asymmetric while this is not the case for the 2-dimensional simulation. Furthermore, the velocity contours of flow for the taller wind turbine show that the 2-dimensional simulations indicate a wake break up before reaching the second turbine. For the small diameter turbine, the wake expands in the 3-dimensional simulation while this is the case for the 2-dimensional case. Table 4-5 and Table 4-6 report the Cp values calculated for all cases discussed above and one additional case for two large-diameter turbines placed at a distance of 2.5D. First note that, as expected the Cp for the 2-dimensional simulation is always larger than the 3-dimensional simulation due to tip effects and flow expansion that are not captured with a 2-dimensional simulation. Second, the downstream turbine has a very low Cp even at a distance of 10D. This is consistent with recent findings in the literature.

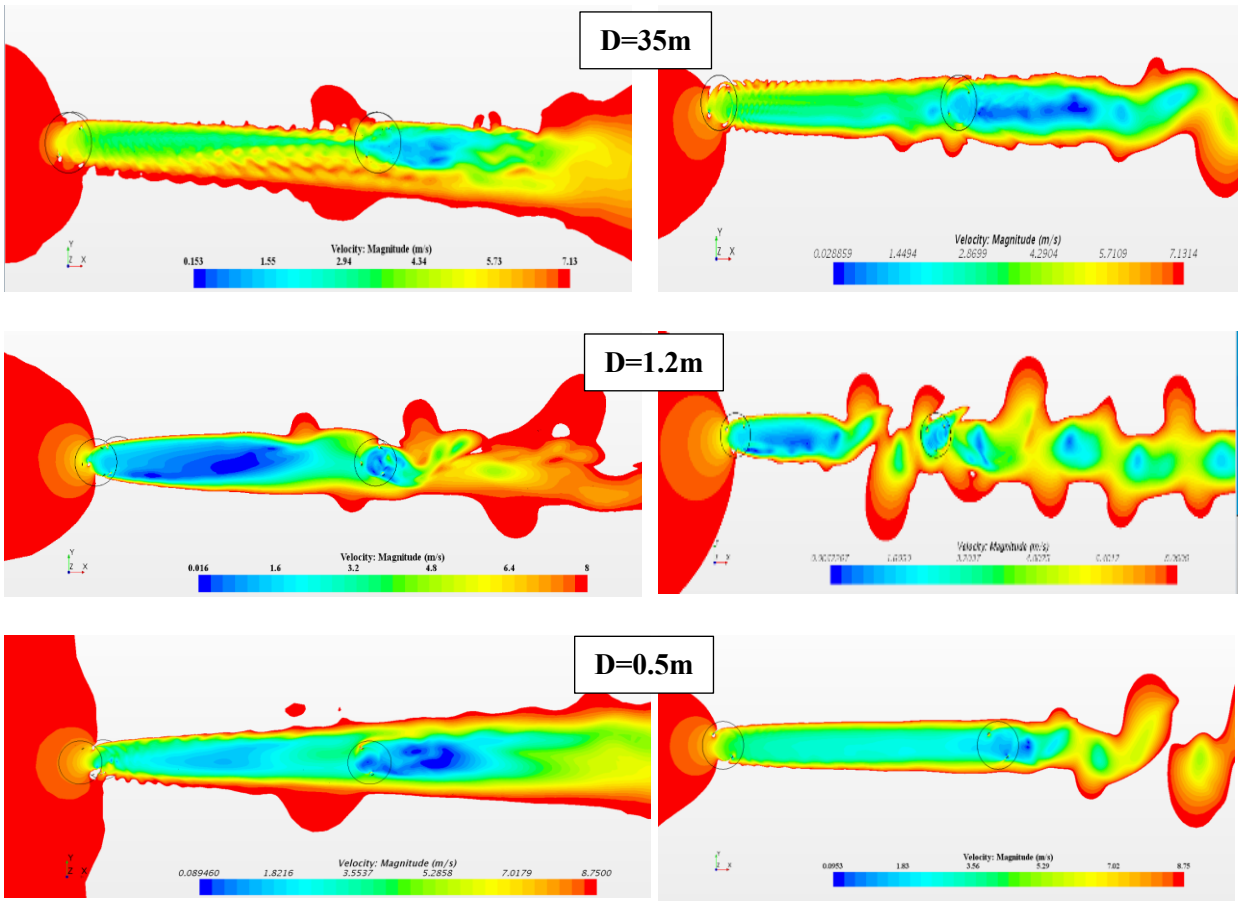

Figure 4-20: Velocity contours at the vertical plane at the middle of the balades for the **3-dimensional** simulations.

Figure 4-21: Velocity contours for the **2-dimensional** simulations.

Table 4-5: The power coefficient (Cp) for Wind turbine diameter **D=35m**.

	Distance of L=2.5D		**Distance of L=10D**	
	Wind turbine diameter **D=35m**			
	Turbine 1	*Turbine 2*	*Turbine 1*	*Turbine 2*
(Cp)2D	0.440	0.032	0.440	0.022
(Cp)3D	0.309	0.027	0.309	0.083
(Cp1-Cp2)2D	0.408 (93%)		0.418 (95%)	
(Cp1-Cp2)3D	0.282 (92%)		0.226 (73%)	

Lastly, the percentage decrease in the Cp for the second turbine is captured similarly for both 2 and 3-dimensional simulations for the largest turbine and the smallest turbine. There is a

big discrepancy for the tall turbine which may be due to its high Aspect Ratio (H/D) close to 5.08. Nevertheless, these results suggest that for a turbine with an aspect ratio of around 1, the 2-dimensional simulation provides a reasonable estimate of the power loss of the second turbine in comparison with the power of the turbine upstream.

Table 4-6: The power coefficient (Cp) for Wind turbines diameter **D=1.2m** and **D=0.5m**.

	Distance of L=10D			
	Wind turbine diameter ***D=1.2m***		Wind turbine diameter ***D=0.5m***	
	Turbine 1	*Turbine 2*	*Turbine 1*	*Turbine 2*
(Cp)2D	0.271	0.138	0.33	-0.05
(Cp)3D	0.193	-0.088	0.18	-0.02
(Cp1-Cp2)2D	0.133 (49%)		0.38 (115%)	
(Cp1-Cp2)3D	0.281 (146%)		0.20 (111%)	

4.4.2 Velocity correction of the 2-Dimensional simulation

The flow upstream of the wind turbine will tend to deviate around the entire turbine as the rotating blades effectively block its path. However, in a 2-dimensional numerical model, this effect is limited, causing the flow to only deviate around both sides of the turbine. In contrast, with a finite aspect ratio turbine, there is no such limitation, allowing the flow to pass the upper and lower sides of the area covered by the sweep of the turbine [14]. To consider these disparities, it is possible to apply a flow velocity correction factor denoted by κ. This adjustment ensures a more accurate representation of the upstream velocity perceived by the two-dimensional numerical model before normalizing its results. This concept is studied in this section with a focus on the wake. The proposed correction that is described below will affect the wake and the power of the second turbine that is operating in the wake of the first turbine.

To start, the effective flow velocity is introduced as follows:

$$V_{eff} = k\mathrm{U}_{\infty} \tag{4-15}$$

A velocity correction factor captures the increase in the flow velocity in the numerical model, therefore, the dynamic pressure force and available power in the incoming 2D flow are augmented. As a consequence, the effective blade speed ratio of the turbine is reduced, alongside the predicted

amplitudes of the force and power coefficients. The effective power coefficient is related to the power coefficient in the following way:

$$Cp_{eff} = \frac{P}{0.5\rho U_{eff}^3 A_s} = \frac{Cp}{k^3} \tag{4-16}$$

The factor k can be calculated based on the power coefficients obtained from the 3-dimensionnal simulation which is assumed to be an accurate representation of the flow and the 2-dimensional simulation calculation of the Cp which is assumed to be overestimated. The following equation is proposed:

$$k = \sqrt[3]{\frac{(Cp)_{2-Dimensional}}{(Cp)_{3-Dimensional}}} \tag{4-17}$$

The velocity correction factor can also be estimated by determining the square root of the ratio between the 2-dimensional calculation and the power coefficients derived experimentally minus mechanical losses. To obtain the value of the corrected flow velocity for the 2-dimensional simulation inflow condition is divided by the correction factor:

$$(U_\infty)_{Corrected} = \frac{U_\infty}{k} \tag{4-18}$$

To compensate for the error arising from the flow deviation in the 2-dimensional simulation, the inflow boundary condition is reduced but all other calculations such as TSR and Cp use U_∞.One of the objectives of this work is to evaluate if this approach works for modeling the wake accurately with a 2-dimensional model. To this end, the correction process is applied for all three wind turbines and results are compared with the 3-dimensional simulations. First, the large wind turbine is analysed, with two distances between the rotors: L = 2.5D and L = 10D. When the TSR is set to 3.5, it was determined that reducing the velocity of the approaching wind to 6.34 m/s in the 2-dimensional computational model (while maintaining the reference wind speed at 7.1314 m/s) produces the power coefficient and torque coefficient variation that are the most similar to the 3-dimensional model but also the experimental values as the 3-dimensional model compared well with the experimental values. As illustrated in Table 4-7, the corrected power coefficient of the first turbine resulting from the reduction in the free stream speed for both cases is very close to the value obtained in the 3-dimensional simulation. Nevertheless, the power coefficient of the

second wind turbine is much lower suggesting less wind velocity arriving to the second turbine than predicted by the 3-dimensional model.

Table 4-7: Comparison between the calculated and the corrected power coefficients with different distances for the large wind turbine.

	Distance of L=2.5D		**Distance of L=10D**	
	Wind turbine diameter **D=35m**			
	Turbine 1	*Turbine 2*	*Turbine 1*	*Turbine 2*
(Cp)2D	0.448	0.032	0.448	0.022
(Cp)3D	0.309	0.027	0.309	0.083
k		1.125		
V_{Eff}		7.131		
$V_{Corrected}$		6.338		
$(Cp)_{2D\text{-}Corrected}$	**0.31**	**0.008**	**0.31**	**0.007**

Next, the two small wind turbines are examined using the distance of L= 10D, with two wind turbines having different H/D ratios, namely 5.08 and 1.6, corresponding to wind turbines with diameters of 1.2m and 0.5m, respectively. Table 4-8 presents the corrected power coefficient obtained for these wind turbines. The smallest wind turbine has a behavior comparable to those of the large wind turbine which predicts a reduced performance of the second turbine. The wind turbine with a higher H/D ratio does not have the same behavior as the performance of the second turbine is relatively better when simulated with the correction method. Velocity profiles at L=8D are illustrated in Figure 4-22 and compared with the calculated 2-dimensional original simulation for each wind turbine.

The wake contours are very similar between the correction and original models. The main difference is that for the wake in the case of D=35m and D=0.5m, the wake is smooth until it reaches the second wind turbine, however, for the case of D=1.2m, the wake breaks up before reaching the second wind turbine. This turbine is quite different from the other two as it has 3 blades, therefore a higher solidity, but also in addition a higher Aspect Ratio. As seen before this turbine has a different behavior leading to a much different behavior between the 2-dimensional and the 3-dimensional simulations.

Table 4-8: Comparison between the calculated and the corrected power coefficients with different distances for the small wind turbine.

	Distance of L=10D			
	Wind turbine diameter ***D=1.2m***		Wind turbine diameter ***D=0.5m***	
	Turbine 1	*Turbine 2*	*Turbine 1*	*Turbine 2*
(Cp)2D	0.271	0.138	0.33	-0.05
(Cp)3D	0.193	-0.088	0.18	-0.02
k	1.11		1.22	
V_{Eff}	8		8.72	
$V_{Corrected}$	7.2		7.15	
$(Cp)_{2D\text{-}Corrected}$	0.188	0.098	0.176	-0.09

The wake looks similar for the largest and smallest turbines. We clearly see that the incoming velocity is lower for the correction method. For the high Aspect Ratio turbine (D=1.2m), the instantaneous wake is different because the wake breaks down into vortices before it reaches the second turbine. To illustrate the wake difference between the correction and the original models, the velocity contours are presented in Figure 4-23 and Figure 4-24. The wake contours are very similar between the correction and original models. The main difference is that the wake for the case of D=35m and D=0.5m, the wake is smooth until it reaches the second wind turbine, however, for the case of D=1.2m, the wake breaks up before reaching the second wind turbine. This turbine is quite different from the other two as it has 3 blades, therefore a higher solidity, but also in addition a higher Aspect Ratio. As seen before this turbine has a different behavior leading to a much different behavior between the 2-dimensional and the 3-dimensional simulations.

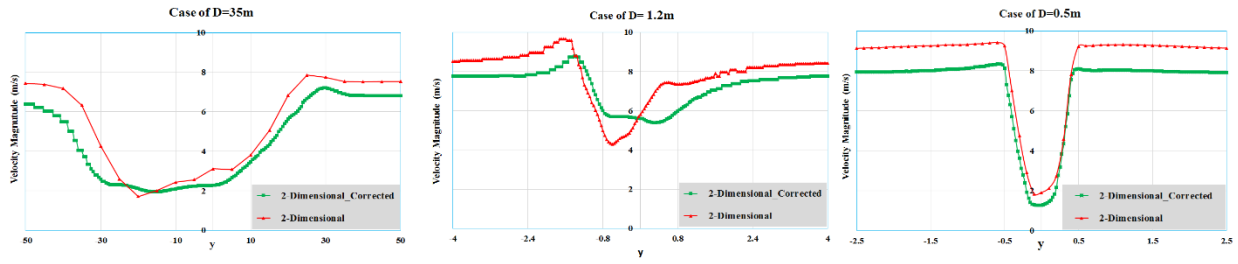

Figure 4-22: Velocity magnitude at the horizontal plane of L=8D **Corrected vs. Not-Corrected cases.**

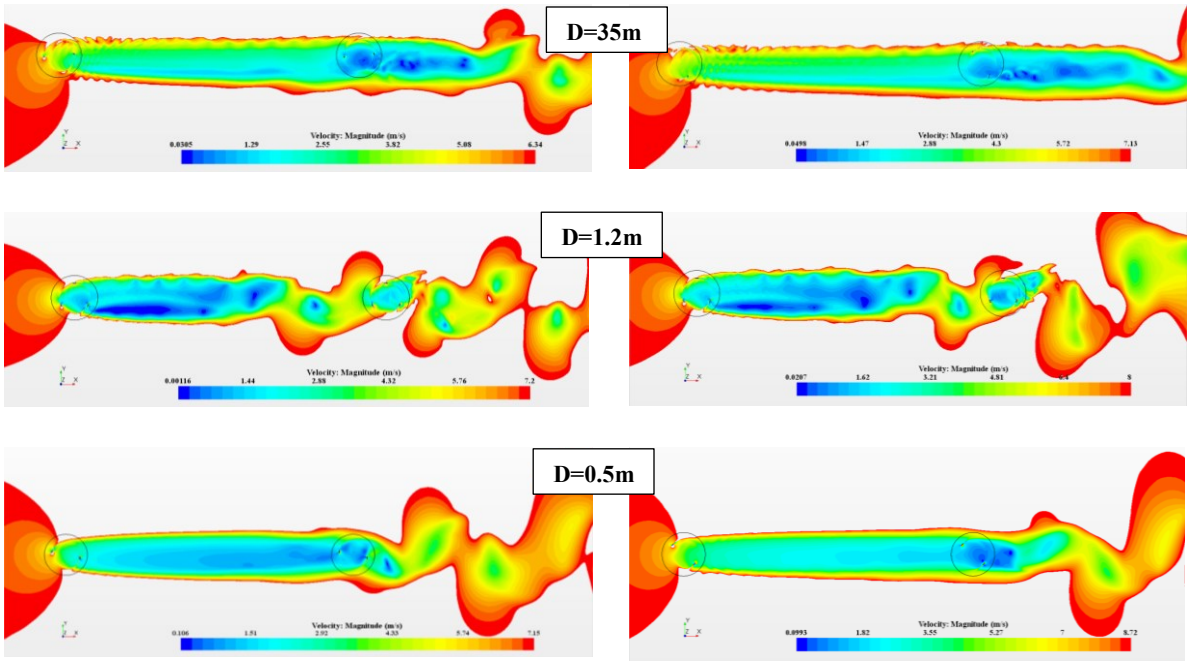

Figure 4-23: Velocity contours for the case of the **Corrected** simulation.

Figure 4-24: Velocity contours for the case of the **not Corrected** simulation.

4.5 Conclusions

This study has investigated the performance of a downstream Vertical-Axis Wind Turbine operating in the wake of a similar turbine placed either 2.5D or 10D upstream. Three different VAWTs were analyzed, considering aspects such as aspect ratio, turbine size, and the number of blades. The analysis could converge on Computational Fluid Dynamics (CFD) to assess the accuracy of 2-dimensional models compared to 3-dimensional models. The following points can be condensed as follows:

- The Cp of the downstream wind turbine operating in the wake of an upstream turbine remains very low, even at a distance of 10 diameters between the two turbines. This behavior was consistently observed for all three turbines.
- As expected, the 2-dimensional investigations consistently overestimated the power coefficient of the upstream turbine compared to the 3-dimensional simulations. However, this pattern did not consistently apply to the second turbine.
- The 2-dimensional simulations proved useful in predicting the percentage decrease of the Cp of the second turbine for turbines with aspect ratios ranging from 0.6 to 1.6.

- The correction method, which involves reducing the inflow velocity in the 2-dimensional model simulation, effectively predicted the Cp of the first turbine for all investigated turbines. However, it did not give a remarkable share to predicting the Cp of the second turbine.
- The turbine with a high aspect ratio of 5.08 and high solidity has a very different wake behavior and the 2 and 3-dimensional model comparison behaves differently than the other two turbines.

This work suggests that 2-dimensional models can be used for low-aspect-ratio and low-solidity turbines to estimate the distance between turbines. It is important to acknowledge that the 2-dimensional approach overestimates the power coefficient but is able to offer a good evaluation of the amount of power lost by the second turbine operating the wake.

5 CHAPTER 5: Conclusion and future work

5.1 Conclusion

Simulations based on solving the Navier-Stokes equations were employed to extensively explore the three and two-dimensional unsteady wake aerodynamics of multiple H-Darrieus rotors. The CFD code named STAR CCM+ was used for this purpose. It exhibited high parallel efficiency, ensuring efficient and accurate analysis. By utilizing this advanced tool, a comprehensive investigation into the aerodynamic behavior of the rotor-wake and turbulence-rotor interaction was conducted, shedding light on its complex flow dynamics and providing valuable insights into its performance and efficiency.

Due to the rapid progress in high-performance computing and the growing availability of large computational resources, I employed CFD in the context of multiple VAWTs to study the complex flow around and between VAWTs. CFD tools offer cost-effective, versatile, and accurate means to improve the understanding of the unsteady aerodynamics of Darrieus wind turbines. For the study of Darrieus rotors, I used more than 24, 32-core nodes, each with 512 GB of memory and approximately 1 TB of volatile-scratch disk space on a High-Performance Computing (HPC) Facility named Speed. Several highly refined simulation models were used, with the largest mesh having a grid of about 43 million elements. After a series of verification and studies of different parameters to create our simulation methodologies, such as wall treatment, time step and mesh independency, and influence of temporal scheme parameters; I successfully validated the coefficient of power (Cp) for three distinct types of turbines with different sizes ranging from rotors with a diameter of 0.5m to 35m. The validation was performed by comparing the calculated power coefficient (Cp) to the experimental data found in the literature. By utilizing CFD, I was able to investigate the complex fluid dynamics involved in VAWT operation and ascertain the Cp values for each turbine design. This comprehensive approach allowed me to gain valuable insights into the performance and efficiency of these VAWTs, aiding in the optimization of their design and contributing to the advancement of renewable energy technologies.

The studies presented in this thesis focus on the effects of turbulence intensity and wake interaction effects on the performance of VAWTs. After validating different parameters used in the simulations, the first study demonstrates that turbulence intensity has a significant but limited

impact on the power performance of small-scale VAWTs. The power coefficient improves by 22% when turbulence intensity increases from 0.07% to 20%, but no further improvement is observed beyond this value. This work indicates that dynamic stall is affected by turbulence intensity and is the main reason for this improvement. The influence of turbulence intensity decreases with increasing Reynolds number of the flow over the blade. Therefore turbulent intensity did affect the performance of large-scale turbines.

The second study investigates the performance of large VAWTs arranged in different configurations, such as behind each other or in a triangular pattern. Two-dimensional CFD analysis is found to be effective in assessing the relative performance of downstream turbines compared to the first turbine, although it overestimates the power coefficient value. First, it is observed that the wake of the first turbine develops into larger eddies after 10 to 20 rotor diameters downstream. Secondly, the wake effect is especially noticeable when the second turbine is on the port side of the first turbine. Finally, the triangular configuration shows a 20% improvement in power output over operating the turbines separately. For more accurate quantitative results of downstream turbine performance, three-dimensional CFD modeling is suggested.

The third study investigates how a downstream VAWT performs in the wake of another similar turbine placed at a 2.5-diameter distance or 10-diameter distance upstream. The study compares three different VAWTs with varying aspect ratios, turbine sizes, and number of blades. The study uses CFD to assess the accuracy of 2-dimensional models versus 3-dimensional models. The results indicate that 2-dimensional models can estimate the distance between turbines for low aspect and low solidity turbines, but they overestimate the power coefficient and underestimate the power loss of the second turbine in the wake. These studies enhance the knowledge of turbulence intensity effects and wake interactions for VAWT design and optimization.

This thesis presents three studies on how turbulence intensity and wake interactions affect the performance of VAWTs. The first study examines the effect of turbulence that exists in the atmospheric boundary layer, where urban turbulence intensity can reach up to 30%, making it favorable for small turbines. The second study explores the wake behind a VAWT, which results from the energy extraction from the wind. The wake has various features and changes downstream, affecting the performance of a downstream turbine. The second study uses a 2-dimensional CFD model to analyze the wake characteristics and interactions. The third study evaluates the accuracy

of the 2-dimensional model for different types of turbines. It finds that the model is accurate for low-aspect and low-solidity turbines, but not for high-solidity and high-aspect-ratio turbines. The third study concludes that the 2-dimensional model can be used to estimate the optimal spacing between turbines for low-aspect and low-solidity turbines, but it overestimates the power coefficient. The model is not suitable for high-solidity and high-aspect turbines.

The behavior of VAWTs under different conditions is investigated in these studies, which provide valuable insights for the design and optimization of VAWT systems. The first study shows that turbulence intensity has an effect on small-scale VAWTs but little on large VAWTs, while the second study reveals that wake effects are important and that power output can be increased by optimizing turbine placement. The third study examines downstream turbine performance and suggests using two-dimensional models for some turbine configurations. These studies enhance the understanding of the factors affecting the performance of multiple VAWT in atmospheric boundary layer flows and guide the design and optimization of VAWT systems.

5.2 Future works

Four areas for future research are proposed to further advance the understanding and optimization of VAWTs, paving the way for their broader adoption and utilization in renewable energy applications.

Turbulence Effects on VAWTs: A Further Investigation

The previous study showed that turbulence intensity affects the power output of small-scale vertical axis wind turbines (VAWTs). However, turbulence may also have other impacts on VAWT performance, such as structural loads, fatigue life, and noise generation. These aspects need to be further investigated to gain a comprehensive understanding of how turbulence influences VAWTs. Future studies could focus on these areas and provide more insights into the optimal design and operation of VAWTs in turbulent environments.

Two-Dimensional CFD Modeling: A Key Tool for VAWT Optimization

The previous study demonstrated the limitations of two-dimensional CFD modeling for predicting the downstream performance of some types of VAWTs. Nevertheless, due to the low computational expense, two-dimensional CFD models, actuator disk and actuator line models are

recommended to investigate and optimize the design and operation of VAWTs in wind farms with multiple turbines.

Optimization of Wake Interactions:

The third study revealed how the power performance of VAWTs is affected by the wake interactions among them. Future research can aim to optimize the power output and minimize wake interference by finding the best placement and configuration of VAWTs in wind farms. Advanced optimization techniques, along with CFD simulations, can help to determine the optimal turbine arrangements and design parameters for improved VAWT performance.

Scaling Effects and Comparative Studies:

The studies highlighted the differences in wake behavior and performance between small-scale and large-scale VAWTs. Future investigations could explore these scaling effects in more detail and compare the performance characteristics of VAWTs with other wind turbine types, such as Horizontal Axis Wind Turbines (HAWTs). Comparative studies can provide valuable insights into the strengths and limitations of VAWTs and help guide their optimal integration into wind energy systems.

References

[1] S. Afsharian, B. Afsharian, and M. Shiea, "Perspectives on offshore wind farms development in Great Lakes," *Journal of Marine Science*, vol. 2, no. 3, 2020.

[2] T. Brahimi, F. Saeed, and I. Paraschivoiu, "Aerodynamic Models for the Analysis of Vertical Axis Wind Turbines (VAWTs)," *Int. J. Mech. Aerospace, Ind. Mechatron. Manuf. Eng*, vol. 10, no. 1, 2016.

[3] "Canadian wind energy association 'CanWEA' wind vision 2025, Powering canada's future retrieved september 2015 From http://www.energybc.ca/cache/wind2/www.canwea.ca/images/uploads/File/Windvision_summary_e.pdf."

[4] G. Li, W. Xu, Y. Li, and F. Wang, "Univariate analysis of scaling effects on the aerodynamics of vertical axis wind turbines based on high-resolution numerical simulations: The Reynolds number effects," *Journal of Wind Engineering and Industrial Aerodynamics*, vol. 223, p. 104938, 2022.

[5] A. B. Suresh *et al.*, "Computational investigations of aluminum-based airfoil profiles of helical shaped vertical axis wind turbines suitable for friction stir joining and processing," *International Journal on Interactive Design and Manufacturing (IJIDeM)*, pp. 1–16, 2023.

[6] C. Gerrie, S. Z. Islam, S. Gerrie, N. Turner, and T. Asim, "3D CFD Modelling of Performance of a Vertical Axis Turbine," *Energies*, vol. 16, no. 3, p. 1144, 2023.

[7] I. Janajreh, L. Su, and F. Alan, "Wind energy assessment: Masdar City case study," *Renewable energy*, vol. 52, pp. 8–15, 2013.
[8] F. Balduzzi, A. Bianchini, and L. Ferrari, "Microeolic turbines in the built environment: Influence of the installation site on the potential energy yield," *Renewable Energy*, vol. 45, pp. 163–174, 2012.
[9] S. Bianchi, A. Bianchini, G. Ferrara, and L. Ferrari, "Small wind turbines in the built environment: influence of flow inclination on the potential energy yield," *Journal of Turbomachinery*, vol. 136, no. 4, 2014.
[10] A. Bianchini, G. Ferrara, and L. Ferrari, "Design guidelines for H-Darrieus wind turbines: Optimization of the annual energy yield," *Energy Conversion and Management*, vol. 89, pp. 690–707, 2015.
[11] S. Eriksson, H. Bernhoff, and M. Leijon, "Evaluation of different turbine concepts for wind power," *renewable and sustainable energy reviews*, vol. 12, no. 5, pp. 1419–1434, 2008.
[12] "'www.lemoniteur.fr/article/comment-ca-marche-energie-eolienne-20844033.'"
[13] D. Araya and J. Dabiri, "Transition to bluff body dynamics in the wake of vertical axis turbines," in *APS division of fluid dynamics meeting abstracts*, 2015, p. H12. 002.
[14] M. Kinzel, Q. Mulligan, and J. O. Dabiri, "Energy exchange in an array of vertical-axis wind turbines," *Journal of Turbulence*, vol. 13, no. 1, p. N38, 2012.
[15] J. O. Dabiri, "Potential order-of-magnitude enhancement of wind farm power density via counter-rotating vertical-axis wind turbine arrays," *Journal of renewable and sustainable energy*, vol. 3, no. 4, p. 043104, 2011.
[16] R. W. Whittlesey, S. Liska, and J. O. Dabiri, "Fish schooling as a basis for vertical axis wind turbine farm design," *Bioinspiration & biomimetics*, vol. 5, no. 3, p. 035005, 2010.
[17] G. Feng, T. De Troyer, and M. Runacres, "Optimizing land use for wind farms using vertical axis wind turbines," in *EWEA Annual Event, 2014*, European Wind Energy Association (EWEA), 2014, p. PO_192.
[18] D. B. Araya, A. E. Craig, M. Kinzel, and J. O. Dabiri, "Low-order modeling of wind farm aerodynamics using leaky Rankine bodies," *Journal of renewable and sustainable energy*, vol. 6, no. 6, p. 063118, 2014.
[19] "'https://www.conservationmagazine.org/2016/08/offshore-northeast-us-winds-turbulent-mean-wind-power/'."
[20] J. F. Manwell, J. G. McGowan, and A. L. Rogers, *Wind energy explained: theory, design and application*. John Wiley & Sons, 2010.
[21] H. K. Versteeg and W. Malalasekera, *An introduction to computational fluid dynamics: the finite volume method*. Pearson education, 2007.
[22] S. Yahaya and J. Frangi, "Cup anemometer response to the wind turbulence-measurement of the horizontal wind variance," 2004.
[23] S. Wharton and J. K. Lundquist, "Atmospheric stability affects wind turbine power collection," *Environmental Research Letters*, vol. 7, no. 1, p. 014005, 2012.
[24] A. C. Molina, T. De Troyer, T. Massai, A. Vergaerde, M. C. Runacres, and G. Bartoli, "Effect of turbulence on the performance of VAWTs: An experimental study in two different wind tunnels," *Journal of Wind Engineering and Industrial Aerodynamics*, vol. 193, p. 103969, 2019.
[25] L. Battisti, E. Benini, A. Brighenti, S. Dell'Anna, and M. R. Castelli, "Small wind turbine effectiveness in the urban environment," *Renewable energy*, vol. 129, pp. 102–113, 2018.

[26] K. C. Anup, J. Whale, and T. Urmee, "Urban wind conditions and small wind turbines in the built environment: A review," *Renewable energy*, vol. 131, pp. 268–283, 2019.
[27] D. R. Drew, J. F. Barlow, and T. T. Cockerill, "Estimating the potential yield of small wind turbines in urban areas: A case study for Greater London, UK," *Journal of Wind Engineering and Industrial Aerodynamics*, vol. 115, pp. 104–111, 2013.
[28] F. Balduzzi, A. Bianchini, E. A. Carnevale, L. Ferrari, and S. Magnani, "Feasibility analysis of a Darrieus vertical-axis wind turbine installation in the rooftop of a building," *Applied Energy*, vol. 97, pp. 921–929, 2012.
[29] "T. Maeda et al., 'Wind tunnel study on wind and turbulence intensity profiles in wind turbine wake', Journal of Thermal Science, vol. 20, no. 2, pp. 127–132, 2011."
[30] "E. Möllerström, 'Noise, eigenfrequencies and turbulence behavior of a 200 kW H-rotor vertical axis wind turbine', Acta Universitatis Upsaliensis, 2017."
[31] "R. Wagner, I. Antoniou, S. M. Pedersen, M. S. Courtney, and H. E. Jørgensen, 'The influence of the wind speed profile on wind turbine performance measurements', Wind Energy: An International Journal for Progress and Applications in Wind Power Conversion Technology, vol. 12, no. 4, pp. 348–362, 2009."
[32] L. Liu, Y. Shi, Z. Zhang, K. Zhang, and F. Hu, "Analysis of Turbulence Intensity in the Megacity by High-Frequency Observations on a 325-M Tower," *Available at SSRN 4086332*.
[33] X. Jin, G. Zhao, K. Gao, and W. Ju, "Darrieus vertical axis wind turbine: Basic research methods," *Renewable and Sustainable Energy Reviews*, vol. 42, pp. 212–225, 2015.
[34] R. Lanzafame, S. Mauro, and M. Messina, "2D CFD modeling of H-Darrieus wind turbines using a transition turbulence model," *Energy Procedia*, vol. 45, pp. 131–140, 2014.
[35] M. H. Mohamed, "Performance investigation of H-rotor Darrieus turbine with new airfoil shapes," *Energy*, vol. 47, no. 1, pp. 522–530, 2012.
[36] L. A. Danao, J. Edwards, O. Eboibi, and R. Howell, "A numerical investigation into the influence of unsteady wind on the performance and aerodynamics of a vertical axis wind turbine," *Applied Energy*, vol. 116, pp. 111–124, 2014.
[37] Q. Xiao, W. Liu, and A. Incecik, "Flow control for VATT by fixed and oscillating flap," *Renewable Energy*, vol. 51, pp. 141–152, 2013.
[38] S. Armstrong, A. Fiedler, and S. Tullis, "Flow separation on a high Reynolds number, high solidity vertical axis wind turbine with straight and canted blades and canted blades with fences," *Renewable energy*, vol. 41, pp. 13–22, 2012.
[39] H. F. Lam and H. Y. Peng, "Study of wake characteristics of a vertical axis wind turbine by two-and three-dimensional computational fluid dynamics simulations," *Renewable Energy*, vol. 90, pp. 386–398, 2016.
[40] F. R. Menter, "Two-equation eddy-viscosity turbulence models for engineering applications," *AIAA journal*, vol. 32, no. 8, Art. no. 8, 1994.
[41] F. R. Menter, M. Kuntz, and R. Langtry, "Ten years of industrial experience with the SST turbulence model," *Turbulence, heat and mass transfer*, vol. 4, no. 1, Art. no. 1, 2003.
[42] F. Menter, "Zonal two equation kw turbulence models for aerodynamic flows," in *23rd fluid dynamics, plasmadynamics, and lasers conference*, 1993, p. 2906.
[43] H. X. Zou, L. C. Zhao, Q. H. Gao, L. Zuo, F. R. Liu, T. Tan, K. X. Wei, and W. M. Zhang, "Mechanical modulations for enhancing energy harvesting: Principles, methods and applications," *Appl. Energy, vol. 255, p. 113871,* 2019.

[44] N. Han, D. Zhao, J. U. Schluter, E. S. Goh, H. Zhao, and X. Jin, "Performance evaluation of 3D printed miniature electromagnetic energy harvesters driven by air flow," *Applied energy*, vol. 178, pp. 672–680, 2016.
[45] A. Abdelkefi, "Aeroelastic energy harvesting: A review," *International Journal of Engineering Science*, vol. 100, pp. 112–135, 2016.
[46] J. Wang, L. Geng, L. Ding, H. Zhu, and D. Yurchenko, "The state-of-the-art review on energy harvesting from flow-induced vibrations," *Applied Energy*, vol. 267, p. 114902, 2020.
[47] J Wang, S Gu, C Zhang, G Hu, G Chen, K Yang, Hang Li, Y Lai, G Litak, and D Yurchenko., "Hybrid wind energy scavenging by coupling vortex-induced vibrations and galloping," *Energy Conversion and Management, 213, 112835*.
[48] K.-Y. Lee, S.-H. Tsao, C.-W. Tzeng, and H.-J. Lin, "Influence of the vertical wind and wind direction on the power output of a small vertical-axis wind turbine installed on the rooftop of a building," *Applied Energy*, vol. 209, pp. 383–391, 2018.
[49] M. Ahmadi-Baloutaki, R. Carriveau, and D. S.-K. Ting, "Performance of a vertical axis wind turbine in grid generated turbulence," *Sustainable Energy Technologies and Assessments*, vol. 11, pp. 178–185, 2015.
[50] H. Y. Peng, H. F. Lam, and H. J. Liu, "Power performance assessment of H-rotor vertical axis wind turbines with different aspect ratios in turbulent flows via experiments," *Energy*, vol. 173, pp. 121–132, 2019.
[51] J. Su, H. Lei, D. Zhou, Z. Han, Y. Bao, H. Zhu, and L. Zhou, "Aerodynamic noise assessment for a vertical axis wind turbine using Improved Delayed Detached Eddy Simulation," *Renewable Energy, 141, 559-569.*, 2019.
[52] E. Möllerström, F. Ottermo, A. Goude, S. Eriksson, J. Hylander, and H. Bernhoff, "Turbulence influence on wind energy extraction for a medium size vertical axis wind turbine," *Wind Energy*, vol. 19, no. 11, Art. no. 11, 2016.
[53] T. Bertényi, C. Wickins, and S. McIntosh, "Enhanced energy capture through gust-tracking in the urban wind environment," in *48th AIAA aerospace sciences meeting including the new horizons forum and aerospace exposition*, 2010, p. 1376.
[54] S. J. Kooiman and S. W. Tullis, "Response of a vertical axis wind turbine to time varying wind conditions found within the urban environment," *Wind Engineering*, vol. 34, no. 4, Art. no. 4, 2010.
[55] L. C. Pagnini, M. Burlando, and M. P. Repetto, "Experimental power curve of small-size wind turbines in turbulent urban environment," *Applied Energy*, vol. 154, pp. 112–121, 2015.
[56] M. Z. Shiraz, A. Dilimulati, and M. Paraschivoiu, "Wind power potential assessment of roof mounted wind turbines in cities," *Sustainable Cities and Society*, vol. 53, p. 101905, 2020.
[57] F. Balduzzi, J. Drofelnik, A. Bianchini, G. Ferrara, L. Ferrari, and M. S. Campobasso, "Darrieus wind turbine blade unsteady aerodynamics: a three-dimensional Navier-Stokes CFD assessment," *Energy*, vol. 128, pp. 550–563, 2017.
[58] I. E. Evgenevna, I. T. Evgenevna, and B. P. Viktorovich, "Analysis of the application of turbulence models in the calculation of supersonic gas jet," *American J. of Applied Sciences*, vol. 11, no. 11, Art. no. 11, 2014.
[59] D. B. Spalding, "Kolmogorov's two-equation model of turbulence," *Proceedings of the Royal Society of London. Series A: Mathematical and Physical Sciences*, vol. 434, no. 1890, Art. no. 1890, 1991.
[60] D. C. Wilcox, *Turbulence modeling for CFD*, vol. 2. DCW industries La Canada, CA, 1998.

[61] D. C. Wilcox, “Simulation of transition with a two-equation turbulence model,” *AIAA journal*, vol. 32, no. 2, Art. no. 2, 1994.
[62] G. Bedon, S. De Betta, and E. Benini, “Performance-optimized airfoil for Darrieus wind turbines,” *Renewable Energy*, vol. 94, pp. 328–340, 2016.
[63] I. D. Mays, C. A. Morgan, M. B. Anderson, and S. J. R. Powles, “Experience with the VAWT 850 demonstration project,” in *Proceedings of European Community Wind Energy Conference*, 1990.
[64] S. N. Zadeh, M. Komeili, and M. Paraschivoiu, “Mesh convergence study for 2-D straight-blade vertical axis wind turbine simulations and estimation for 3-D simulations,” *Transactions of the Canadian Society for Mechanical Engineering*, vol. 38, no. 4, pp. 487–504, 2014.
[65] S. Cd-Adapco, “STAR CCM+ user guide version 12.04,” *CD-Adapco: New York, NY, USA*, vol. 62, 2017.
[66] I. Paraschivoiu, *Wind turbine design: with emphasis on Darrieus concept*. Presses inter Polytechnique, 2002.
[67] X. Amandolese and E. Széchényi, “Experimental study of the effect of turbulence on a section model blade oscillating in stall,” *Wind Energy: An International Journal for Progress and Applications in Wind Power Conversion Technology*, vol. 7, no. 4, pp. 267–282, 2004.
[68] A. Vergaerde, T. De Troyer, J. Kluczewska-Bordier, N. Parneix, F. Silvert, and M. C. Runacres, “Wind tunnel experiments of a pair of interacting vertical-axis wind turbines,” in *Journal of Physics: Conference Series*, 2018.
[69] S. Acarer, “Peak lift-to-drag ratio enhancement of the DU12W262 airfoil by passive flow control and its impact on horizontal and vertical axis wind turbines,” *Energy*, vol. 201, p. 117659, 2020.
[70] S. Zanforlin and T. Nishino, “Fluid dynamic mechanisms of enhanced power generation by closely spaced vertical axis wind turbines,” *Renewable Energy*, vol. 99, pp. 1213–1226, 2016.
[71] A. Rezaeiha, I. Kalkman, H. Montazeri, and B. Blocken, “Effect of the shaft on the aerodynamic performance of urban vertical axis wind turbines,” *Energy conversion and management*, vol. 149, pp. 616–630, 2017.
[72] A. Tummala, R. K. Velamati, D. K. Sinha, V. Indraja, and V. H. Krishna, “A review on small scale wind turbines,” *Renewable and Sustainable Energy Reviews*, vol. 56, pp. 1351–1371, 2016.
[73] N. Qin, R. Howell, N. Durrani, K. Hamada, and T. Smith, “Unsteady flow simulation and dynamic stall behaviour of vertical axis wind turbine blades,” *Wind Engineering*, vol. 35, no. 4, pp. 511–527, 2011.
[74] A. J. Buchner, M. W. Lohry, L. Martinelli, J. Soria, and A. J. Smits, “Dynamic stall in vertical axis wind turbines: comparing experiments and computations,” *Journal of Wind Engineering and Industrial Aerodynamics*, vol. 146, pp. 163–171, 2015.
[75] F. Arpino *et al.*, “CFD simulations of power coefficients for an innovative Darrieus style vertical axis wind turbine with auxiliary straight blades,” in *Journal of Physics: Conference Series*, IOP Publishing, 2017, p. 012036.
[76] B. Belabes and M. Paraschivoiu, “Numerical study of the effect of turbulence intensity on VAWT performance,” *Energy*, vol. 233, p. 121139, 2021.
[77] T. Kinsey and G. Dumas, “Impact of channel blockage on the performance of axial and cross-flow hydrokinetic turbines,” *Renewable energy*, vol. 103, pp. 239–254, 2017.

[78] H. Y. Peng, H. J. Liu, and J. H. Yang, "A review on the wake aerodynamics of H-rotor vertical axis wind turbines," *energy*, vol. 232, p. 121003, 2021.
[79] K. H. Wong, W. T. Chong, S. C. Poh, Y.-C. Shiah, N. L. Sukiman, and C.-T. Wang, "3D CFD simulation and parametric study of a flat plate deflector for vertical axis wind turbine," *Renewable energy*, vol. 129, pp. 32–55, 2018.
[80] F.-Z. Tai, K.-W. Kang, M.-H. Jang, Y.-J. Woo, and J.-H. Lee, "Study on the analysis method for the vertical-axis wind turbines having Darrieus blades," *Renewable energy*, vol. 54, pp. 26–31, 2013.
[81] Z. N. Ashrafi, M. Ghaderi, and A. Sedaghat, "Parametric study on off-design aerodynamic performance of a horizontal axis wind turbine blade and proposed pitch control," *Energy Conversion and Management*, vol. 93, pp. 349–356, 2015.
[82] R. Kumar, K. Raahemifar, and A. S. Fung, "A critical review of vertical axis wind turbines for urban applications," *Renewable and Sustainable Energy Reviews*, vol. 89, pp. 281–291, 2018.
[83] L. A. Danao, O. Eboibi, and R. Howell, "An experimental investigation into the influence of unsteady wind on the performance of a vertical axis wind turbine," *Applied Energy*, vol. 107, pp. 403–411, 2013.
[84] L. Wang, A. C. Tan, and Y. Gu, "Comparative study on optimizing the wind farm layout using different design methods and cost models," *Journal of Wind Engineering and Industrial Aerodynamics*, vol. 146, pp. 1–10, 2015.
[85] W. Tian, A. Ozbay, and H. Hu, "An experimental investigation on the aeromechanics and wake interferences of wind turbines sited over complex terrain," *Journal of Wind Engineering and Industrial Aerodynamics*, vol. 172, pp. 379–394, 2018.
[86] Z. Zhao, D. Wang, T. Wang, W. Shen, H. Liu, and M. Chen, "A review: Approaches for aerodynamic performance improvement of lift-type vertical axis wind turbine," *Sustainable Energy Technologies and Assessments*, vol. 49, p. 101789, 2022.
[87] L. Kuang *et al.*, "Flow characteristics and dynamic responses of a parked straight-bladed vertical axis wind turbine," *Energy Science & Engineering*, vol. 7, no. 5, pp. 1767–1783, 2019.
[88] A. Rezaeiha, H. Montazeri, and B. Blocken, "Characterization of aerodynamic performance of vertical axis wind turbines: Impact of operational parameters," *Energy Conversion and Management*, vol. 169, pp. 45–77, 2018.
[89] B. Hand, G. Kelly, and A. Cashman, "Aerodynamic design and performance parameters of a lift-type vertical axis wind turbine: A comprehensive review," *Renewable and Sustainable Energy Reviews*, vol. 139, p. 110699, 2021.
[90] G. Chen, X.-B. Li, and X.-F. Liang, "IDDES simulation of the performance and wake dynamics of the wind turbines under different turbulent inflow conditions," *Energy*, vol. 238, p. 121772, 2022.
[91] Q. Wang and Q. Zhao, "Rotor airfoil profile optimization for alleviating dynamic stall characteristics," *Aerospace Science and Technology*, vol. 72, pp. 502–515, 2018.
[92] Y. Jodai and Y. Hara, "Wind-Tunnel Experiments on the Interactions among a Pair/Trio of Closely Spaced Vertical-Axis Wind Turbines," *Energies*, vol. 16, no. 3, p. 1088, 2023.
[93] T. C. Hohman, L. Martinelli, and A. J. Smits, "The effects of inflow conditions on vertical axis wind turbine wake structure and performance," *Journal of Wind Engineering and Industrial Aerodynamics*, vol. 183, pp. 1–18, 2018.

[94] W. Zuo, X. Wang, and S. Kang, "Numerical simulations on the wake effect of H-type vertical axis wind turbines," *Energy*, vol. 106, pp. 691–700, 2016.
[95] A. Sheidani, S. Salavatidezfouli, G. Stabile, and G. Rozza, "Assessment of URANS and LES methods in predicting wake shed behind a vertical axis wind turbine," *Journal of Wind Engineering and Industrial Aerodynamics*, vol. 232, p. 105285, 2023.
[96] V. F. Rolin and F. Porté-Agel, "Experimental investigation of vertical-axis wind-turbine wakes in boundary layer flow," *Renewable energy*, vol. 118, pp. 1–13, 2018.
[97] G. Tescione, C. S. Ferreira, and G. J. W. Van Bussel, "Analysis of a free vortex wake model for the study of the rotor and near wake flow of a vertical axis wind turbine," *Renewable Energy*, vol. 87, pp. 552–563, 2016.
[98] I. D. Brownstein, N. J. Wei, and J. O. Dabiri, "Aerodynamically interacting vertical-axis wind turbines: Performance enhancement and three-dimensional flow," *Energies*, vol. 12, no. 14, p. 2724, 2019.
[99] A. S. Alexander and A. Santhanakrishnan, "Mechanisms of power augmentation in two side-by-side vertical axis wind turbines," *Renewable Energy*, vol. 148, pp. 600–610, 2020.
[100] S. Sahebzadeh, A. Rezaeiha, and H. Montazeri, "Towards optimal layout design of vertical-axis wind-turbine farms: Double rotor arrangements," *Energy Conversion and Management*, vol. 226, p. 113527, 2020.
[101] S. Kang, X. Yang, and F. Sotiropoulos, "On the onset of wake meandering for an axial flow turbine in a turbulent open channel flow," *Journal of Fluid Mechanics*, vol. 744, pp. 376–403, 2014.
[102] M. Abkar and J. O. Dabiri, "Self-similarity and flow characteristics of vertical-axis wind turbine wakes: an LES study," *Journal of Turbulence*, vol. 18, no. 4, pp. 373–389, 2017.
[103] F. M. White, *Fluid Mechanics: Frank M. White; Adapted by Professor Rhim Yoon Chul*. McGraw Hill Education, 2018.
[104] J. Sangwan, T. K. Sengupta, and P. Suchandra, "Investigation of compressibility effects on dynamic stall of pitching airfoil," *Physics of Fluids*, vol. 29, no. 7, p. 076104, 2017.
[105] X. Huang, M. Albers, P. S. Meysonnat, M. Meinke, and W. Schröder, "Analysis of the effect of freestream turbulence on dynamic stall of wind turbine blades," *International Journal of Heat and Fluid Flow*, vol. 85, p. 108668, 2020.
[106] P. Ouro, T. Stoesser, and L. Ramirez, "Effect of blade cambering on dynamic stall in view of designing vertical axis turbines," *Journal of Fluids Engineering*, vol. 140, no. 6, 2018.
[107] S. Jain and U. K. Saha, "On the influence of blade thickness-to-chord ratio on dynamic stall phenomenon in H-type Darrieus wind rotors," *Energy Conversion and Management*, vol. 218, p. 113024, 2020.
[108] R. R. Leknys, M. Arjomandi, R. M. Kelso, and C. H. Birzer, "Dynamic stall flow structure and forces on symmetrical airfoils at high angles of attack and rotation rates," *Journal of Fluids Engineering*, vol. 141, no. 5, 2019.
[109] B. Hand, G. Kelly, and A. Cashman, "Numerical simulation of a vertical axis wind turbine airfoil experiencing dynamic stall at high Reynolds numbers," *Computers & Fluids*, vol. 149, pp. 12–30, 2017.
[110] N. Franchina, G. Persico, and M. Savini, "2D-3D computations of a vertical axis wind turbine flow field: Modeling issues and physical interpretations," *Renewable Energy*, vol. 136, pp. 1170–1189, 2019.

[111] F. Balduzzi *et al.*, "Understanding the aerodynamic behavior and energy conversion capability of small darrieus vertical axis wind turbines in turbulent flows," *Energies*, vol. 13, no. 11, p. 2936, 2020.
[112] K. Svitil, "Wind-turbine placement produces tenfold power increase, researchers say," *PhysOrg. (July 13, 2011)*, 2011.
[113] M. L. Shur, P. R. Spalart, M. K. Strelets, and A. K. Travin, "A hybrid RANS-LES approach with delayed-DES and wall-modelled LES capabilities," *International journal of heat and fluid flow*, vol. 29, no. 6, pp. 1638–1649, 2008.